Modeling and simulation of non-linear bioelectronic systems applied to cell culture assays

Juan Alfonso Serrano Viseas

Supervised by:

Dr. Alberto Yúfera García

Dra. Gloria Huertas Sánchez

December 2021

I would like to dedicate this thesis to my parents, my brother and all my family, for their support throughout this journey.

To Alicia, for encouraging me at every step of the way.

To all my friends, for each and every one of their phrases in the best and worst situations.

To my colleagues at the Seville Institute of Microelectronics (IMSE-CNM), without whose contribution this thesis would not be possible.

To my tutors, for their guidance during these years.

Acknowledgements

This thesis would not have been possible without the help of many people. Each and every one of them has provided both technical and support in other ways. If I neglect to mention another name, just remember that I have not forgotten your support and that you have done your bit to make this thesis possible.

The first persons to be mentioned are Prof. Alberto Yúfera García and Prof. Gloria Huertas Sánchez. They have guided me during these years, providing me with encouragement, technical support and their experience for the successful completion of this thesis. Thank you both for the excellent support you have given me, I am very proud and it has been a pleasure to have you as my tutors.

Thanks to my colleagues at Seville Institute of Microelectronics (IMSE-CNM), especially to the PA34 members for helping me in some technical details. I will never forget his friendship and support to follow and complete this journey.

I would also like to thank Prof. Antonio José Ginés Arteaga. During almost all this period, and especially during one year, he has shared and transmitted much of his knowledge and experience. I am very grateful for your help and I am very proud to have worked with you.

Prof. Paula Daza and Prof. María Martín of the Cell Biology Department in the Seville University, for their essential contribution to obtain the required data without which this work could not have been completed. Also, to all the staff of the Institute of Biomedicine of Seville (IBiS), where extra data were obtained from cell cultures and tissues. Thanks to all of you for helping to obtain the biological data that have made this work possible.

My parents, Alfonso and Concepción, and my aunt, Encarna, have always encouraged me and helped me to choose the right decisions at this stage and in all the previous stages of my life. Also, to my brother, Antonio, who helped me with his ideas in some technical aspects to continue in some moments of this thesis. Thank you very much, for everything.

Finally, thank you Alicia for caring for me in every bad moment, for helping me smile when my ideas didn't work, and for being my daily support during almost all this stage of my life.

Abstract

Monitoring the properties of biological samples (BS) is expensive in terms of time consumption and cost in resources and human effort. There are monitoring methods using different techniques, depending on the type of biological sample (cells, tissues, blood, etc.). In this thesis, we improve the accuracy of the ECIS (electrical cell-substrate impedance spectroscopy) technique of bioimpedance (BI) measurement of a monolayer cell-culture (CC), which measures the electrical response of a CC when an alternating current is applied to it at several frequencies. Specifically, this dissertation is focused on the modeling of the cell-electrode (CE) block, and the real-time monitoring and acquisition of the cell concentration in a CC assay experiment. In addition, using as a database the CE model obtained in the modeling stage, a toolbox has been built to perform efficient electrical real-time simulations with Ngspice, launching these simulations from Matlab.

Herein, the BI measurement is applied indirectly. Instead of injecting a signal, the CE block is connected to an electronic oscillator, which fulfills the Barkhausen Stability Criterion (BSC) to ensure that self-maintained and self-sustained oscillations are generated. The technique is known as Oscillation Based Test (OBT) [1]. Instead of measuring the changes between the output and input signal, the oscillation frequency and amplitude are acquired and, using the BSC, the parameters of the CE model used can be obtained on the fly. As can be seen, this technique is much more powerful than injecting a signal, since instead of obtaining the BI for a given frequency, the whole CE electrical model of the CE block is obtained.

The CE model used is based on previous work, but some improvements are introduced to increase its accuracy. The data base for this work are real measurements made by the research group in CC assays with three different cell lines using an OBT circuit. From these data, the parameters of the CE model block are successfully obtained. The modeling technique is tested on some variations of the CE model, reaching better results by increasing its complexity, making the model closer to reality or introducing Fractional Oden (FO) elements.

Data from real experiments, and the best variants of the electrical model are used to build a simulator of a CC assay experiment. The simulator calculates model parameters and cell concentration in real-time (without taking into account future measurements) using the minimization of a cost function (CF). The minimization of an appropriate CF ensures that the oscillation requirements are satisfied and that the obtained CE model parameter values are consistent with the theoretical values. The acquired results are very satisfactory since the simulation of a real-time experiment demonstrates that the technique of minimizing a CF can be used to obtain the cell concentration in real-time. As a result, cell concentration data are attained whose trend and values present a relatively low error when compared to the cell concentration achived by traditional optical cell counting methods.

Electrical simulations of an electronic circuit are very useful during the design and testing process prior to the build of the circuit. The model parameters obtained during

the simulation of a CC assay experiment, in addition to showing the feasibility of the technique, can be used in electrical simulations of the OBT circuit. For future improvements of the OBT measurement circuit, which are discussed at the end of this dissertation, electrical simulations must be performed with realistic data to ensure that the measurement circuit will work robustly. To perform such simulations, a toolbox has been built in Matlab, which performs electrical simulations using Ngspice (open-source Spice simulator) in an efficient way. This toolbox is applied to the oscillator circuit simulation successfully, being able to perform multiple simulations, varying the CE model automatically, in an efficient way. In addition, it can be applied to any electronic circuit to launch electrical simulations from Matlab.

Table of contents

List of figures

List of tables

Glossary of abbreviations

AC	Alternative Current
BSC	Barkhausen Stability Criterion
BI	Bioimpedance
BPF	Band-Pass Filter
BD	Bode Diagram
BS	Biological Sample
CE	Cell-Electrode
CC	Cell-culture
CPE	Constant Phase Element
CF	Cost Function
DF	Descriptive Function
DE	Differential Equation
DC	Direct Current
ECIS	Electrical Cell-substrate Impedance Spectroscopy
EC	Environmental Conditions
ES	Electrical Simulation
FE	Finite Elements
FO	Fractional Order
HPF	High-Pass Filter
IO	Integer Order
LPF	Low-Pass Filter
NA	Network Analyzer
OBT	Oscillation-Based Test
OCF	Oscillation Condition Function
OHP	Outer Helmholtz Plane
PI	Proportional-Integral
REW	Real-Electrode Well
RT	Real-Time
SUT	Sample Under Test
SEW	Single-Electrode Well
TF	Transfer Function

Chapter 1   Introduction

Throughout history, humanity has tried to understand everything that is around it. It started with relatively simple-to-understand elements until today, where it is possible to treat complex diseases, design and fabricate electronic circuits, etc. The study of nature, and all the microorganisms that reside in it, is a subject that, although great progress has been achieved, is still in the process of research. Biologists from all over the world are currently involved in the study of cells, tissues, blood studies, etc. Many tools used in this kind of research have progressed a lot, such as electron microscopes, incubators, and other tools that are used today. However, there are still processes such as optical cell counting, cell differentiation analysis, disease detection, etc. that are still too "rudimentary" compared to the enormous advances seen in other research areas. In the area of cell biology, specifically in Cell Culture (CC) assays studies, CC monitoring methods require a very large amount of time and resources. All tasks and experiments performed with CC require one or more people to monitor the status of the culture every time. This means, for example, that the researcher must count the number of cells 1 by 1 in each culture (the traditional method of counting is explained in detail later), check their morphology, size, etc. This is done, for evident reasons, using a microscope. In order to observe a cell under a microscope, it must be dead and have been stained with a colorant. Once the cells are killed and stained, this culture can no longer be monitored since, as mentioned above, the cells (the CC) have died. Researchers, in order to know the state of a CC assay, must perform a complex and expensive process. To take a single measurement of the cell concentration present in a well, they must take a CC assay, kill and stain the cells, and then perform an optical count through a microscope. The optical (or traditional) counting with the microscope is statistical, several samples (or zones) of the culture are counted and extrapolated to the whole CC using the mean of the taken measurements. This process is long and, moreover, is expensive, since for each measurement that biologist want to perform, they must "waste" a CC assay. Considering the present level of technology, it is coherent to think that it is possible to develop an easier and more efficient method to perform all these tasks.

In recent years, some methods to solve this problem have emerged, such as image processing to calculate the number of cells in a CC assay [2], [3], flow cytometry (a sophisticated instrument measuring multiple physical characteristics of a single cell) [4], or bioimpedance (BI) measurement [5], [6]. The BI is the resistance to the current flow produced by any biological sample (BS). There are many studies on BI, its modeling and applications, but there are also many unsolved problems, such as the translation of BI into useful parameters for the field of biology, such as cell concentration, differentiation level, composition of a cell, etc. This work focuses on the use of BI to try to solve or go a step further in solving this problem these points. Concretely, the main goal is to find a method to measure the cell concentration of a CC assay using the BI.

The structure of the present document begins with Chapter 1, which contains an introduction, where the current state of the art of the agents with which it has been working (CC assays, BI modeling methods, measurement circuits, data acquisition and processing, and simulation) will be explained. The current state of the art of BS and its electrical modeling is reviewed. After that, the challenges of BS modeling is presented. The fourth point is to choose and compare the different ways of data acquisition when taking electrical measurements of biological samples. This is a very complex field, because there are many types of sensors and acquisition methods. Finally, the starting point and objectives of this thesis are presented.

In Chapter 2, the model of the chosen measurement circuit and the possible models that can be used to predict the behavior of a CC assay are studied. Details are given about how the chosen measurement circuit, an oscillator, works. On the other hand, different ways of processing the data (bode diagrams, Barkhausen criterion, etc.) are studied. Finally, the parameters of three variants of the same model are fitted using data from a CC growth experiment, and the results are compared with each other and with data obtained in the traditional experimental way (optical counting with microscope).

Then, in Chapter 3, two types of simulations applicable to BI measurement are presented and tested. The first one is the simulation of a cell growth experiment in which the cell concentration is estimated in real-time. To perform real-time estimation electric models of the CC must be used, which is the reason why these models have been studied in Chapter 2. The second one is the electrical simulation (ES) and its use for the design of BI measurement circuits, exposing an efficient method to perform electrical simulations applied to this work. In the future, these electrical simulations will be very useful when an improvement of the measurement circuit is required, since the real-time simulation data is used to predict the behavior of the circuit.

Finally, Chapter 4 presents the conclusions reached in this study and possible future work that might be derived from it.

1.1 Biological samples

A BS is a sample of biological material from humans, animals or plants, such as blood, cells, tissue, DNA, etc. Each type of sample has its own composition, morphology and size, which can be measured in different ways, which are defined as properties of a BS. The present work focuses on the study of CC assays, which possess properties of their own that can be quantified. For example, cell differentiation is a process by which cells are transformed into more complex cell types or even tissues. The differentiation level is a fundamental property of a CC assay when performing a cell differentiation study [7] and there are many techniques for sensing and acting on tissues [8]. Another property, and one of the targets of this thesis, is the growth of a CC assay. The growth or proliferation of a cell culture is the process by which the number of cells and / or the size of cells in a CC assay grows. This process can be of the cell division type, in which a cell divides into two smaller ones; cell growth, which occurs when a cell increases in

size; growth and cell division, in which the cell increases its size to then divide into two cells of the same size as the original cell. There are many works devoted to the study of cell proliferation, such as [9], which details the process of cell counting by optical density (a less accurate technique than direct counting).

Fig. 1.1 shows the growth curve of a CC, which has been reproduced from [9], which also details the six different zones (labeled with numbers in the figure) of the CC growth.

1. **Lag phase**: The cells adapt to the new culture medium and the new environmental conditions.

2. **Acceleration phase**: Some structural components of the cells increase sequentially and the cell concentration in the well begins to increase.

3. **Exponential phase**: The growth rate reaches its maximum and the cell concentration increases quickly.

4. **Deceleration phase**: the cells face fewer growth factors that enhance growth, so the growth rate of the concentration decreases.

5. **Steady-state phase**: The birth rate is equal to the mortality rate, so the growth rate of the CC concentration is negligible.

6. **Apoptosis (death phase)**: The mortality rate exceeds the birth rate, so the growth rate is negative. This means that the cell concentration decreases.

As previously explained, cell counting by traditional methods (or direct counting) is very laborious and expensive in terms of time and cost. The researchers must spend time preparing several CCs in order to count, for example, each day, the number of cells in
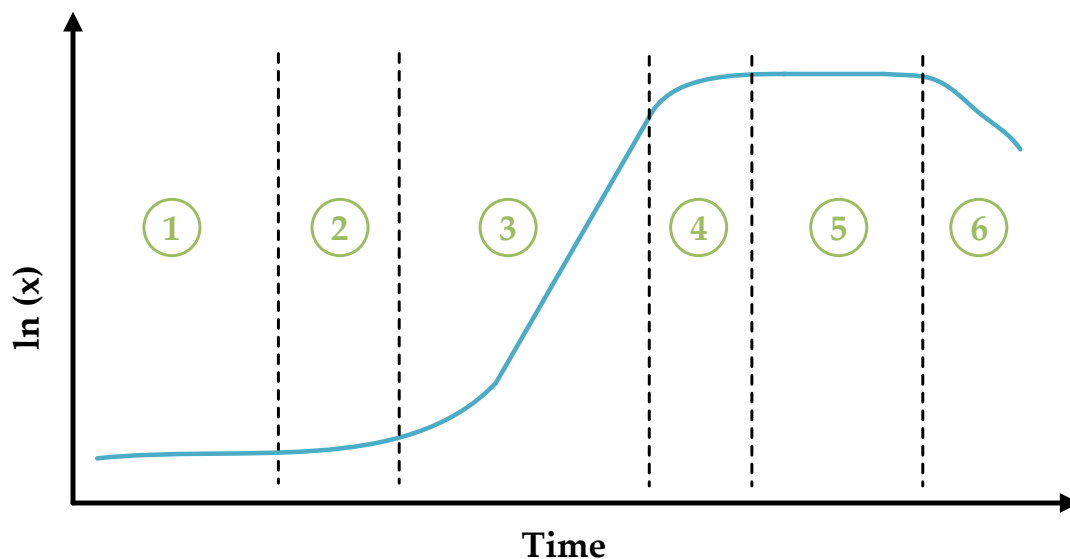
Fig. 1.1 Growth curve of a CC. There are six different zones which are labeled in the figure. Variable x is the cell concentration on each moment.

that CC. If a fairly accurate growth curve is required (Fig. 1.1), it is necessary to kill, stain and count cells from several similar CC cell cultures (seeded at the same time) on the same day. Even then there may be errors with respect to what would be a growth curve measured each day on the same CC assay, since the counting is based on obtaining measurements from several CC and obtaining the statistical mean. As can be deduced, this process is not optimal, since it requires the expenditure of many materials (cells, petri dishes, etc...), and a lot of time performing the whole process.

1.2 Electrical modeling and applications

As mentioned, this work focuses, among other topics, on the measurement of BI, a property that all BS exhibit. The BI property is based on the electrical properties reported in [10] in 1957 by Schwan, the dielectric constant (ε) and the conductivity (σ). These two properties are frequency dependent as shown in Fig. 1.2 (obtained from [10]) and three frequency dependent dispersion zones are observed: α, β and γ.
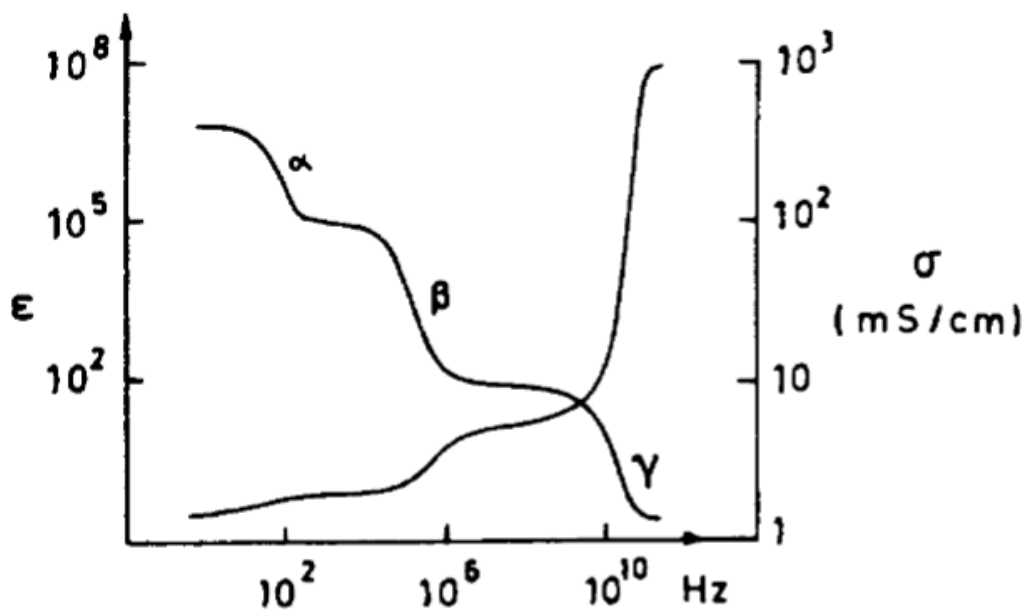
Fig. 1.2 Dielectric constant (ε) and the conductivity (σ) change depends on frequency. There are three different dispersion zones related to the frequency (α, β and γ). Figure from [10].

Each BS, depending on its morphology and composition, has a different BI. The BI can be translated into one of the properties of the BS, thus making an indirect measurement of the desired property. For example, in [11], the measurement of BI, specifically conductivity, is used to determine the blood glucose level. The study [12] describes a method to estimate interstitial fluid volume and peripheral blood volume in hemodialysis patients using whole body and calf bioimpedance spectroscopy techniques. On the other hand, for CC assays there are a lot of researches that study the

relationship of CC BI and some of its properties. In [13] the BI of some CCs is tracked to find relationships between BI and cell differentiation. There are also many studies focused on research for a robust, reliable and accurate non-invasive technique to study and estimate cell growth in a CC [5], [14]–[17]. In addition, cell number quantification has also been targeted for various research purposes and techniques, such as toxicity assays [18], cancer characterization experiments [19], [20], biochemical [21], immune-assays [22], stem cell differentiation protocols [23], etc. All of these studies have at least one thing in common, they all seek to use the BI to indirectly quantify one or more properties of a BS.

To translate the BI into the desired property, electrical models are used. Electrical models predict the behavior of a given material or object in the presence of electric current, i.e., they indicate how the material or object will react against the flow of current. Furthermore, depending on the complexity level of the model, they will be composed of a certain number of parameters. These parameters are usually linked to some property of the material or object, such as its density, size, shape, etc. In the case of BS, the same applies. When the electric current flows through a BS, it faces an impedance, which depends on the type of BS (blood, cells, tissue, etc.) and its properties and characteristics (size, shape, composition, concentration of some chemical substance, etc.). These parameters are the key to obtain and quantify, indirectly, the properties of a BS.

The Bioimpedance-based measurement approach, also called ECIS (electrical cell-substrate impedance spectroscopy) measures the response of a CC when an alternating current is applied to it at several frequencies. Impedance spectroscopy or ECIS technique is used because it is a reliable and robust non-invasive technique to estimate and study cell growth on cell-culture assays. This technique requires robust electrical models of the cell-electrode (CE) block and accurate electronic circuits to extract the signals to be measured [24]. Note that this technique is based on the idea that in a CC assay, cells are seeded in a well filled with culture medium and adhere to the bottom of the well, thus forming the CE block through which the electric current flows.

BI monitoring and modeling has been previously studied in several works [5], [17], [25], [26], [27]. In [5] and [27] the authors solve the electrical equations that model the electrical behavior of the BS under study. Research of [25], [26] use Finite-Element simulations of the whole system (cell-electrode-culture medium system) to extract the relationships between the conductivity, morphology and electrical behavior of the system. Many of the studies mentioned above are the base for this paper, in particular the works [17], [25], [28]. In [17] the model of an electrode immersed in a saline solution (without the presence of cells or other BS) is studied and derived. In [28] a motility experiment is performed with mammalian cells and determines the impedance of a cell-covered electrode and a non-cell-covered electrode. The work [25] performs finite element simulation to find the value of some elements of the electrical models used by the previously described works and, in addition, introduces a new parameter.

1.3 Challenges of cell-culture assay modeling

The CE model used in this work is based on the model of an electrode immersed in a saline solution (culture medium) [17], including in the model the presence of cells [19]. About this model, promising test have been reported, due to the good results obtained in the cited works.

In [17] it is explained how to calculate some of the parameters of the model (Fig. 1.3), which is shown in 2.1.2. The diffusion-related elements (R_w and C_w, named Warburg resistance) are calculated theoretically by [29]. These elements, for the frequencies used in this study, are removed because their effect on the model is negligible. The charge transfer resistance (R_{ct}) depends on exchange current density (J_0) and the thermal voltage (V_t), which are parameters that can vary easily, because their theoretical determination depends on the properties of the electrode and the saline solution, as well as temperature and other variables. In the computation of R_{ct} there can be errors due to the number of parameters and their variability, and the same occurs in the calculation of the interfacial capacitance (C_{dl}), because it depends on much more parameters with similar or greater variability. Finally, as for the spreading resistance (R_s), its estimation is relatively more accurate and easier than the previous parameters, since it depends on the electrode geometry and its resistivity. However, when cells are involved, R_s is more complex to estimate and can even change, as reported in [25] and [30]. The model of an electrode immersed in a saline solution is very complex and presents a high variability. The calculation of the parameters (2.1.2), although relatively accurate, is complex, since there are many variables that can deviate the value of any of them. One of the main challenges of the present work is to find experimental values, or ranges of values, of these
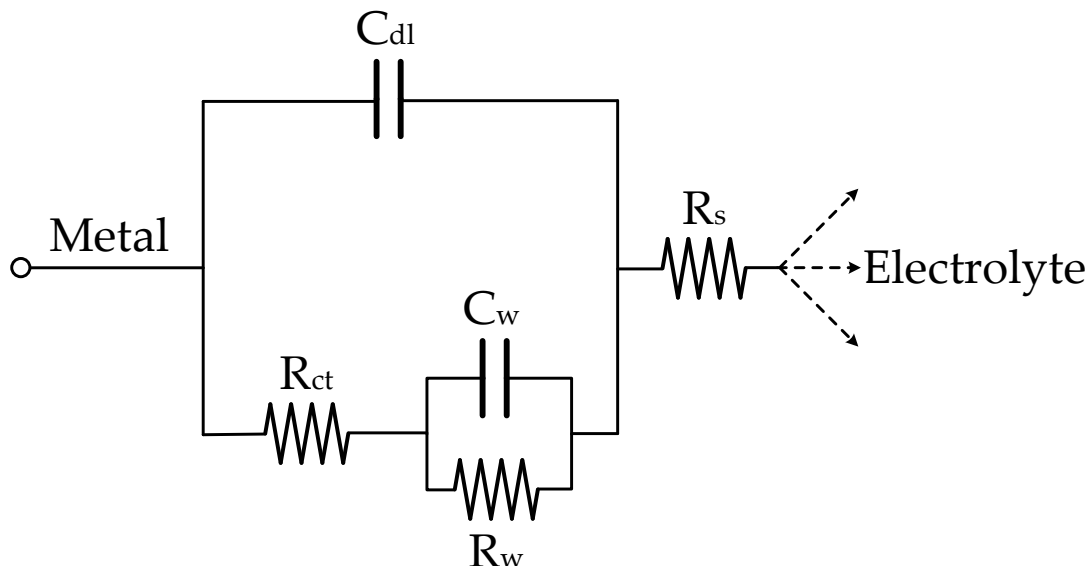
Fig. 1.3 Model of an electrode immersed in an saline solution, reported by [17]. C_{dl} is the interfacial capacitance, R_{ct} is the charge transfer resistance, Rs represent the solution (or spreading resistance) and C_w and R_w are the Warburg elements which are related to diffusion effects.

parameters. The theoretically estimated parameters are used as a starting point to know the approximate behavior of the model and design the experiments accordingly.

An effect not included in [17], is the gap resistance (R_{gap}), which is found by [25] using Finite-Element simulations. The model, included cells and its effects, like R_{gap}, is shown in Fig. 1.4, where these effects are shown. $Z(\omega)$ is the impedance of the electrode immersed in a saline solution, ω is the angular frequency, A_e is the area of the electrode and A_{cell} is the area of the cells. $Z(\omega)$ is divided in two parts, the covered by cells and the uncovered one. In addition, the R_{gap} effect is added after the impedance of the cell covered electrode. R_{gap} represents the effect of the current flowing between the cells attached to the bottom of the well and the well itself, and is highly dependent on the space (gap) between cell and well, which can takes values of 15-150 *nm* as explored in [25], [31]. In [25] R_{gap} values of 10^5 Ω are considered, while in [31], the resistance assumes values of 90 kΩ.

The model of Fig. 1.4 contains the theoretical behavior of an electrode covered by cells and immersed in a saline solution when an electric current is flowing through it. This model is composed of different parameters that model each of the parts of the system, except for one. Cells are considered to be an infinite resistance, i.e., no electric current flows through them. In other works, the cell impedance is considered as a capacitor [32], or as a capacitor and a resistor [33]. In the present work it has not been considered since the impedance division model of the electrode immersed in a saline solution, combined with R_{gap} and R_s, seems to predict well the behavior of the system.

The parameters of the model are difficult to estimate theoretically, due to the fact that the size and composition of the elements that are part of the system are complex to accurately calculate. In addition, the model contains a considerable number of variables, which must be computed and fitted to the data of a real experiment. Finally, biological elements usually exhibit nonlinear behavior, i.e., they cannot be fully modeled using conventional passive elements. There are techniques, such as the fractional-order (FO) models, which can be applied to the BS modeling. In [34], FO models are used to
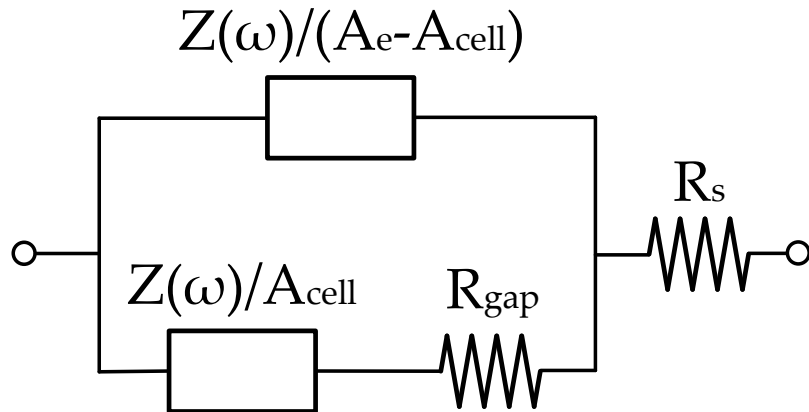
Fig. 1.4 Model of an electrode immersed in a saline solution covered by cells. $Z(\omega)$ is the impedance of the electrode immersed in a saline solution, ω is the angular frequency, A_e is the electrode area, and A_{cell} is the area covered by cells.

characterize vegetable tissue. It is also widely applied in animal tissue modeling [35], and, therefore, is a technique to be considered herein.

1.4 Data Acquisition solutions

To measure BI, two main decisions must be done: the choice of the type of circuit, and the type and number of electrodes. These questions should be discussed considering the type of BS to be monitored, i.e., its theoretical electric model. which predicts the electrical behavior, or BI, of the BS. The fundamental BI measurement circuit is shown in Fig. 1.5. Current is introduced through the BS and the voltage difference between the input and output of the BS is measured. Using Ohm's law, the BI of the BS is calculated. Reality is always more complex, so complex circuits are needed to perform such measurements.

The electrodes influence the electrical behavior of the circuit their electrical model must be considered, since they are vital elements to perform the measurement of the BI. For example, in the works [36]–[40] the electrical behavior of electrodes made of different materials immersed in ionic liquids is studied. The algorithm for extracting the real and imaginary parts is important when measuring BI. In [41] coherent demodulation principle is used, while in [42] synchronous sampling is applied. These methods require an external excitation, i.e., a current (or voltage) source to provide the input signal to the BS. Feedback measurement techniques do not require external excitation, such as the oscillation-based test (OBT) technique [43] which is based on a self-sustained oscillator circuit, where the oscillation amplitude and frequency are used to indirectly acquire the BS impedance.

The electrode number also influences the measurement. The most commonly used are the two-wires ones, which modify the electrical behavior of the BS, and the four-wires ones, which minimize and even make negligible the electrical effect of the electrodes on the BS. Work [44] compares both electrode measurement strategies. In addition, there are other electrode configurations, as in [45], which test two and three electrode configurations in a glucose measurement sensor.

$$V_1 \xrightarrow{\;i\;} \boxed{\text{Biological Sample}} \quad V_2$$

$$Z(\omega) = (V_2 - V_1)/i$$
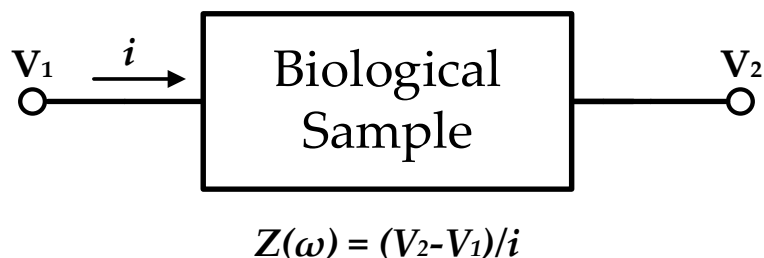
Fig. 1.5 Basic BI measurement circuit. Current flow through the BS, voltage between the edges of the BS is measured, and the Ohm`s Law is used to calculate the BI or $Z(\omega)$.

For this study, the OBT measurement technique was chosen, using two-wire configuration for the measurements. Therefore, it is important to know the electrical model of the electrode, since its effects are included in the measurements. A source is not necessary to generate the electrical signal, since the OBT circuit produces the oscillation signal by itself. In this case, an indirect measurement is made by monitoring the signal oscillation amplitude and frequency, instead of observing the output signal for a given input signal. The advantage of measuring the frequency and amplitude of oscillation, as discussed below, is that the entire electrical model of the CE block can be obtained from these parameters, and not only its BI at a specific frequency.

1.5 Objectives

Currently cell counting techniques are slow and very expensive. The main and most widely used is the optical microscope counting method, for which a lot of resources in terms of time and cost in resources and human effort must be invested. Today's technology must advance to improve this kind of task and save these important resources (for example [4]). Therefore, the main goal of this work has been to research, design and build a system that allows the monitoring of a cell culture, showing in real-time the cell concentration.

On the other hand, the project developed in this thesis has the objective of finding a method to estimate the cellular concentration of a CC through BI data. The diagram of the method is shown in Fig. 1.6. The CC is placed, with culture medium, in wells with electrodes [46]. These electrodes are the connection between the CC and an oscillator circuit (OBT). The OBT is a circuit that oscillates permanently with a frequency (f_{osc}) and amplitude (a_{osc}) determined by the components of the circuit itself, within which are the electrodes and the CC. Depending on the cell concentration, the BI changes, so the OBT will oscillate at different a_{osc} and f_{osc}. The oscillator circuit collects the f_{osc} and a_{osc} every hour and these parameters are used to estimate the cell concentration in real-time. To calculate the cell concentration, the relationship between the cell concentration and the oscillation parameters must be identified. For this purpose, electrical models of an electrode immersed in a saline solution and covered with cells are used.

There are some details to consider:

- Wells are of commercial origin, manufactured by Applied Biophysics [46], and are used to perform CC electrical measurements using a two-electrode technique.

- Experiments have been performed with various different cell lines to test and in order to validate the performance of the circuit and the cell concentration estimation method.

OBT

f_{osc}

a_{osc}

Cell concentration estimation

Cell-culture
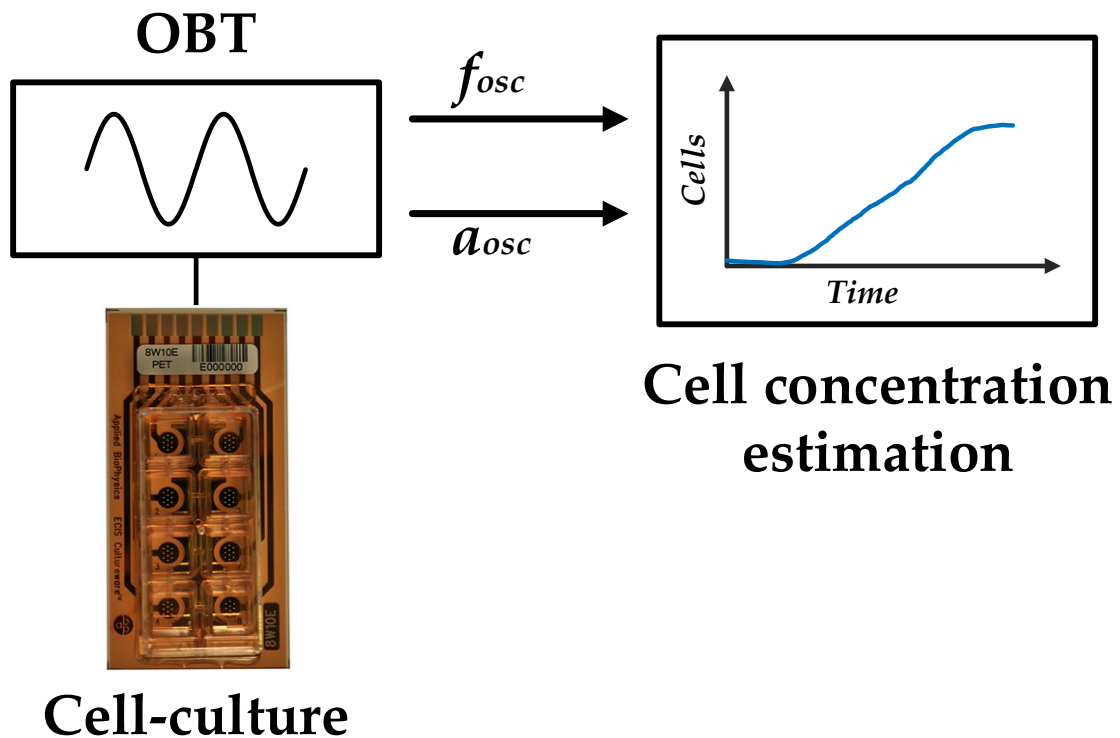
Fig. 1.6 Cell concentration estimation project. A CC is connected as a load to an OBT circuit. The changes in the oscillation parameters (f_{osc} and a_{osc}) are used by an algorithm to estimate the cell concentration of the CC at each moment.

- The OBT circuit produces self-sustained oscillations, but to ensure that the oscillations are in the desired frequency range, and to decrease the settling time of the oscillations, a start-up circuit was implemented.

- To calculate the cell concentration, the electrical behavior of the electrode-cell block (CE) must be known. The electrical model used is only a starting model, and some more complex variants will be studied and tested.

- The electrical model is essential for the estimation of the cell concentration, since it is based on the oscillation condition established by Barkhausen [1]. Therefore, the electrical model of all circuit elements must be known.

- The measurement prototype, in addition to the included OBT circuit, has other circuits to obtain the data, analyze it, and send it to a database. All details were reported in the thesis [47].

Therefore, the two main objectives are:

1. To find and explain a way to fit the experimental data to the electrical model (Chapter 2). In that way, variations of the used electrical model and fitting techniques are considered and tested.

2. To define and simulate a protocol for real-time monitoring of a CC assay experiment (Chapter 3). This objective must consider from the prototype design to the algorithm for estimating the cell concentration in a real-time CC, including the optimal time between measurements (sampling time).

Chapter 2   Electrical modeling of biological samples

Bioimpedance (BI) measurement is a non-invasive, cheap and fast method to estimate the state of the biological sample (BS) under test. If one tries to use the measured impedance to obtain the state of a BS (cell, tissue, blood, etc.), it is needed to know the meaning of each impedance value, i.e., translating the BI value to another variable which gives information about the biological material. That is, the sensor doesn't provide the BI value, the designer has to measure the variation of voltage or current, calculating the impedance and then, using the mathematical model of the sensor, obtains value of the BS property. In that way, mathematical or electrical models can be used to translate BI measures to a biological variable.

BI is a key property of any BS, which value can be converted or interpreted into another property. Depending on the property to be measured, the model to translate the value of BI to that property will be chosen. Fig. 2.1 shows, for the sake of illustration, some properties of a cell-culture (CC) assay. In that way, if the main goal is to know the mean size of the cells in a CC and BI is the parameter (property) known, a mathematical model (chemical, electrical, etc.) and an adequate assay could be used to find the mean cell size.

Mathematical models are used to understand the relationship between some variables of a system. Usually, it is a relationship between an input (u) and an output (y). These variables can be measured directly or indirectly. Models contain the relationships between system variables, and allow to get some variables from another variable. This "translation" can be done by several kind of models:

- Gain model: It is a proportional relationship between two parameters (mathematical formulas).

$$y = K \cdot u \tag{2.1}$$

  where K is the constant gain ratio between u and y.

- Transfer function (TF): It is a linear relationship between u and y. Usually, there is a time-dependent dynamic. This model is usually expressed in the Laplace frequency domain [48] obtained from a differential equation (DE) by Laplace Transform.

$$Y(s) = H(s) \cdot U(s) \tag{2.2}$$

  where s is the Laplace variable ($s = \sigma + j\omega$, since σ is the real part of s, j is the complex variable and ω is the angular frequency) and $H(s)$ is the TF.
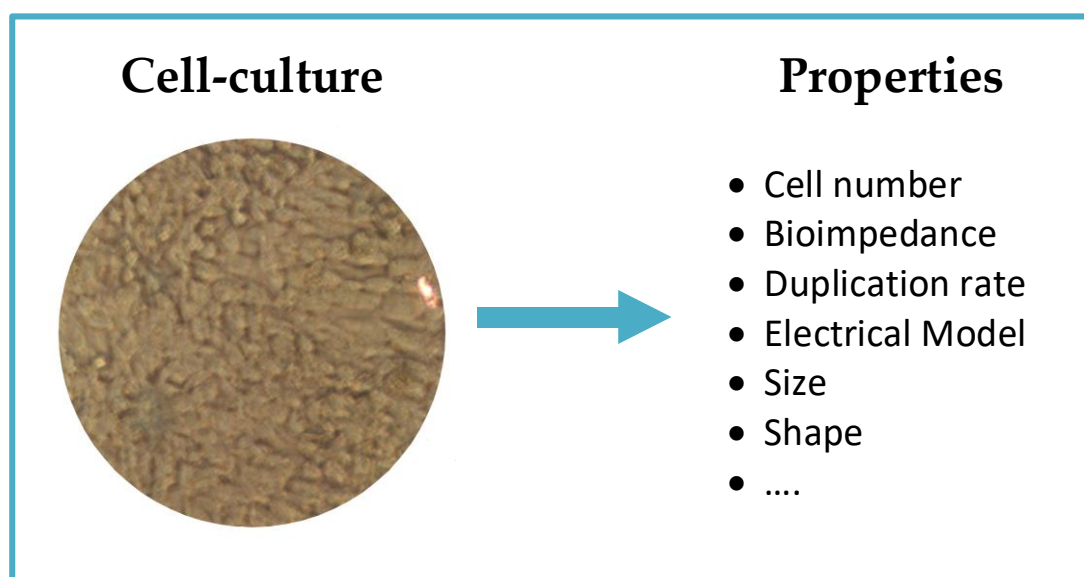
Fig. 2.1 Each CC property can be used to know other ones, since some mathematical relation could exist.

- Differential equation (DE): A DE is a mathematical equation that relates a function to its derivatives. If one focused on the solution of a time-dependent DE, the relation between u and y can be gotten. A DE could be linear or non-linear. If it is linear, it can be solved by Laplace transform, i.e., transforming it in a TF. If it is non-linear, there is some solving methods like linearizing in a working point, numerical solving, etc.

In this work an electronic oscillator is proposed to monitoring the growth of a CC assay. The CC assay is connected as a load to the oscillator, which produces changes in oscillation frequency and amplitude. The oscillation frequency and amplitude are used, in combination with electrical models of the CC, to predict the growth of the CC assay. This chapter describes the oscillator circuit and the electrical model of the CC assay on which this work is based, as well as all the modifications of the model, which will be tested throughout the chapter. Finally, the model parameters will be fitted to real experimental data performed with three different cell lines and the results achieved will be discussed.

2.1 Cell-culture assay modeling

In recent years, a lot of research has been focused on growth monitoring of a cell-culture assay for the development of a non-invasive, cheap and robust technique [5], [14]–[17]. Biomedical setups such as toxicology assays [18], cancer characterization experiments [19], [20], biochemical [21], immune-assays [22], stem cells differentiation protocols [23], etc., seek to quantify the number of cells for characterizing a diversity of research objectives and techniques. As was previously introduced, the modeling of a BS allows to know its electrical behavior and several useful parameters.

ECIS (electrical cell-substrate impedance sensing) technique senses the electrical response generated on a BS ([28], [49]), the CC, when it is excited with an alternating current (AC) electrical source, voltage, or current, at several frequencies, as consequence of its conductivity properties. Since the current applied to the BI must be very low, the ECIS technique requires precise and robust electronics [24]. Usually, the CC is immersed in an ionic solution, the culture medium, and the cells of the CC settle on the substrate of the culture well, where the electrodes are placed. The ideal use of this technique would be to inject a signal whose amplitude and frequency are set at their optimum values, i.e., the values most sensitive to a change in BS. The current-voltage relationship, or Ohm's law, returns an impedance value with a real part and an imaginary part, the so-called BI, which is defined as:

$$Z_{BI} = R_{BI} + j \cdot X_{BI} \tag{2.3}$$

In this way, the value of the BI is obtained, but to understand its value, a model of the electrical behavior of an electrode immersed in an ionic solution must be used. There are some works focused on modeling BI by solve electrical system equations [5], [17] or performing finite elements (FE) simulations [25], [26] of the whole system, which comprises CC and electrodes. Then, the main goal is to obtain a cell-electrode (CE) model which throws up information about the current state of the CC, i.e., about the CC growth.

2.1.1 Cell-culture assay growth

CC assay tests are the best way to known the behavior of cells in specific situations. These tests give data about the response of cells in any isolated scenario, i.e., CC assay tests allow to isolate the effect of a certain situation in cells without the effects of another situation. These "situations" could be cell differentiation scenario, toxicology test, unusual cell behavior characterization, etc. For example, in a cell differentiation test, differentiation data could be obtained without the "perturbation" of another effects in cells. In that way, the cell growth is a basic parameter to characterize a CC.

CC tests must be performing in a controlled environment, i.e., the environmental conditions (EC) must be properly set for cell proliferation. Tests are held in a CC reactor, or "incubator", in which the researcher can chose the EC. Concretely, the data used in this work are obtained from CC assay experiment whose EC are a temperature of 37 °C and 5 % CO_2 in a very humid atmosphere (90 %).

CC assay is placed in a Petri dish or in another well type. Cells take some hours (number of hours varies depending on cell line) to adhere to the substrate in the bottom of the Petri dish [9]. Each certain time period, cells are detached from the bottom and rise to perform cell division (mitosis phase), i.e., cell divides into two identical cells and identical to the cell that originated them. In that way, when there are enough cells, the CC builds a layer over the bottom of the Petri dish. Cell division is repeated until all the bottom is covered by cells, obtaining a monolayer.

2.1.2 Cell-electrode model

ECIS technique is based on the Double-layer interphase explored in [5], [17], [25], [47], among others, and also in the behavior of a CC assay. An electrode immersed in an ionic solution generates an electric-field on the electrode surface. For this purpose, Applied Biophysics [46] commercial electrodes are used. The employed electrodes (model 8W10E PET) contain eight separated wells with ten circular biocompatible gold microelectrodes of 250 μm diameter (Fig. 2.2), which are labeled in Fig. 2.2. Each well also contains a reference electrode (reference electrodes of each well are connected to each other) which has an area approximately 400 larger than each circular electrode.
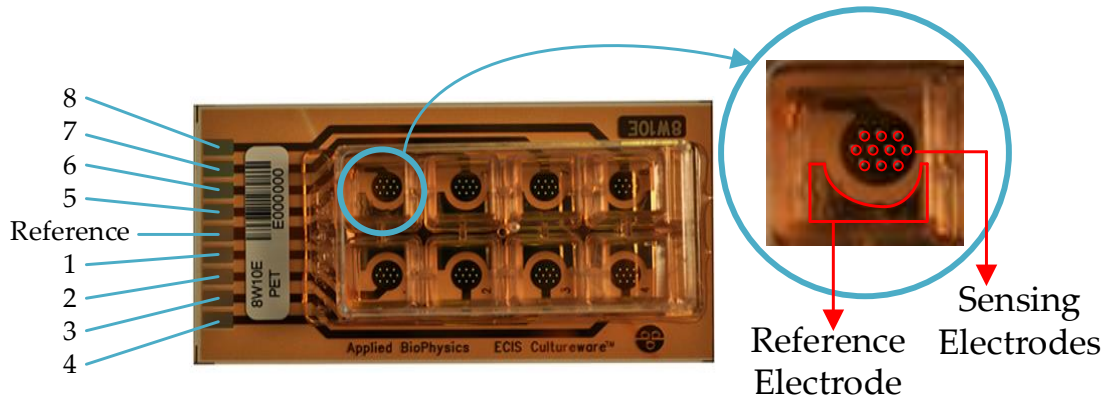
Fig. 2.2 8W10E PET Applied BioPhysics electrodes. Eight separated wells with ten circular biocompatible gold microelectrodes of 250 μm diameter, and a large reference electrode with an area approximately 400 larger than each circular microelectrode.

Reference [17] models the electrochemical behavior of an electrode immersed in an ionic solution. This idea is displayed in Fig. 2.3; the electrical model of the impedance of an electrode immersed in an ionic solution (CC medium). That is, the electrical behavior of an electrode immersed in an ionic solution is modeled as a resistance (R_{ct}) in parallel with a capacitor (C_{dl}), whose total impedance is Z_e. In [17], [47] the physical meaning of each component of the electrical model (Fig. 2.3) is explained in detail, so in this work each parameter will be explained and its theoretical estimation:

- Charge transfer resistance (R_{ct})

    R_{ct}, depends on exchange current density (J_0) and the thermal voltage (V_t). J_0 is the absolute value of current per area in the electrode, and it depends on the electrode properties and ionic solution. According to [36], referenced by [17] and [47], for a gold micro-electrode immersed in a saline solution, the value is $J_0 = 3.98 \cdot 10^{-6} \ A/cm^2$.

Thermal voltage is estimated by:

$$V_t = \frac{k \cdot T}{q} = 26.71 \ mV \tag{2.4}$$
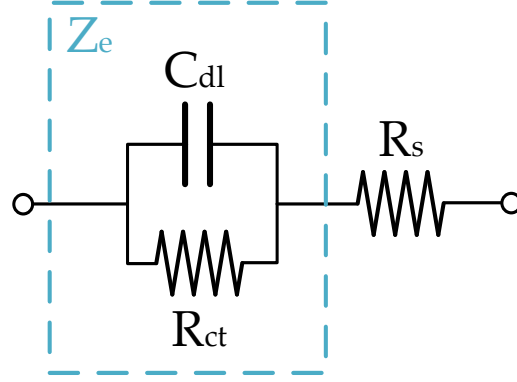
Fig. 2.3 Electrical model of an electrode immersed in an ionic solution impedance without the presence of cells.

where T is the temperature in kelvin (K) set at 310.15 K (37 °C), q is the electron charge and it is set to 1.60218·10^{-19} C, and k is the Boltzmann's constant that has a value of 1.38·10^{-23} J/K.

The charge transfer resistance per area is calculated by (2.5). Then, the expression to estimate R_{ct} of a gold microelectrode of area A_e immersed in an ionic solution is (2.6).

$$R_{ct}^{'} = \frac{V_t}{J_0} = 671.21 \ G\Omega \cdot \mu m^2 \tag{2.5}$$

$$R_{ct} = \frac{R_{ct}^{'}}{A_e} \ [\Omega] \tag{2.6}$$

- Double layer capacitance (C_{dl})

Over the electrode immersed in an ionic solution, a charged capacitive layer is created. This layer was modeled by Stern [50], basis in works of Helmholtz [51], and Gouy [52] and Chapman [53]. Helmholtz capacitance (C_H) in terms of capacity per unit area is defined by:

$$C_H = \frac{\varepsilon_0 \cdot \varepsilon_r}{d_{OHP}} \ [F/m^2] \tag{2.7}$$

where ε_0 is the vacuum permittivity (8.85419·10^{-12} F/m), ε_r is the relative permittivity of the solution (value of 6.8), and d_{OHP} is the distance between electrode surface and Outer Helmholtz Plane (OHP) ([17], [54]) whose value is 8.25·10^{-10} m. For these values, C_H is 0.073 F/m^2.

The second capacitance included in that model is the Gouy capacitor (C_G), and can be estimated[17] by:

$$C_G = \frac{\varepsilon_0 \cdot \varepsilon_r}{L_D} \cdot \cosh(\frac{z \cdot V_o}{2 \cdot V_t}) \ [F/m^2] \tag{2.8}$$

where z is the valence of the ions present in the reaction of creation of the double layer ($z = 1$), V_o is the maximum electrode potential (provided by [46]) whose value is 100 mV [47], and L_D is the Debye Length, models the drop in potential along its length [17]. L_D is defined by:

$$L_D = \sqrt{\frac{\varepsilon_0 \cdot \varepsilon_r \cdot V_t}{2 \cdot n^0 \cdot z^2 \cdot q}} \quad [m] \tag{2.9}$$

n^0 is the concentration of ions in the electrolyte whose value, for a saline solution, is $n^0 = 140$ mol/m^3 [47]. q is the electron charge, $q = 1.60218 \cdot 10^{-19}$ C. Then, using this data L_D has a value of $2.44 \cdot 10^{-10}$ m and $C_G = 0.821$ F/m^2.

The total capacitance per unit area (C'_{dl}) is the series of Helmholtz capacitance (C_H) and Gouy-Chapman capacitance (C_G). C_{dl} of a gold microelectrode of area A_e immersed in an ionic solution can be calculated by (2.11).

$$\frac{1}{C'_{dl}} = \frac{1}{C_H} + \frac{1}{C_G} \quad \rightarrow \quad C'_{dl} = 0.067 \ F/m^2 \tag{2.10}$$

$$C_{dl} = C'_{dl} \cdot A_e \ [F] \tag{2.11}$$

- Spreading resistance (R_s)

Spreading resistance is the opposition to current flow through saline solution in contact with electrode. This resistance is generally determined by (2.12), but (2.13) is the equation to calculate R_s for a circular electrode [17].

$$R_s = \frac{\rho \cdot L}{A} \quad [\Omega] \tag{2.12}$$

$$R_s = \frac{\rho}{4 \cdot r_e} = \frac{\rho \cdot \sqrt{\pi}}{4 \cdot \sqrt{A_e}} \quad [\Omega] \tag{2.13}$$

where ρ is the electrolyte resistivity, whose value for a saline solution of NaCl is $5 \cdot 10^5$ $\Omega \cdot \mu m$, L is the length, A is the cross-sectional area (cm^2) of the solution through which the current passes and r_e is the electrode radius ($r_e = 125$ μm). The theoretical value of R_s for a circular electrode of radius r_e is 1 $k\Omega$.

- Gap resistance (R_{gap})

The last parameter of the basis electrical CE model is R_{gap}, which is shown in Fig. 2.5. This resistor models the resistive gap region through which the current flows laterally, and it was modeled in [25] using finite elements simulations. R_{gap} depends on adhesion distance of the cell to the electrode, which varies between 15 nm and 150 nm [31]. In this reference, a value for R_{gap} of 75 $k\Omega$ is considered, but in [30], [55] values near to 1 $k\Omega$ was obtained. In the present work, R_{gap} is estimated from real experimental data

When CC growths, it covers the electrode as a cell layer. The cell layer, act as an impedance whose effects is added to the effect of the electrode. In that way, the real
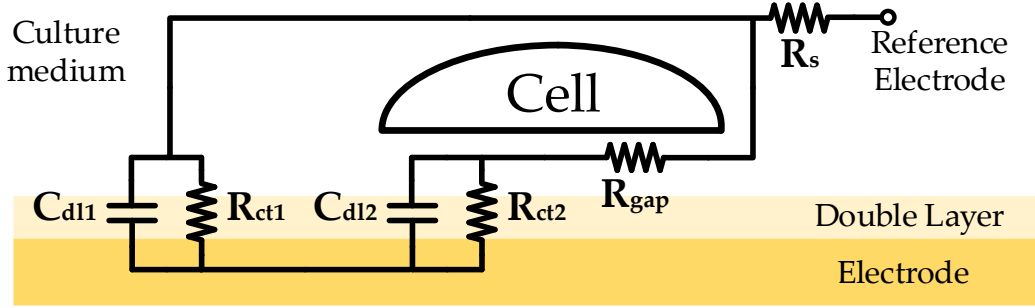
Fig. 2.4 Double-layer interphase diagram, where double layer effect is divided in two terms: electrode covered by cells and electrode non-covered by cells.

electrical behavior of the CE system has been reported in [30], [55]–[58]. Fig. 2.4 and Fig. 2.5 shows the model of CE covered by cells. First shows the layout of the electrical model components in a real CC, while in the second figure illustrates the schematic of the electrical model as seen from above the CC. The electrical model presents the division of R_{ct} and C_{dl} in two parallel branches, modeling the electrode area covered by cells (A_C) and not covered (A_e - A_c) by cells, equation (2.14). That division is shaped by two impedances.

$$Z_C = \frac{Z_e}{A_C} \qquad Z_{nC} = \frac{Z_e}{(A_e - A_C)} \tag{2.14}$$

where Z_C is the impedance of the circuit covered by cells and Z_{nC} is the impedance of the circuit non-covered by cells. Since cell growth is the main parameter to measure, the electrical model must include a parameter that informs as an indicator of cell growth. This parameter is the fill-factor (*ff*), which is the percentage of electrode area covered by cells in %₁, i.e., if $A_C = A_e$ the value of *ff* is 1, but if $A_C = 0$ the value of *ff* is 0. In that way R_1, C_1, R_2 and C_2 are defined by next equations:

$$R_{ct1} = \frac{R_{ct}}{1 - ff} \qquad C_{dl1} = C_{dl} \cdot (1 - ff) \tag{2.15}$$

$$R_{ct2} = \frac{R_{ct}}{ff} \qquad C_{dl2} = C_{dl} \cdot ff \tag{2.16}$$

where R_{ct1} and C_{dl1} are the contribution of R_{ct} and C_{dl} in the area not covered by the cells, and R_{ct2} and C_{dl2} are the contribution of R_{ct} and C_{dl} in the area covered by the cells.

The TF which models the CE impedance is obtained by solving the circuit of Fig. 2.5. Equation (2.17) shows the BI TF, which has two poles and two zeros. Poles and zeros are directly dependent on *ff* (among other things), which means that the number of cells covering the electrode influences the BI model. Equation (2.17) has been parameterized because the equation is too big.
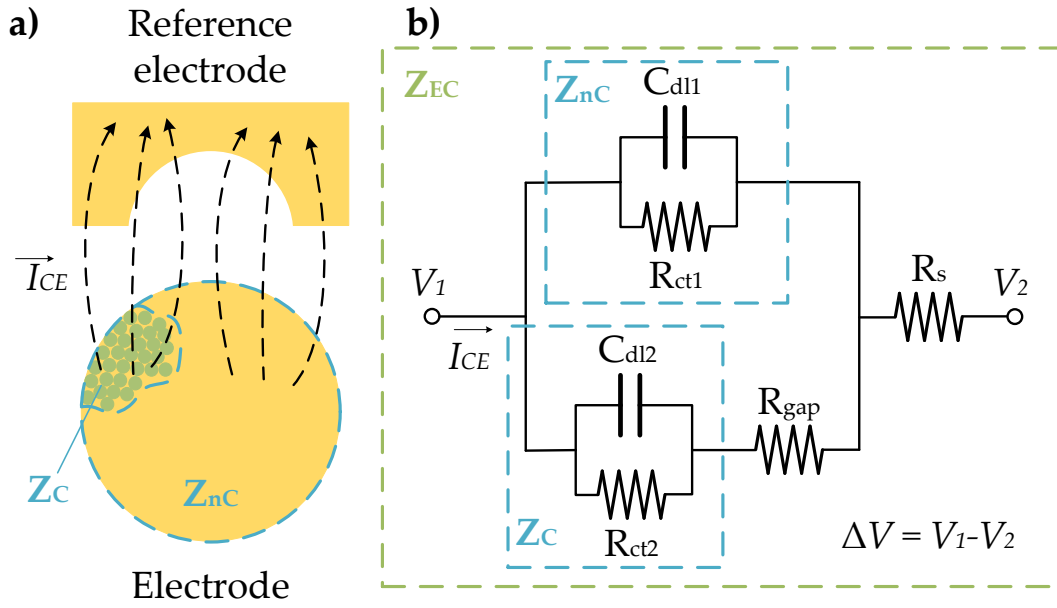
Fig. 2.5 Double-layer interphase model. **a)** CE diagram seen from the top, which shows the electrode area covered by cells (Z_C), the electrode area not covered by cells (Z_{nC}), the reference electrode and the current flow lines flowing through electrode and cells to reference electrode. This is a diagram for illustration purpose, electrodes have not the real size seen at Fig. 2.2. **b)** Equivalent electrical circuit that models the electrical behavior of the CE system.

$$Z_{CE}(s) = \frac{k_2 \cdot s^2 + k_1 \cdot \dfrac{\omega_{0z}}{Q} \cdot s + k_0 \cdot \omega_{0z}^2}{s^2 + \dfrac{\omega_{0z}}{Q} \cdot s + \omega_{0z}^2} \tag{2.17}$$

where k_2, k_1, k_0, ω_n and Q are the model parameters. These parameters are defined below as:

$$k_2 = R_s \tag{2.18}$$

$$k_1 = R_s + \frac{R_{gap} \cdot R_{ct1}}{2 \cdot R_{gap} + R_{ct1} + R_{ct2}} \tag{2.19}$$

$$k_0 = R_s + \frac{R_{ct1} \cdot (R_{gap} + R_{ct2})}{R_{gap} + R_{ct1} + R_{ct2}} \tag{2.20}$$

$$\omega_{0z} = \sqrt{\frac{R_{gap} + R_{ct1} + R_{ct2}}{R_{gap} \cdot (C_{dl} \cdot R_{ct})^2}} \tag{2.21}$$

$$Q = \omega_{0z} \cdot \frac{R_{gap} \cdot C_{dl} \cdot R_{ct}}{2 \cdot R_{gap} + R_{ct1} + R_{ct2}} \tag{2.22}$$

The described model (Fig. 2.5) is the main model proposed in this work, but in next sections will be discussed and improved, for the sake of completeness.

2.1.3   Measurement circuit theory

Traditionally, the BI measurement is performed by applying AC current signals of different frequencies [31]. Depending on the frequency and the cell type, each impedance measure is different. By applying a signal, a complex measured impedance is obtained. The impedance value, without a model to translate it to another property, can only be used during the experiment to see the trend of a certain property which is known to vary when impedance changes. In that way, when experiment is over, if the relationship between impedance and the property to be measured is unknown, the typical approximation between the two properties is to find the relationship between the property to be measured and the relative impedance, for example, based on the full range of the observed impedance along the experiment or its initial value. Equations (2.23) show these examples. Where i is the time index of the experiment and its range is $1 \leq i \leq k$ (where k is the i value where impedance is maximum), $r_Z(i)$ is the relative impedance in the i moment, $Z(i)$ is the impedance in i moment, $Z(1)$ is the first impedance measurement, and $Z(k)$ is the maximum and last impedance measurement. These equations show the typical relative impedances used to obtain information from a BS under test:

$$r_Z(i) = \frac{Z(i) - Z(1)}{Z(1)} \qquad r_Z(i) = \frac{Z(i) - Z(1)}{Z(k) - Z(1)} \tag{2.23}$$

Due to ECIS technique is used to perform an estimation of change in one or more properties of a BS, and this change is related to an impedance change, it is hard to find a relationship between an absolute property value of a CC assay (for example, the cell growth in a CC assay) and a relative property value of a CC assay, the impedance relative variation. By known the impedance in a certain frequency, the model parameters cannot be obtained (the only available parameter is the impedance at this frequency). If the model parameters are not estimated, a lot of information could be ignored or lost.

To obtain the value of each model parameter, the measured data must be more than the impedance at a certain frequency. The Oscillation-based test is a good option for this purpose. This measurement technique applied to ECIS is based on an indirect measurement of the BI collecting data of the oscillation parameters, i. e., amplitude (a_{osc}) and frequency (f_{osc}). If the BI is connected to an oscillator, as a load, a_{osc} and f_{osc} depends on the BI features. If BI changes during an experiment the oscillation parameters will change as well.

2.1.3.1   Oscillation-based test

A non-linear system could produce oscillations of constant amplitude and frequency under some conditions, which are called self-excited oscillations or limit cycles. Van der Pol oscillator proposed one of the first equations to analyze these systems.

A self–starting and self-sustained oscillator is a circuit which has two main parts (Fig. 2.6), linear part and non-linear part, and it has to meet some requirements:

1. There is only **one non-linear element**.

2. **Non-linear** element is **time invariant**.

3. **Non-linear** element is **symmetrical**.

4. **Linear** part must have a **low-pass filter** behavior.

If these conditions are met by the circuit, there would exist oscillations at a constant amplitude (a_{osc}) and frequency (f_{osc}). Oscillation parameters (a_{osc} and f_{osc}) depend on linear and non-linear parts of the entire system. These parameters could be estimated by the Barkhausen stability criterion (BSC) [1] (it will be explained later), but to apply it, the non-linear element must be linearized. The Descriptive Function (DF) method is employed to obtain the linearized response of a periodic non-linear component from the truncated Fourier Transform. The model of the system added to these two tools is the way to know the behavior of a non-linear oscillator.
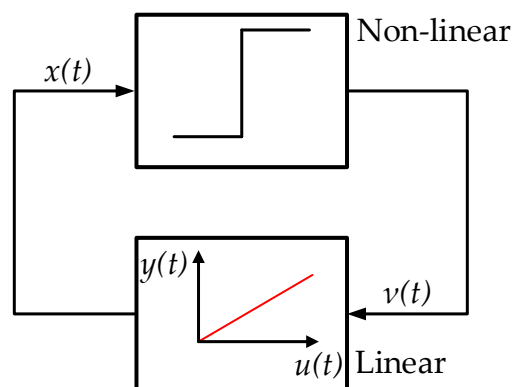
Fig. 2.6   Basic block diagram of a self-sustained oscillator.

2.1.3.1.1   Describing function method

The DF is a method based on the frequency response of the system which ignores the higher harmonics. DF method replaces the non-linear system by the first component of the Fourier series. As mentioned above, if the linear part of the system behaves as a low-

pass filter or a band pass-filter, the decision to truncate the Fourier series is a reasonable approach. First, it is considered that the input of non-linear element is a sine of amplitude a_{osc} and angular frequency of ω. By making the variable change $\theta = \omega \cdot t$, where t is the time variable, the input of non-linear element is $y(a_{osc}, \theta) = a_{osc} \cdot \sin \theta$. Fig. 2.7 shows the non-linear feedback system block diagram, where m is defined by:

$$m(t) = f(y(a_{osc}, \theta)) \tag{2.24}$$
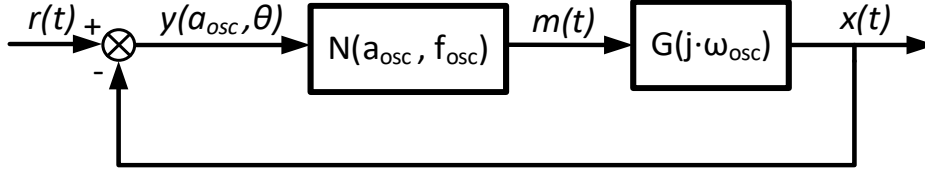
Fig. 2.7 Non-linear linear feedback system where there are two different parts, the linear ($G(j \cdot \omega_{osc})$) and the non-linear part ($N(a_{osc}, f_{osc})$).

The non-linear element DF, N, can be presented by using the Fourier coefficients, in complex notation, as:

$$N(a_{osc}) = f_1(a_{osc}) + j \cdot f_2(a_{osc}) \tag{2.25}$$

The next steps and considerations to estimate the DF are based on section 2.2 of [59]. Since the non-linear component is symmetric, the offset Fourier component is equal to 0. $f_1(a_{osc})$ and $f_2(a_{osc})$ coefficients are the normalized Fourier coefficients.

$$f_1(a_{osc}) = \frac{a_1}{a_{osc}} \qquad f_2(a_{osc}) = \frac{b_1}{a_{osc}} \tag{2.26}$$

where a_1 and b_1 are the Fourier coefficients. Then the normalized coefficients could be estimated by

$$f_1(a_{osc}) = \frac{1}{\pi a_{osc}} \int_0^{2\pi} f[a_{osc} \sin(\theta)] \sin(\theta) d\theta \tag{2.27}$$

$$f_2(a_{osc}) = \frac{1}{\pi a_{osc}} \int_0^{2\pi} f[a_{osc} \sin(\theta)] \cos(\theta) d\theta \tag{2.28}$$

The DF estimation can be applied to the non-linear component of the OBT circuit of this work, an inverter comparator with hysteresis. Fig. 2.8 presents the comparator hysteresis in *a)*, the comparator output in *b)* and the comparator input in *c)*. These figures show that there are four different zones in terms of θ. The comparator output takes the value M or $-M$ depending on θ, where M is the comparator output according to the input. These regions are defined in the expression (2.30). The angle θ_1 has a value of:

$$\theta_1 = \sin^{-1}\left(\frac{y(\theta_1)}{a_{osc}}\right) \tag{2.29}$$
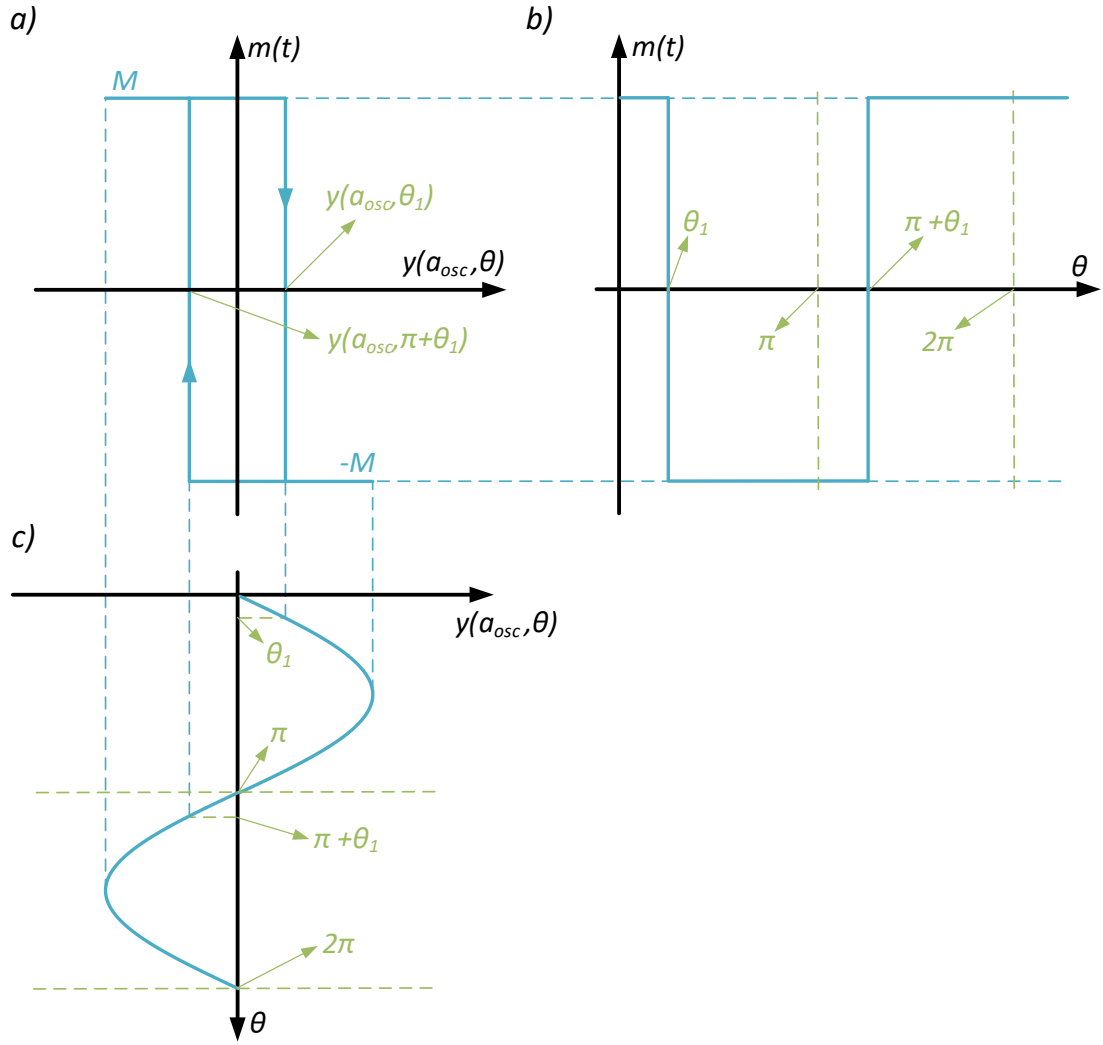
Fig. 2.8 Comparator hysteresis (a), comparator output (b) and comparator input (c).

$$m(t) \begin{cases} M & 0 \leq \theta < \theta_1 & (1) \\ -M & \theta_1 \leq \theta < \pi & (2) \\ -M & \pi \leq \theta < \pi + \theta_1 & (3) \\ M & \pi + \theta_1 \leq \theta < 2\pi & (4) \end{cases} \tag{2.30}$$

There are two clearly differentiated regions, when $m(t)$ is M and when $m(t)$ is $-M$. Since the value of $m(t)$ is used to estimate the coefficients $f_1(a_{osc})$ and $f_2(a_{osc})$ integrals can be easily solved:

$$f_1(a_{osc}) = \frac{M}{\pi a_{osc}} \left(\int_0^{\theta_1} \sin(\theta) d\theta - \int_{\theta_1}^{\pi + \theta_1} \sin(\theta) d\theta + \int_{\pi + \theta_1}^{2\pi} \sin(\theta) d\theta \right)$$

$$f_1(a_{osc}) = \frac{-4M}{\pi a_{osc}} \cos(\theta_1) \tag{2.31}$$

42

$$f_2(a_{osc}) = \frac{M}{\pi a_{osc}} \left(\int_0^{\theta_1} \cos(\theta)d\theta - \int_{\theta_1}^{\pi+\theta_1} \cos(\theta)d\theta + \int_{\pi+\theta_1}^{2\pi} \cos(\theta)d\theta \right)$$

$$f_2(a_{osc}) = \frac{4M}{\pi a_{osc}} \sin(\theta_1)$$

(2.32)

Then, by substituting in (2.25), DF of the inverter comparator with hysteresis is:

$$N(a_{osc}) = \frac{4M}{\pi a_{osc}} \left(-\cos(\theta_1) + j\sin(\theta_1) \right)$$

(2.33)

where θ_1 can be estimated by (2.29).

2.1.3.1.2   Barkhausen stability criterion

The BSC is the mathematical condition that the closed-loop feedback system must fulfill to obtain sustained oscillations. Fig. 2.7 shows the linear block $G(j \cdot \omega_{osc})$), which is a TF where $s = j \cdot \omega_{osc}$. The angular frequency oscillation is directly related to f_{osc} by the expression $\omega_{osc} = 2\pi f_{osc}$. Depending of the non-linearity type, N could depend on only a_{osc} or only f_{osc}, or both parameters. As previously mentioned, the oscillation parameters a_{osc} and f_{osc} can be estimated by the BSC. The condition the circuit must meet is:

$$f(a_{osc}, f_{osc}) \equiv 1 + G(s = j\omega_{osc}) \cdot N(a_{osc}, f_{osc}) = 0$$

(2.34)

where $f(a_{osc}, f_{osc})$ is the oscillation condition function (OCF). This function can be rewritten as:

$$f(a_{osc}, f_{osc}) = h_1(a_{osc}, f_{osc}) + j \cdot h_2(a_{osc}, f_{osc})$$

(2.35)

where h_1 and h_2 are de real and imaginary parts respectively of the OCF.

The main goal of using BSC is obtaining the oscillation parameters. Then, since OCF must be equal to 0, in phasorial form, the condition is:

$$f(a_{osc}, f_{osc}) \equiv h \angle \varphi = 0 \angle 0°$$

$$h = \sqrt{h_1^2 + h_2^2} = 0$$

$$\varphi = \tan^{-1}\left(\frac{h_2}{h_1} \right) = 0°$$

(2.36)

where h and φ are, respectively, the module and angle of $f(a_{osc}, f_{osc})$ and must be equal to 0 and 0° to meet this condition.

2.1.4 OBT measurement circuit

In this work, cell growth measurement has been performed by connecting the CE system, as a load, to an OBT system. The self-sustained oscillator reaches an oscillation amplitude and an oscillation frequency which depend on the whole system. This means that, in addition to the linear and non-linear parts of the OBT, a_{osc} and f_{osc} depend on the impedance of the CE system. The block diagram of the prototype used to perform the measures on this work is shown in Fig. 2.9. OBT system consists of a band-pass filter (H_{BP}), a comparator, a current source and the BI connected as a load. In the next subsections, all the elements of the OBT system will be explained in detail.
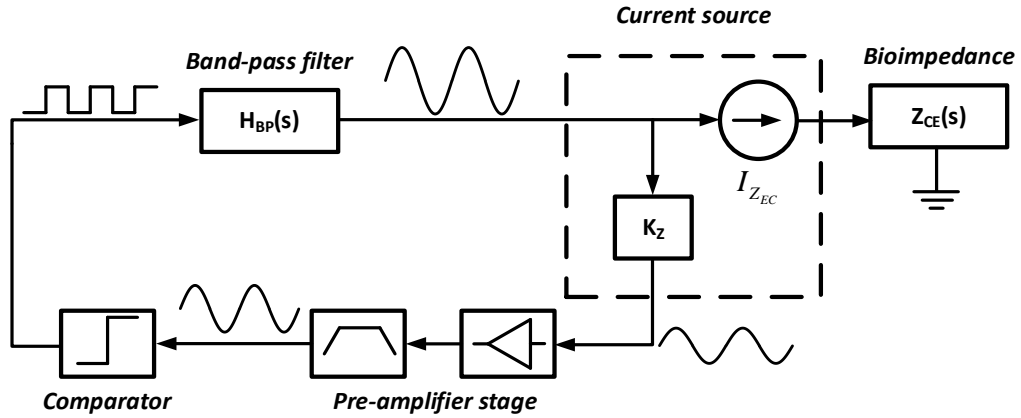
Fig. 2.9 Block diagram of the OBT prototype. The oscillator consists of the linear part: a band-pass filter (H_{BP}) and a current source; and a non-linear part: the comparator. CE system (Z_{CE}) is connected as a load to the current source.

2.1.4.1 Band-pass filter

The main purpose of the band-pass filter (BPF) is to reject the high-frequency harmonics of the comparator output signal (square signal). Therefore, the output of the comparator is connected to the input of the filter. A BPF is used instead of a low-pass filter to choose the oscillator operating point. Using the resonant frequency of the filter, it is ensured that the oscillation frequency will be in the desired frequency range. Fig. 2.10 shows the used topology to implement the BPF, which has been used due to the simplicity of choosing the different filter parameters: gain (K_{BP}), resonant frequency (ω_{0BP} in rad/s or f_{0BP} in Hz) and quality factor (Q_{BP}).

The BPF is implemented using four operational amplifiers. It is designed to have a K_{BP} of -1 V/V, a f_{0BP} of 1 kHz and a Q_{BP} of 10. Q_{BP} is set to 10 to set the oscillation frequency range. f_{0BP} is set to 1 kHz due to the frequency characteristics of the CE system. The values of these parameters have been chosen considering the frequency response of the CE system.

After the analysis of the circuit, the transfer function of the BPF is obtained:
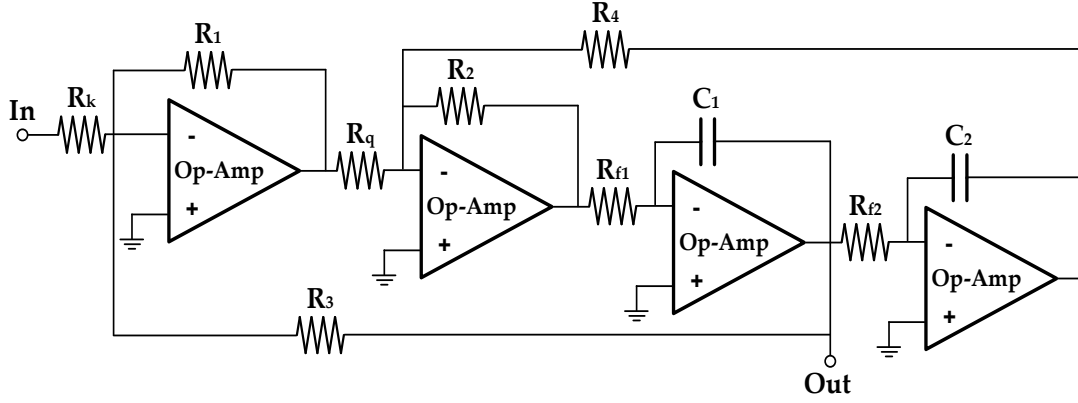
Fig. 2.10 Band-pass filter implemented by using operational amplifiers OPA4227UA. Each filter parameter can be independently fixed.

$$H_{BP}(s) = \frac{K_{BP}\dfrac{\omega_{0BP}}{Q_{BP}}s}{s^2 + \dfrac{\omega_{0BP}}{Q_{BP}}s + \omega_{0BP}^2} \tag{2.37}$$

where K_{BP} is the filter gain, ω_{0BP} is the resonant central frequency in *rad/s* and Q_{BP} is the filter quality factor. These parameters can be estimated from the circuit analysis:

$$K_{BP} = \frac{-R_3}{R_k} \qquad \omega_{0BP}^2 = \frac{R_2}{R_4 C_1 C_2 R_{f1} R_{f2}} \qquad Q_{BP} = \frac{\omega_{0BP}}{\left(\dfrac{R_1 R_2}{R_3 C_1 R_{f1} R_q}\right)} \tag{2.38}$$

Firstly, the filter gain is defined with the resistor R_k. After that, the resistors R_{f1} and R_{f2} must be chosen to select the resonance frequency (ω_{0BP}). Finally, with the resistor R_q the filter quality factor Q_{BP} is fixed, which adjusts the filter bandwidth (BW_{BP}) to 100 *Hz*, that is defined as:

$$BW_{BP} = \frac{f_{0BP}}{Q_{BP}} \tag{2.39}$$

The BPF is an active filter, implemented with OPA4227UA operational amplifiers. To compare the accuracy of the model, the band pass filter bode diagram (BD) has been obtained in Matlab® [60] using the TF and in Spice using Ngspice [61] (more details of the Spice simulation in section 3.2). Both BDs are shown in Fig. 2.11. The only difference appears at high frequencies, where high frequency effects in electrical simulation (Spice) can be observed.
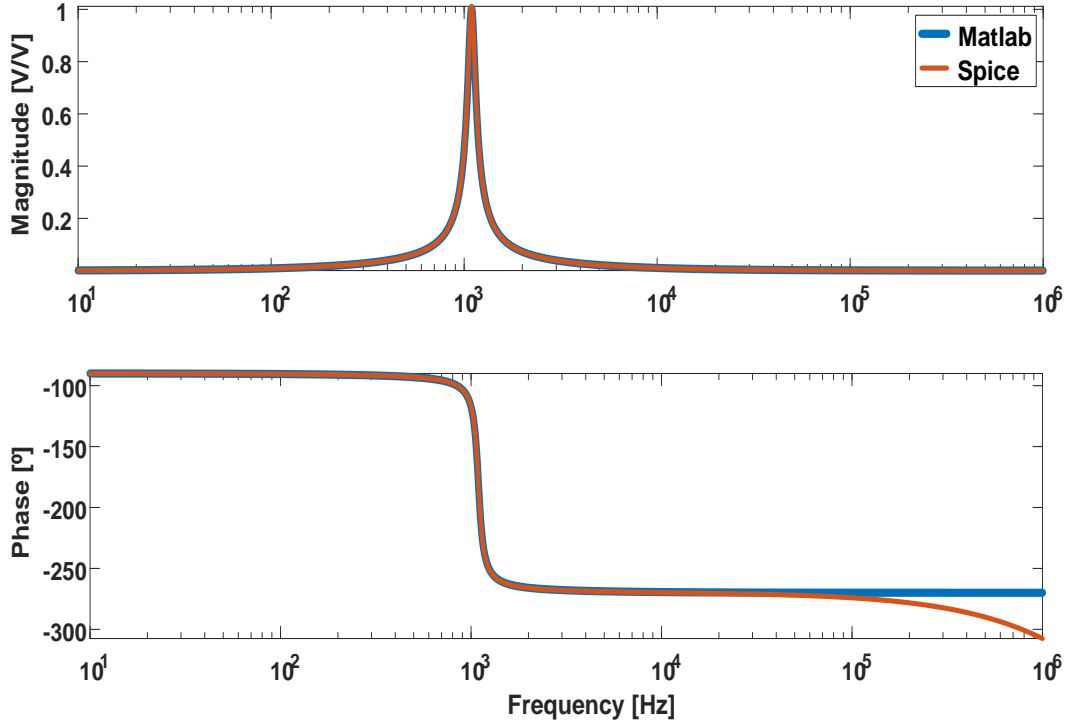
Fig. 2.11 Bode diagram of band-pass filter. Comparison between the bode diagram obtained from TF (Matlab®) and electrical simulation (Spice).

2.1.4.2   Comparator

The comparator block is composed of the comparator and the pre-amplifier stage. The pre-amplifier stage ensures that the signal that reaches the comparator input is filtered (avoiding high and low frequencies) and has an adequate amplitude.

2.1.4.2.1   Pre-amplifier stage

As was said, the first part of pre-amplifier stage is composed by two op-amps. A non-inverting amplifier, and an inverting amplifier (Fig. 2.12). Gain and inverse stages are independent of each other so that they can be configured separately. Through simple mathematical calculations the TF can be obtained:

$$H_K = \frac{V_o}{V_i} = \frac{-R_{22}}{R_{21}} \frac{(R_{11} + R_{12})}{R_{11}} \tag{2.40}$$

The second and the most important part of the pre-amplifier stage is the filter part. It is composed by a high-pass filter (HPF) and a low-pass filter (LPF). In Fig. 2.13 is shown the whole circuit composed by HPF and LPF. By operating on the electrical equations of the filters, their TFs (H_{HPF} and H_{LPF}) can be obtained:
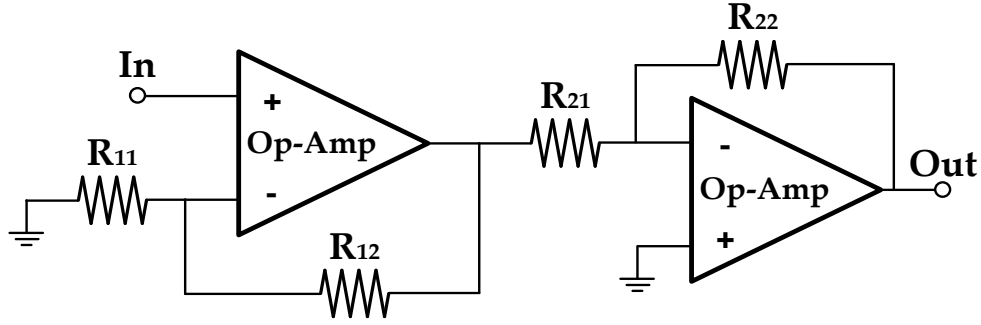
Fig. 2.12 First part of the pre-amplifier stage. The first op-amp is a non-inverting circuit to amplifier the signal, and the second op-amp is an inverting circuit to invert the signal. Gain and inverse stages are independent of each other so that they can be configured separately.

$$H_{HPF}(s) = \frac{K_{HPF}s^2}{s^2 + \frac{\omega_{HPF}}{Q_{HPF}}s + \omega_{HPF}^2} \qquad H_{LPF}(s) = \frac{K_{LPF}}{s^2 + \frac{\omega_{LPF}}{Q_{LPF}}s + \omega_{LPF}^2} \qquad (2.41)$$

The cut frequencies (ω_{HPF} and ω_{LPF}) of each filter, its gains (K_{HPF} and K_{LPF}) and its quality factors (Q_{HPF} and Q_{LPF}):

$$\omega_{LPF} = \sqrt{\frac{1}{R_{l2}R_{l3}C_{l1}C_{l2}}} \qquad\qquad \omega_{LPF} = \sqrt{\frac{1}{R_{l2}R_{l3}C_{l1}C_{l2}}}$$

$$K_{HPF} = \frac{-C_{h1}}{C_{h3}} \qquad\qquad K_{LPF} = \frac{-1}{C_{l1}C_{l2}R_{l1}R_{l2}} \qquad (2.42)$$

$$Q_{HPF} = \frac{C_{h2}C_{h3}R_{h2}\omega_{HPF}}{(C_{h1} + C_{h2} + C_{h3})} \qquad Q_{LPF} = \frac{C_{l1}R_{l1}R_{l2}R_{l3}\omega_{HPF}}{(R_{l1}R_{l2} + R_{l1}R_{l3} + R_{l2}R_{l3})}$$

The filters cut frequencies ($f_{HPF} = 2\pi\omega_{HPF}$ and $f_{LPF} = 2\pi\omega_{LPF}$), in Hz, are defined by using the filters parameters:

$$f_{HPF} = 50\ Hz \quad f_{LPF} = 15.2\ kHz \qquad (2.43)$$
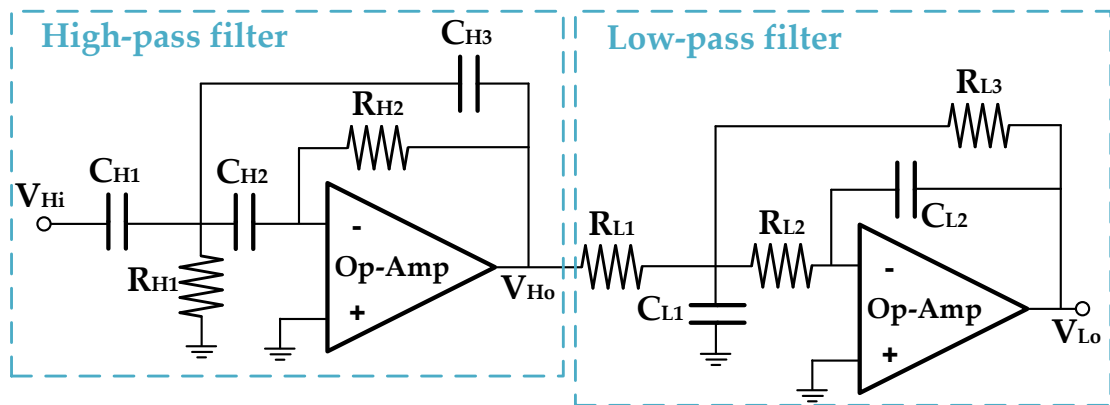
Fig. 2.13 High-pass filter and low-pass filter previous to comparator.

As BPF filters of pre-amplifier stage circuits are implemented using OPA4227UA op-amps. TF of the two filters in series is obtained to analyze the entire system in Matlab® [60] to compare the accuracy of the model with the Spice filters [61]. In Fig. 2.14 are presented the BDs of the filter union. The mathematical model is very accurate since it has a low error compared to Spice electrical simulation.
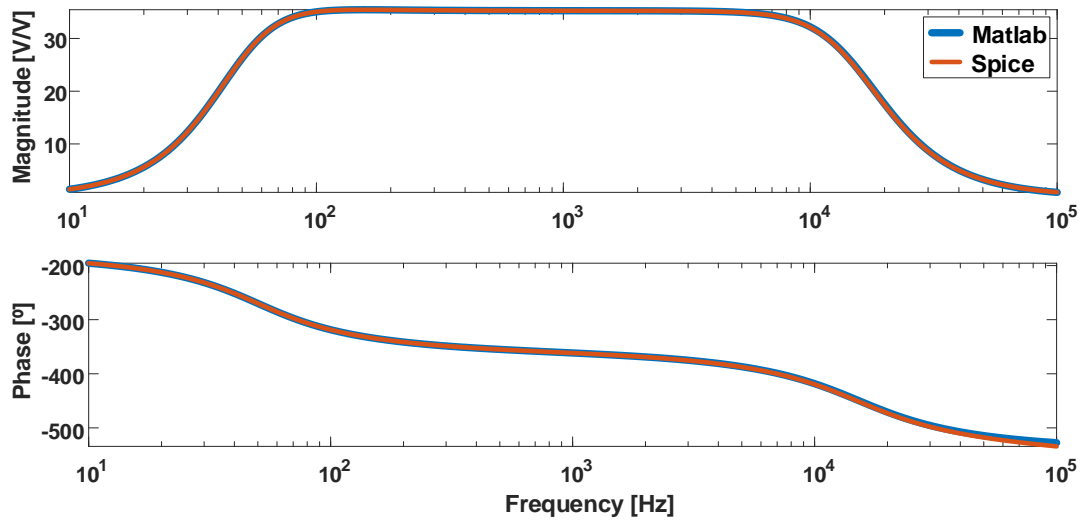
Fig. 2.14 High-pass filter and low-pass filter BD. Blue line represents Matlab® simulation, and the red line represents the electrical simulation in Ngspice.

2.1.4.2.2   Comparator stage

The comparator stage includes the comparator, the hysteresis passive elements and the diodes to limit the output amplitude. Fig. 2.15 shows the comparator stage. Comparator is implemented in the circuit using an integrated circuit LMC7211 [62]. The comparator has a response time of 4 μs (at 5 V of supply voltage). R_o is the output resistor. Resistors R_H and R_F, and capacitor C_F compose the hysteresis circuit, which set the thresholds to ± 20 mV. The last part of the comparator stage is the diode net, where D_1 and D_2 limit the negative output voltage and D_3 and D_4 limit the positive output voltage.
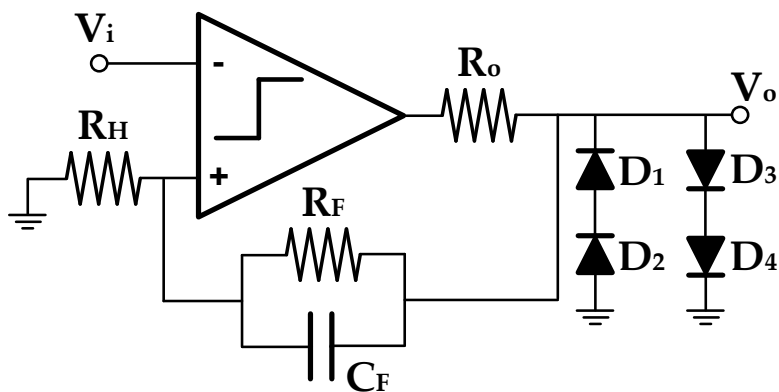
Fig. 2.15 Comparator stage, which includes hysteresis and voltage limit diodes.

The Spice transient simulation of the circuit in Fig. 2.15 can be compared with the expected signals (Fig. 2.8). For this purpose, in Fig. 2.16, the output versus input of the comparator is shown. The comparator has a response time of 6 μs (near of expected in datasheet from LMC7211), and its thresholds voltages are near to ±20 mV (observed in simulations). There is a small difference between the positive and negative threshold, so the response of the comparator is somewhat asymmetrical. Considering the work frequencies of the oscillator (10 Hz to 100 kHz), this is not a significant limit.
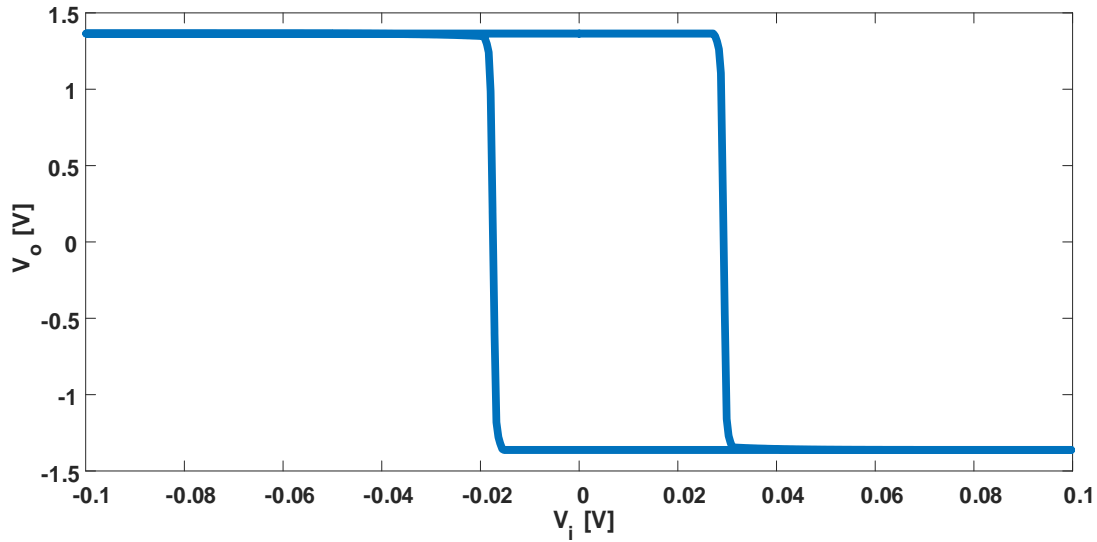
Fig. 2.16 Comparator output presented against input (comparator negative pin).

2.1.4.3 Current source

Current source is responsible for ensuring that the current supplied to the CE system is adequate. If the current is too large it could burn the cells and electrodes and, on the other hand, if it is too low, the measurements could be wrong as well. For that reason, a current source independent of the load has been used. The current will be not dependent on the impedance changes due to cell growth. Fig. 2.17 shows the current source input.

Taking into account the relationships $R_3=R_1/2$ and $R_4=R_2/2$, by analyzing the circuit, the current expression in CE is obtained:

$$I_{CE} = \frac{-R_2}{R_1 R_5} V_i \tag{2.44}$$

where I_{CE} is the current that flows through BI. From this expression, the voltage gain of the circuit (gain between V_i and V_o) can be obtained:

$$V_o = \frac{-R_2 Z_{CE}(s)}{R_1 R_5} V_i \quad \rightarrow \quad H_{CS}(s) = \frac{-R_2 Z_{CE}(s)}{R_1 R_5}$$

Resistor values are chosen to obtain a gain current of $I_{CE} = -5 \cdot 10^{-6} V_i$, which means that the current in CE system is in the order of $I_{CE} = 7$ μA (safe value for cells).
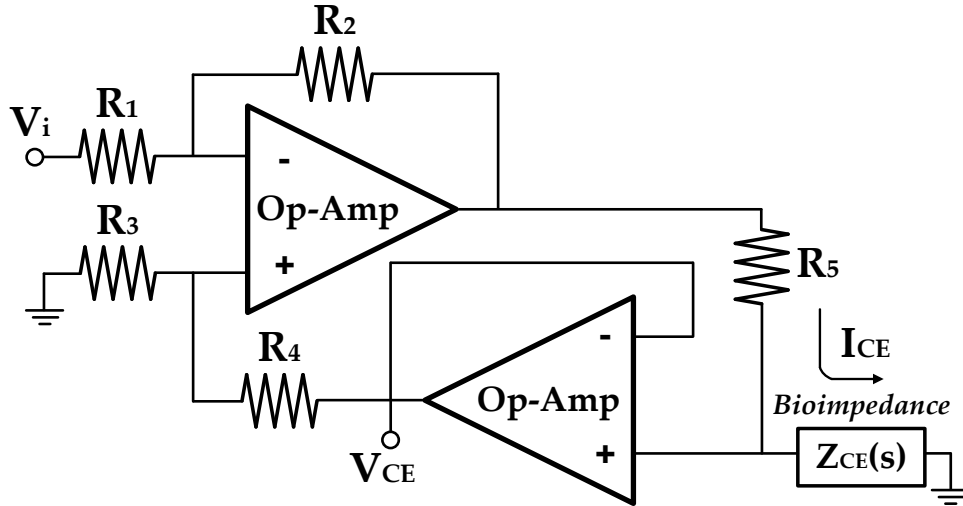
Fig. 2.17 Current source with CE connected as load. Current in CE system is independent of BI.

2.1.5 Empirical cell-electrode model

In this section the CE model is obtained the from empirical data. $Z_{CE}(s)$ (2.17) parameters are estimated using experimental data obtained from the test performed with some cell lines for the sake of illustration [55], [63]. In next subsections, cell lines specifications and the method to obtain the empirical models are shown.

2.1.5.1 Cell lines specifications

For this work, three cell lines have been used. The origin of cells, the culture medium, the growth environment conditions and the number of cells seeded is explained below.

The first biological Sample Under Test (SUT) is formed by Chinese hamster ovarian fibroblasts: This cell line is identified as AA8 (American Type Culture Collection). This sample is immersed in McCoy's medium supplemented with 10 % (*v/v*) foetal calf serum; 2 *mM* L-glutamine, 50 *µg/ml* streptomycin and 50 *U/ml* penicillin.

The second and third biological samples under test are two Mouse neuroblastoma cell lines. The N2a cell line and its cell line stably expressing wildtype human amyloid precursor protein, N2a-APP. Cells were cultured in medium consisting of 50% DMEM High glucose (Biowest) and 50% Opti-MEM (Gibco) supplemented with 10% (*v/v*) foetal bovine serum (FBS) (Gibco), 2 *mM* L-glutamine, 50 *µg/ml* streptomycin and 50 *U/ml* penicillin (Sigma-Aldrich). N2a-APP was also supplemented with 0.4% Geneticin (Gibco).

All cell lines were maintained at 37° C in a humidified atmosphere with 5% CO_2 and they were routinely subcultured. Different initial number of cells (N_{ini}) was seeded for our experiments: 2500, 5000 and 10000 cells. The AA8 experiments start with a N_{ini} of

2500 cells in wells 1 and 3, 5000 cells in wells 4 and 5, and 10000 cells in wells 7 and 8. On the other hand, the N2a and N2aAPP experiments start with a N_{ini} of 2500 cells in wells 2 and 6, 5000 cells in wells 3 and 7, and 10000 cells in wells 4 and 8. Numbers of the wells were defined in Fig. 2.2.

2.1.5.2 Single-electrode well model

Single-electrode well (SEW) model is referred to estimate the empirical model by considering that the cells are on top of a single large electrode, and the effect of the reference electrode (grounded) is negligible.

The first step to understand the changes in the model when the CC assay growth is to know to position of the poles and zeros fo the system in the important points of the experiments. These ones are when the experiment is started ($ff \rightarrow 0$) and when the well is full ($ff \rightarrow 1$). Poles (2.45), zeros (2.46) and gain (2.47) of the biological system can be obtained from (2.17), and are:

$$p_1 = \frac{R_{gap}\,ff\,(1-ff)+R_{ct}}{C_{dl}R_{ct}R_{gap}\,ff\,(1-ff)} \qquad p_2 = \frac{-1}{C_{dl}R_{ct}} \tag{2.45}$$

$$z_{1,2} = \frac{R_{ct}R_s \pm n_1 + R_{ct}R_{gap}\,ff + 2R_{gap}R_s\,ff - 2R_{gap}R_s\,ff^2}{2C_{dl}R_{ct}R_{gap}R_s\,ff\,(1-ff)} \tag{2.46}$$

$$n_1 = R_{ct}\sqrt{R_{gap}^2\,ff^2 + 4R_{gap}R_s\,ff^2 - 2R_{gap}R_s\,ff + 2R_s^2}$$

$$k_{CE} = R_s + \frac{1}{\dfrac{1}{R_{gap} + R_{ct}/ff} - \dfrac{1-ff}{R_{ct}}} \tag{2.47}$$

As can be observed the expressions are very large, but if ff is set to 0 or 1, poles, zeros and gain are greatly reduced:

$$p_{ff \rightarrow 0} = \frac{-1}{C_{dl}R_{ct}} \qquad z_{ff \rightarrow 0} = \frac{-(R_{ct}+R_s)}{C_{dl}R_{ct}R_s} \qquad k_{CE}^{ff \rightarrow 0} = R_{ct}+R_s \tag{2.48}$$

$$p_{ff \rightarrow 1} = \frac{-1}{C_{dl}R_{ct}} \qquad z_{ff \rightarrow 1} = \frac{-(R_{ct}+R_s+R_{gap})}{C_{dl}R_{ct}(R_s+R_{gap})} \qquad k_{CE}^{ff \rightarrow 1} = R_{ct}+R_s+R_{gap} \tag{2.49}$$

Poles and zeros for $ff \rightarrow 0$ and $ff \rightarrow 1$ provide key information since the model changes from a two-pole two-zero model to a one-pole one-zero model when the well is empty and full. The limit models, for $ff \rightarrow 0$ and $ff \rightarrow 1$, are defined by (2.48) and (2.49) respectively. The limit models are obtained applying the limit when ff tends to 0 and when tends to 1:

$$Z_{CE}^{ff \to 0}(s) = k_{CE}^{ff \to 0} \frac{p_{ff \to 0}}{z_{ff \to 0}} \frac{s + z_{ff \to 0}}{s + p_{ff \to 0}} \tag{2.50}$$

$$Z_{CE}^{ff \to 1}(s) = k_{CE}^{ff \to 1} \frac{p_{ff \to 1}}{z_{ff \to 1}} \frac{s + z_{ff \to 1}}{s + p_{ff \to 1}} \tag{2.51}$$

In the next sections, two different fitting methods using the experimental BD and the oscillation parameters will be detailed.

2.1.5.2.1   Bode fitting method

The first proposed fitting method is to use an experimental bode analysis. For that method, AA8 cells in the amounts indicated in section 2.1.5.1. Cells were seeded in 8W10E PET Applied BioPhysics electrodes. Two wells per initial cell concentration were seeded, i.e., 2x5000 cells (wells 1 and 3) and 2x10000 cells (wells 7 and 8). CC was growing for 6 days. Each day at the same time a frequency analysis was performed using
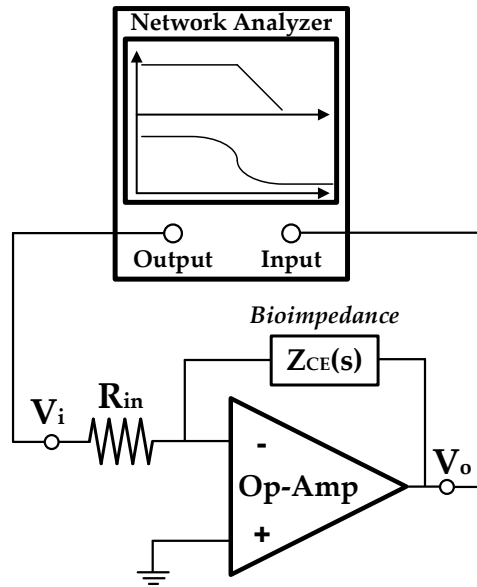
Fig. 2.18 Measurement circuit used to obtain the real BD of the CE system in the network analyzer.

a network analyzer (NA), the HP 3589A Spectrum Network Analyzer , to estimate the BD of each well. The measurement circuit is shown in Fig. 2.18. V_i is connected to the NA output and V_o is connected to the NA input.

Fig. 2.19 displays the BD of the wells 7 and 8 (10000 cells at the beginning of the experiment) the first day of the experiment and the day when *ff* is near to 1 (day 5). From the BDs the cut frequency of the pole and the zero can be obtained:

$$
\begin{array}{lll}
\text{Well 7:} & p_{ff \to 0} = 24.06 \text{ Hz} & z_{ff \to 0} = 18.844 \ kHz \\
\text{Well 8:} & p_{ff \to 1} = 22.73 \text{ Hz} & z_{ff \to 1} = 49.124 \ kHz
\end{array} \tag{2.52}
$$
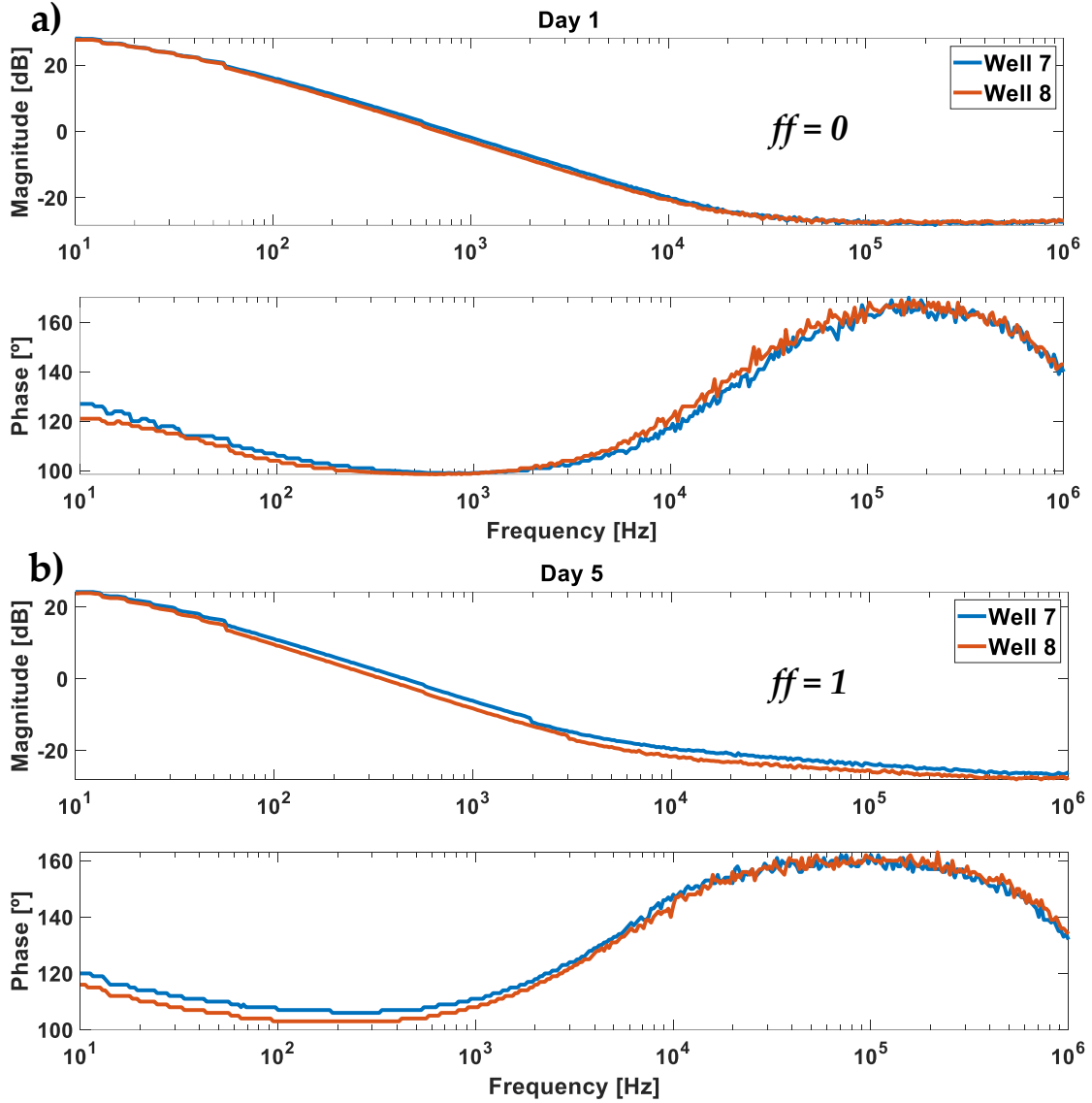
Fig. 2.19 BDs of wells 7 and 8. **a)** Data of the first day of the experiment ($ff \rightarrow 0$). **b)** Data of the fifth day of experiment ($ff \rightarrow 1$)

Due to poles when $ff \rightarrow 0$ and $ff \rightarrow 1$ have similar expressions ((2.48) and (2.49)) and its values are very close to each other, the value of $p_{ff \rightarrow 0}$ is taken to the estimation. At this point there are 3 equations ($p_{ff \rightarrow 0}$, $z_{ff \rightarrow 0}$ and $z_{ff \rightarrow 1}$) and 4 variables (R_{ct}, C_{dl}, R_s and R_{gap}). But the limit of the TFs (2.50) and (2.51) when the frequency ($s = j \cdot \omega$) tends to 0 and ∞ can be used to estimate some parameters and provide the following equations:

$$Z_{CE}^{ff \rightarrow 0}(s \rightarrow 0) = \lim_{s \rightarrow 0} \frac{s + z_{ff \rightarrow 0}}{s + p_{ff \rightarrow 0}} = R_{ct} + R_s$$

$$Z_{CE}^{ff \rightarrow 0}(s \rightarrow \infty) = \lim_{s \rightarrow 0} \frac{s + z_{ff \rightarrow 0}}{s + p_{ff \rightarrow 0}} = R_s \tag{2.53}$$

$$Z_{CE}^{ff \to 1}(s \to 0) = \lim_{s \to 0} \frac{s + z_{ff \to 1}}{s + p_{ff \to 1}} = R_{ct} + R_s + R_{gap}$$

$$Z_{CE}^{ff \to 1}(s \to \infty) = \lim_{s \to 0} \frac{s + z_{ff \to 1}}{s + p_{ff \to 1}} = R_s + R_{gap} \qquad (2.54)$$

Note that $Z_{CE}^{ff \to 0}(s \to 0)$ is the gain $k_{CE}^{ff \to 0}$ and $Z_{CE}^{ff \to 1}(s \to 0)$ is the gain $k_{CE}^{ff \to 1}$. If the measurement circuit is taken into account (Fig. 2.18), and the magnitude values at the limit frequencies of the BDs are obtained, the resulting expressions are:

$$Z_{CE}^{ff \to 0}(s \to 0) = \frac{R_{ct} + R_s}{R_{in}} = 10^{(27.8dB/20)}$$

$$Z_{CE}^{ff \to 0}(s \to \infty) = \frac{R_s}{R_{in}} = 10^{(-27.05dB/20)} \qquad (2.55)$$

$$Z_{CE}^{ff \to 1}(s \to 0) = \frac{R_{ct} + R_s + R_{gap}}{R_{in}} = 10^{(24dB/20)}$$

$$Z_{CE}^{ff \to 1}(s \to \infty) = \frac{R_s + R_{gap}}{R_{in}} = 10^{(-26.8dB/20)} \qquad (2.56)$$

Using equations (2.48) and $Z_{CE}^{ff \to 0}(s \to \infty)$ in (2.55), model parameters can be obtained for $ff \to 0$:

$$R_{ct}^{ff \to 0} = 382.14 \ k\Omega \qquad C_{dl}^{ff \to 0} = 17.31 \ nF \qquad R_s^{ff \to 0} = 488.53 \ \Omega \qquad (2.57)$$

Note that it is not required to estimate $R_{gap}^{ff \to 0}$ because it does not affect $Z_{CE}^{ff \to 0}(s)$. This is an important point, R_{gap} has no influence when $ff \to 0$, and in following sections it will be seen that it has a low effect for low ff values. Fig. 2.20 shows the comparison between the BD of empirical model with $ff \to 0$ and the BD of the real CE system. The biggest errors appear for low and high frequencies, in the extremes.
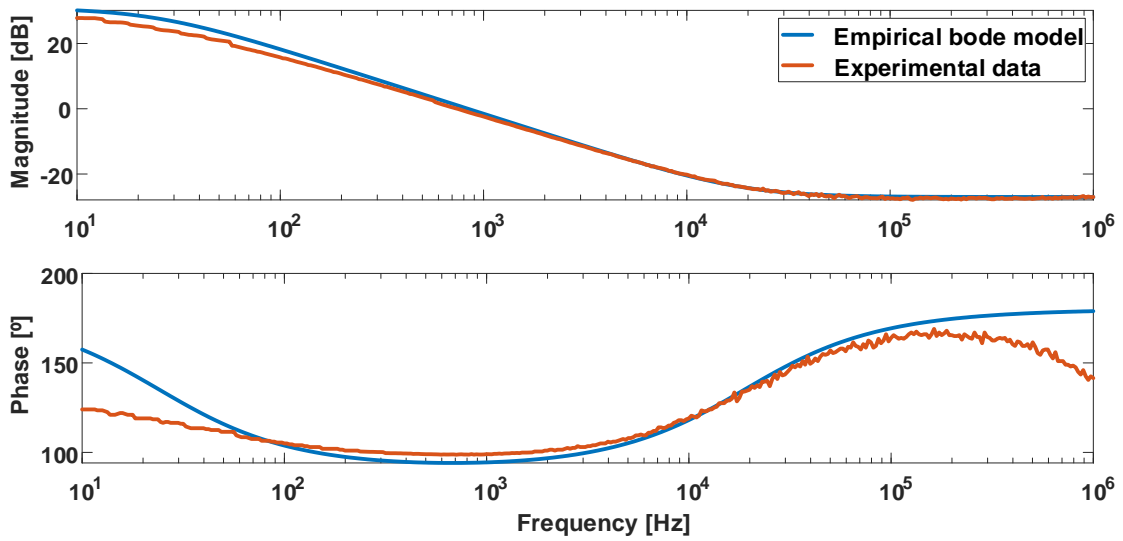
Fig. 2.20 BD of empirical model (blue) when $ff \to 0$. It is compared to the BD of the real CE system (red).

On the other hand, using equations (2.49) and $Z_{CE}^{ff \to 1}(s \to \infty)$ in (2.56), models parameters can be obtained for $ff \to 1$:

$$R_{ct}^{ff \to 1} = 393.29 \ k\Omega \qquad C_{dl}^{ff \to 1} = 16.81 \ nF$$
$$R_{s}^{ff \to 1} = 488.53 \ \Omega \qquad R_{gap}^{ff \to 1} = 14.26 \ \Omega \tag{2.58}$$

$R_s^{ff \to 0}$ has also been used for $ff \to 1$ because there is no way to obtain values of $R_s^{ff \to 1}$, $R_{ct}^{ff \to 1}$ and $R_{gap}^{ff \to 1}$ greater than 0. Then, $Z_{CE}^{ff \to 1}(s \to \infty)$ from (2.56) has been used to estimate $R_{gap}^{ff \to 1}$. The value of $R_{gap}^{ff \to 1}$ seems wrong, since [25], [55] reported higher R_{gap} values. Fig. 2.21 shows the BD of the model when $ff \to 1$. As expected, model cannot establish the gain and phase value because in that point of the experiment, the CE system is highly non-linear. Another type of model or fitting method can improve the accuracy of this model.
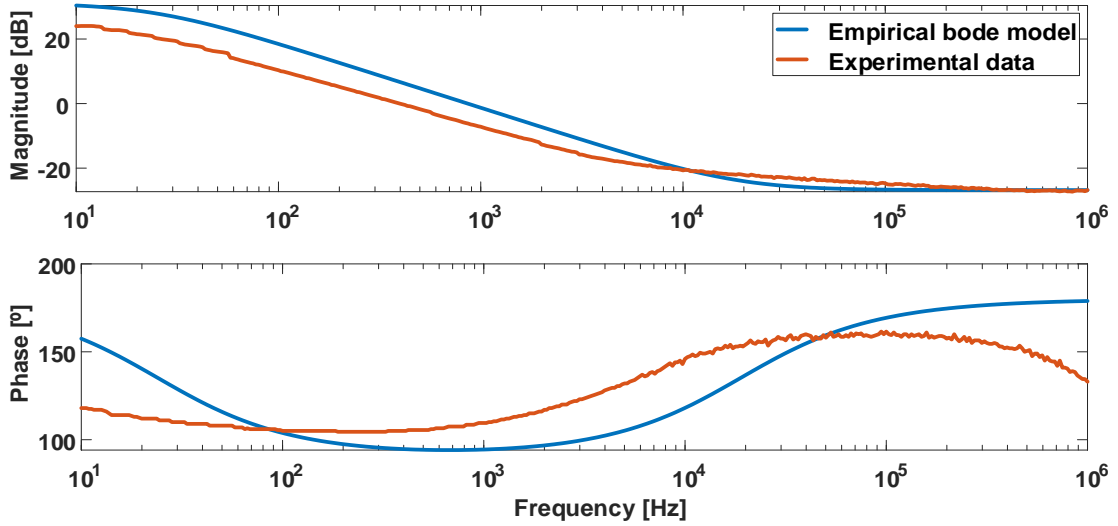
Fig. 2.21 BD of empirical model (blue) when $ff \to 1$. It is compared to the BD of the real CE system (red).

2.1.5.2.2   Empirical fitting method using oscillation parameters

OBT circuit oscillates at a frequency and an amplitude which depend on the load $Z_{CE}(s)$ (Fig. 2.9). The amplitude used to calculate the DF (a_{osc}) in the circuit is the amplitude of the signal V_{Lo} in Fig. 2.13, but the amplitude that will be measured to characterize the CE system is the amplitude of the signal V_{CE} from Fig. 2.17, from now called a_{CE}. Both amplitudes, a_{CE} and a_{osc}, are related each other by the gains of the preamplifier stage of the comparator (2.1.4.2.1).

Therefore, in this section, oscillation amplitude and frequency (oscillation parameters) are employed to estimate the $Z_{CE}(s)$ parameters. Oscillation parameters are obtained from real experiments where CE system is connected to OBT circuit as a load (Fig. 2.9). These experiments are performed by seeded an initial number of cells (N_{ini}) in wells of Fig. 2.2 (different N_{ini} on each well). CC assay grows for a week, from seeding to

confluence, in which the circuit takes a measurement of the oscillation parameters every hour. Oscillation frequency (f_{CE}) and amplitude (a_{CE}) are used in an algorithm to estimate the $Z_{CE}(s)$ parameters.

BSC can be applied to OBT circuit to obtain the oscillation parameters. In this case, there is the inverse problem, oscillation parameters are known and can be used to calculate $Z_{CE}(s)$ model parameters. Equations (2.48) and (2.49) describe the position of the poles and zeros when $ff \rightarrow 0$ and $ff \rightarrow 1$. Since $R_{ct} \gg R_s$ and $R_{ct} \gg R_{gap}$, the zeros equations can be approximated as:

$$z_{ff \rightarrow 0} = \frac{-1}{C_{dl} R_s} \qquad z_{ff \rightarrow 1} = \frac{-1}{C_{dl}(R_s + R_{gap})} \qquad (2.59)$$

BSC applied to the OBT system gets the following equation (where Laplace variable is $s = j\omega_{osc}$):

$$h(a_{osc}, f_{osc}) \equiv 1 + H_{BP}(s) \cdot H_K \cdot H_{HPF}(s) \cdot H_{LPF}(s) \cdot H_{CS}(s) \cdot N(a_{osc}, f_{osc}) \qquad (2.60)$$

The expression in equation (2.60) must be equal to zero in both module and phase. Then, two equations can be derived from BSC:

$$\begin{aligned} h_1(a_{osc}, f_{osc}) &= real(h(a_{osc}, f_{osc})) = 0 \\ h_2(a_{osc}, f_{osc}) &= imag(h(a_{osc}, f_{osc})) = 0 \end{aligned} \qquad (2.61)$$

where *real* and *imag* are the real and imaginary part of $h(a_{osc}, f_{osc})$. The algorithm used to estimate oscillation parameters is simple, and it is divided in two steps:

1. **Initial estimation.** Frequency and amplitude values and equations (2.61) are used to find the initial parameters. The main goal of this step is to obtain $R_{ct}^{ff \rightarrow 0}$, $C_{dl}^{ff \rightarrow 0}$, $R_s^{ff \rightarrow 0}$, $p_{ff \rightarrow 0}$ and $z_{ff \rightarrow 0}$ parameters. R_{gap} has no influence in system behavior at this point ($ff \rightarrow 0$), so it is defined by 600 Ω. $p_{ff \rightarrow 0}$ is calculated because his value is required for the second step. To minimize the number of parameters to be estimated, equation (2.48) and the approach of $z_{ff \rightarrow 0}$ in (2.59) is used to define $R_{ct}^{ff \rightarrow 0}$ and $C_{dl}^{ff \rightarrow 0}$ dependent on $R_s^{ff \rightarrow 0}$, $p_{ff \rightarrow 0}$ and $z_{ff \rightarrow 0}$. Then, $R_{ct}^{ff \rightarrow 0}$ and $C_{dl}^{ff \rightarrow 0}$ are defined by (2.62) and (2.63), and used in $Z_{CE}(s)$ in (2.60).

$$R_{ct}^{ff \rightarrow 0} = \frac{1}{2\pi p_{ff \rightarrow 0} C_{dl}^{ff \rightarrow 0}} \qquad (2.62)$$

$$C_{dl}^{ff \rightarrow 0} = \frac{1}{2\pi z_{ff \rightarrow 0} R_s^{ff \rightarrow 0}} \qquad (2.63)$$

2. **Final estimation.** When wells are fully covered by cells, the oscillation parameters can be used to estimate the CE model parameters when $ff \rightarrow 1$. In the same way that step 1, $R_{ct}^{ff \rightarrow 1}$ and $C_{dl}^{ff \rightarrow 1}$ are defined by (2.64) and (2.65), and depend on $R_s^{ff \rightarrow 1}$, R_{gap}, $p_{ff \rightarrow 1}$ and $z_{ff \rightarrow 1}$. From section 2.1.5.2.1, it is known

that $p_{ff\to 0} \approx p_{ff\to 1}$, that is an approximation which is assumed to be able to estimate the other parameters when $ff \to 1$.

$$R_{ct}^{ff\to 1} = \frac{1}{2\pi p_{ff\to 0} C_{dl}^{ff\to 1}} \tag{2.64}$$

$$C_{dl}^{ff\to 1} = \frac{1}{2\pi z_{ff\to 1}(R_s^{ff\to 1} + R_{gap})} \tag{2.65}$$

Now, the estimation can be performed. The problem is to obtain the value of three parameters from two equations (2.61). As there are more parameters than equations, the choice is to minimize a cost function (CF) to obtain the value of the parameters. The CF must fullfil the condition in such way that real and imaginary parts of (2.60) must be zero. The best way found to meet the condition is to use the module of the complex number $h(a_{osc}, f_{osc})$. Due to $h(a_{osc}, f_{osc}) = h_1(a_{osc}, f_{osc}) + j \cdot h_2(a_{osc}, f_{osc})$, CF can be defined as:

$$h(a_{osc}, f_{osc}) \equiv \sqrt{h_1(a_{osc}, f_{osc})^2 + h_2(a_{osc}, f_{osc})^2} \tag{2.66}$$

The fact of $h_1(a_{osc}, f_{osc})$ and $h_2(a_{osc}, f_{osc})$ are squared assures that terms $h_1(a_{osc}, f_{osc})$ and $h_2(a_{osc}, f_{osc})$ cannot compensate each other.

Data to fit the model are obtained from a one-week experiment of AA8 cell line with initial number of cells of 2500 cells for wells 1 and 3, 5000 cells for wells 4 and 5, and 10000 cells for wells 7 and 8. Oscillation parameters (f_{CE} and a_{CE}) when $ff \to 0$ and when $ff \to 1$ are summarized in Table 2.1. Notice that $f_{CE}^{ff\to 0}$ is the frequency of the signal V_{CE} when $ff \to 0$, $f_{CE}^{ff\to 1}$ is the frequency of the signal V_{CE} when $ff \to 1$, $a_{CE}^{ff\to 0}$ is the amplitude of the signal V_{CE} when $ff \to 0$ and $a_{CE}^{ff\to 1}$ is the amplitude of the signal V_{CE} when $ff \to 1$. Amplitude a_{CE} is different from a_{osc} (amplitude of the comparator input voltage) used in DF. The relationship between a_{osc} and a_{CE} is $a_{osc} = a_{CE}H_K K_{HPF}K_{LPF}$ defined in section 2.1.4.2.1.

Table 2.1 Oscillation frequency (f_{CE}) and amplitude (a_{CE}) at the beginning of the experiment $ff \to 0$ and at the end $ff \to 1$ for AA8 cell line.

Well	$f_{CE}^{ff\to 0}$ [Hz]	$f_{CE}^{ff\to 1}$ [Hz]	$a_{CE}^{ff\to 0}$ [mV]	$a_{CE}^{ff\to 1}$ [mV]
1	783.43	867	9.7	13.94
3	802.14	925.43	7.46	15.19
4	821.73	932.12	6.19	13.39
5	780.75	872.2	10.35	14.97
7	822.15	938.3	7.02	16.19
8	843.86	934.37	6.57	14.19

As was explained, there are two steps per well to characterize it. In the first step, using the oscillation parameters for $ff \to 0$ ($f_{osc}^{ff\to 0}$ and $a_{osc}^{ff\to 0}$) and replacing them on the

CF (2.66), $R_s^{ff \to 0}$, $p_{ff \to 0}$ and $z_{ff \to 0}$ can be estimated by minimizing the CF. Then, $R_{ct}^{ff \to 0}$ and $C_{dl}^{ff \to 0}$ can be calculated using (2.62) and (2.63). In the same way, for $ff \to 1$, $f_{osc}^{ff \to 1}$ and $a_{osc}^{ff \to 1}$ can be replaced on CF to minimize it. $R_s^{ff \to 1}$, R_{gap}, $p_{ff \to 0}$ and $z_{ff \to 1}$ are obtained and are used in equations (2.64) and (2.65) to estimate $R_{ct}^{ff \to 1}$ and $C_{dl}^{ff \to 1}$.

The way to assure that the minimization is enough accurate is to use the function value (f_{val}) for each found solution. It is difficult to obtain a f_{val} value of zero, but the lowest value can be ensured. Table 2.2 summarizes f_{val} for each well in these two steps of the fitting process. Their values are, in general, low enough.

The results of minimizing the CF of (2.66) are shown in next tables. Table 2.3 displays the CE model parameters when $ff \to 0$ and Table 2.4 presents the CE model parameters when $ff \to 1$.

Table 2.2 Function value (f_{val}) for each well in the two steps of model parameters estimation, for $ff \to 0$ and $ff \to 1$.

Well	1	3	4	5	7	8
$f_{val}^{ff \to 0}$ [x 10^{-3}]	0.12	0.18	0.035	0.2	0.04	0.28
$f_{val}^{ff \to 1}$ [x 10^{-3}]	0.25	0.14	0.28	0.033	0.24	0.12

Table 2.3 Model parameters at the beginning of the experiment $ff \to 0$ for AA8 cell line (SEW model).

Well	$R_{ct}^{ff \to 0}$ [$M\Omega$]	$C_{dl}^{ff \to 0}$ [nF]	$R_s^{ff \to 0}$ [$k\Omega$]	$p_{ff \to 0}$ [Hz]	$z_{ff \to 0}$ [kHz]
1	0.40	24.9	0.94	16.02	6.82
3	0.15	34.14	0.67	31.05	7
4	0.43	43.77	0.72	8.51	5.04
5	0.18	23.1	0.73	38.56	9.41
7	0.69	38.6	0.82	6	5.01
8	0.07	44.29	0.58	48.57	6.23

Table 2.4 Model parameters at the end of the experiment $ff \to 1$ for AA8 cell line (SEW model).

Well	$R_{ct}^{ff \to 1}$ [$M\Omega$]	$C_{dl}^{ff \to 1}$ [nF]	$R_s^{ff \to 1}$ [$k\Omega$]	R_{gap} [Ω]	$z_{ff \to 0}$ [kHz]
1	0.44	22.77	0.38	1178.03	4.45
3	0.19	27.41	1.24	451.22	3.46
4	0.58	32.37	0.73	902.34	3.01
5	0.19	21.6	0.46	1002.6	5.02
7	0.96	27.75	1.11	877.28	2.89
8	1.06	30.84	1.15	350.97	3.48

It has been considered that $p_{ff \to 0} \approx p_{ff \to 1}$ but that $z_{ff \to 0}$ is not equal (or similar) to $z_{ff \to 1}$. On the other hand, the obtained results propose that $R_{ct}^{ff \to 0} \neq R_{ct}^{ff \to 1}$, $C_{dl}^{ff \to 0} \neq C_{dl}^{ff \to 1}$ and $R_s^{ff \to 0} \neq R_s^{ff \to 1}$. So, now it is known that R_{ct}, C_{dl} and R_s change with *ff*. In [25] authors report that R_s changes with the area covered by cells (that means with the *ff*), but this approximation is not consistent with the variations found in this work. An alternative work [55] found a way to fit the variations of R_s that match can be implemented with the data herein. It also suggests that if R_s remains constant from $ff \to 0$ to $ff \to 1$ it is not possible to do a good model fitting because a_{osc} cannot be properly calculated. Following the work [55], the spreading can be divided in two terms:

$$R_s(k) = R_{si} + \Delta R_s \cdot ff^{\,n}(k) \tag{2.67}$$

where k is the time index of the experiment, R_{si} is the initial value of R_s, ΔR_s is the change range of R_s (from $ff \to 0$ to $ff \to 1$), $ff(k)$ is the *fill-factor* at time k, and n is the growth rate of R_s from R_{si} to $R_{si} + \Delta R_s$. Note that ΔR_s can be positive or negative, it is only limited by not make R_s lower or equal to zero, i.e., $\Delta R_s > -R_{si}$. Then, initial and final R_s values are translated into this new form, and showed for each well in Table 2.6.

Table 2.6 Parameters to define the evolution of R_s

Well	R_{si} [$k\Omega$]	ΔR_s [$k\Omega$]
1	0.94	-0.56
3	0.67	0.58
4	0.72	0.01
5	0.73	-0.27
7	0.82	0.29
8	0.58	0.57

ff must be estimated for each well in each moment, to test the obtained results. There are also two more model parameters (R_{ct} and C_{dl}) which its initial and final values are known, but its evolution is unknown. Then, there are three model parameters to be estimated for each moment k: R_{ct}, C_{dl} and *ff*. All of them are going to be estimated by minimizing the CF (2.66). Table 2.5 summarizes the limits of each parameter.

Table 2.5 Limits of R_{ct}, C_{dl} and *ff* for minimization of the CF

	R_{ct}	C_{dl}	*ff*
Lower limit	$R_{ct}^{ff \to 0}$	$C_{dl}^{ff \to 1}$	0
Upper limit	$R_{ct}^{ff \to 1}$	$C_{dl}^{ff \to 0}$	1

The limits of R_{ct} and C_{dl} for the minimization are defined for each well for its initial and final value (Table 2.3 and Table 2.4). *ff* has the known limits: 0 and 1.

As expected, in Fig. 2.22 can be observed that wells 1 and 3 are the latest to reach the maximum *fill-factor*, wells 4 and 5 are the second and wells 7 and 8 are the first ones to reach the maximum. This is due to the initial number of cells on each well. The more the initial number of cells, the lower the time to reach the maximum *fill-factor*.
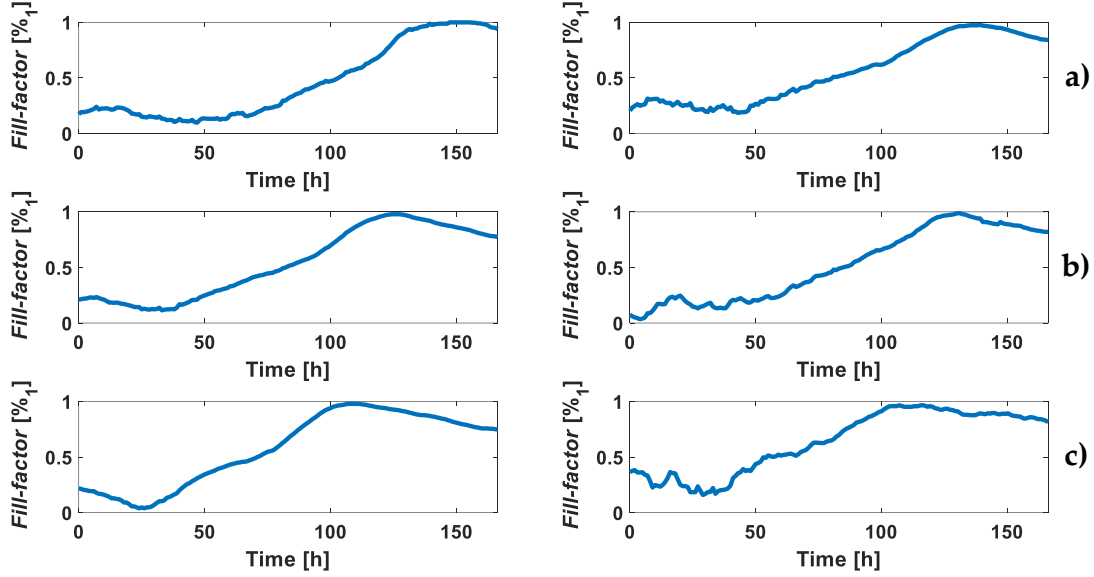
Fig. 2.22 *Fill-factor* evolution for each well of the experiment using SEW model. **a)** Initial number of cells: 2500 cells (well 1 on the left and well 3 on the right). **b)** Initial number of cells: 5000 cells (well 4 on the left and well 5 on the right). **c)** Initial number of cells: 10000 cells (well 7 on the left and well 8 on the right).

To know how good is the fitting method, the results must be compared with the results obtained by traditional counting method. For the sake of illustration, biologists of the department of Cell Biology Department in the Seville University performed an experiment in the same environmental conditions and using cells obtained from the same batch, using the same cell line at an equal cell concentration of the experiments of our data. Then, they performed a traditional optically counting of the number of cells with the Leica DMI1 Inverted Microscopy every 24h until the confluence phase was reached.

The metric used to compare data was the cell concentration. *ff* must be translated to number of cells (N_{cell}). From the traditional experiment, the number of cells in confluence phase ($ff = 1$) is known. Relationship between *ff* and N_{cell} is defined by:

$$ff = N_{cell} \frac{A_{cell}}{A_{well}}$$ (2.68)

where A_{cell} is the mean area of the cells of AA8 cell line, and A_{well} is the well area. Then the AA8 cell mean area is:

$$A_{cell} = \frac{ff \cdot A_{well}^{trad}}{N_{cell}} = \frac{1 \cdot 23.75}{4.3 \cdot 10^6} = 552.5 \ \mu m^2$$ (2.69)

Note that the A_{well}^{trad} used in (2.69) is the area of the well employed in the traditional experiment. The area of the wells from [46], used to perform the OBT experiments, is named as A_{well}. Cell area allows us to kwon the number of cells from each fill factor value using (2.68) in the form:

$$N_{cell} = ff \frac{A_{well}}{A_{cell}} \tag{2.70}$$

where $A_{well} = 0.8 \; cm^2$.

The cell concentration is obtained by divided the number of cells by the well area (traditional data divided by A_{well}^{trad} and OBT data divided by A_{well}). Fig. 2.23 shows the comparison between cell concentration obtained from CF minimization method and traditional method. Note that CF minimization method curves are obtained by making the mean of the *fill-factor* for each initial number of cells. Except at the beginning of the experiment, where there are few cells in the wells and the CF minimization method is not accurate, the results are very similar. The error bars of the traditional optical counting method are shown in Fig. 2.23, and it is observed that the data obtained from the CF minimization method satisfies the error margins.

Using the electrical model of the SEW CE system, results are close to those obtained with traditional optical counting (microscopy). However, this model is not close enough to reality. On the other hand, notice that the values of model parameters obtained (R_{ct}, C_{dl}, R_s and R_{gap}) are not very accurate. The reason is that the used model describes the well as a big electrode, but the real model must contain ten microelectrodes and one big reference electrode. For this reason, the values of C_{dl} and R_{ct} differ significantly from the theoretical values estimated in 2.1.2. The real model of the CE system is explored in the next section.
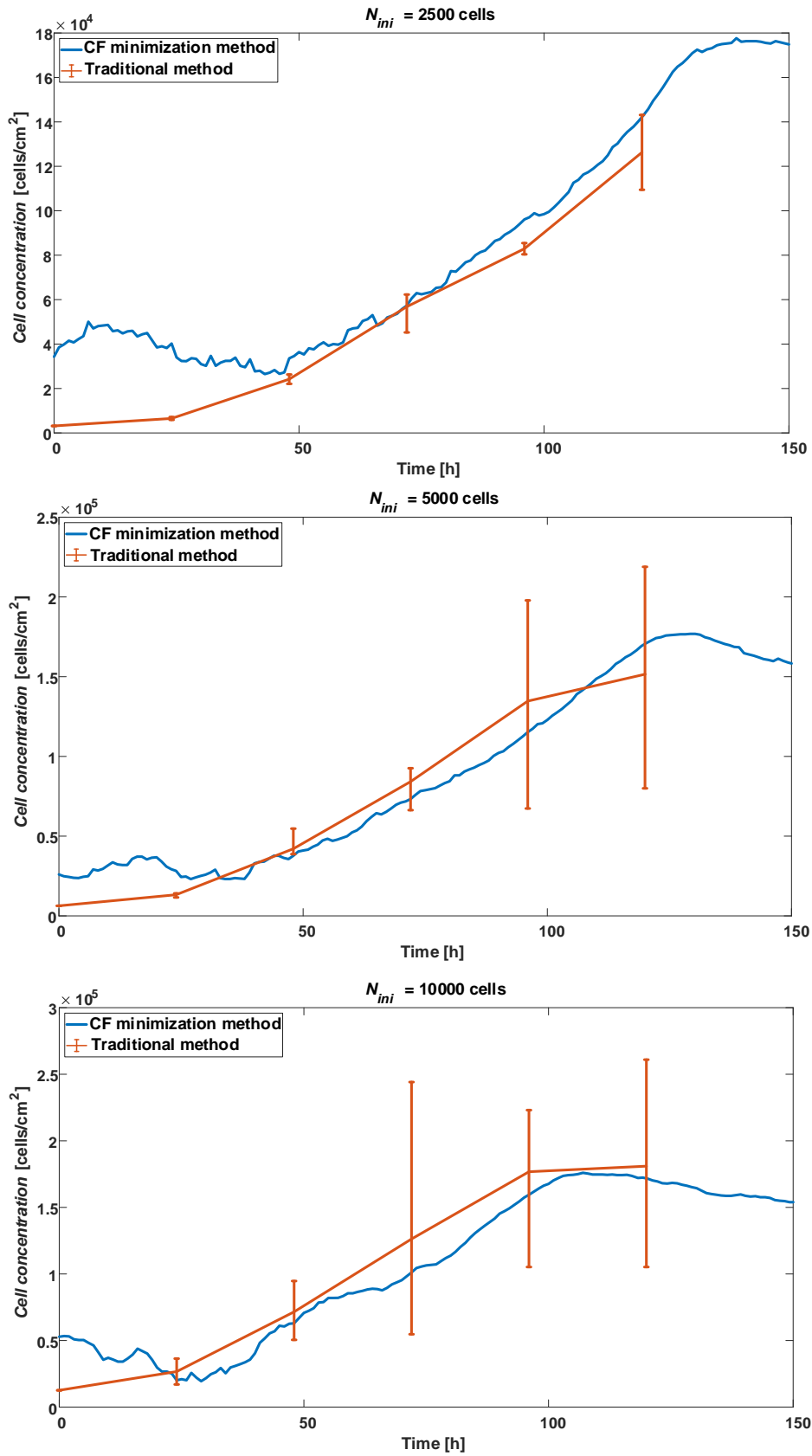
Fig. 2.23 Cell concentration comparison between data from CF minimization method and traditional counting method.

2.1.5.3 Real-electrode well model (11 electrodes)

In the previous section, it was performed a parameter fitting using as a model a SEW system. The problem is that the real wells don't have just one electrode. Employed wells have ten microelectrodes and one big reference electrode. On this section, the model to be fitted is not exactly the circuit on Fig. 2.5.b).

Let us consider that circuit in Fig. 2.5.b) is the circuit inside blocks $Z_{CE}(s)$ in Fig. 2.24. That figure shows how the electrodes are connected to each other. Microelectrodes (e_1 to e_{10}) are connected to the signal V_{CE} and to the reference electrode. The reference electrode (e_r) is connected to the others electrodes and to ground. Microelectrodes and reference electrode are connected to each other by the spreading resistance output terminal. That is the model that is considered in this section.

The model of Fig. 2.24 is complex but must be simplified and analyzed to reduce its complexity. There is a relationship between the parameters of the microelectrode model and the reference electrode model. The relationship between R_{ct} and R_{ctr} can be derived from (2.6):

$$\frac{R_{ctr}}{R_{ct}} = \frac{R_{ct}^{'}}{A_{re}}\frac{A_e}{R_{ct}^{'}} \rightarrow R_{ctr} = R_{ct}\frac{A_e}{A_{re}} \quad [\Omega] \tag{2.71}$$

where R_{ctr} is the change transfer resistance of the reference electrode model and A_{re} is the reference electrode area. In the same way, relationship between C_{dl} and C_{dlr}, and between R_s and R_{sr} can be derived from (2.11) and (2.13) respectively:
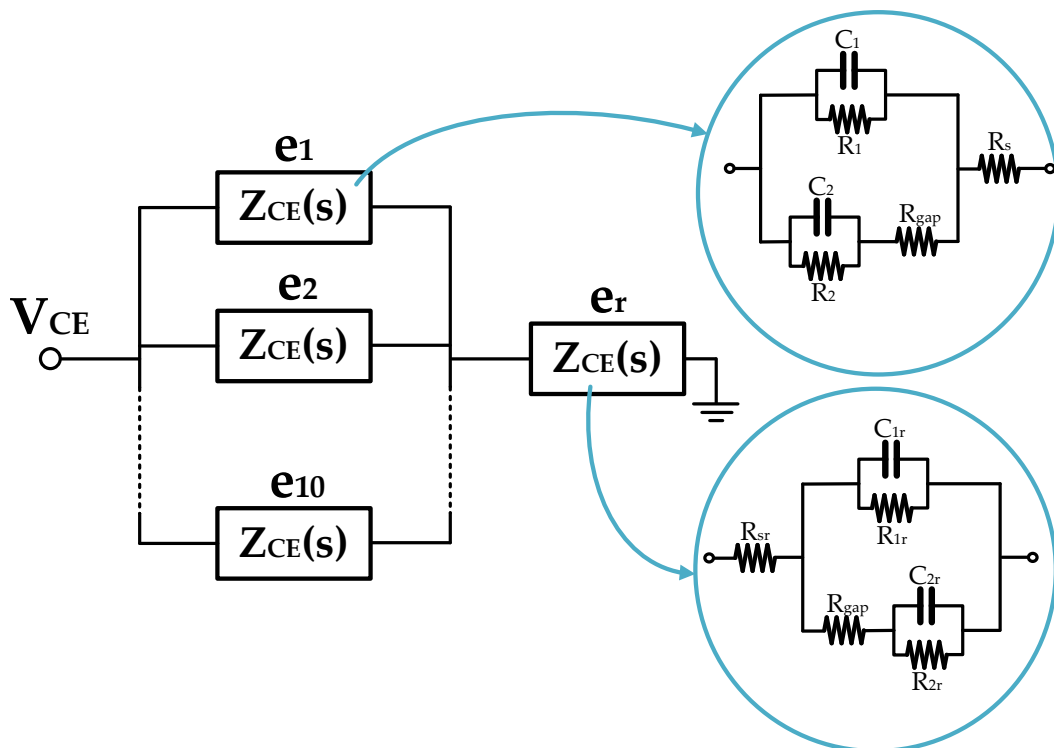
Fig. 2.24 Real-electrode well (REW) model of the well. It has ten microelectrodes (e_1 to e_{10}) and one big reference electrode (e_r).

$$\frac{C_{dlr}}{C_{dl}} = \frac{C'_{dl} \cdot A_{er}}{C'_{dl} \cdot A_e} \rightarrow C_{dlr} = C_{dl} \frac{A_{re}}{A_e} \quad [F] \tag{2.72}$$

$$\frac{R_{sr}}{R_s} = \frac{\rho \cdot \sqrt{\pi}}{4 \cdot \sqrt{A_{re}}} \frac{4 \cdot \sqrt{A_e}}{\rho \cdot \sqrt{\pi}} \rightarrow R_{sr} = R_s \sqrt{\frac{A_e}{A_{re}}} \quad [\Omega] \tag{2.73}$$

where C_{dlr} is the interfacial capacitance of the reference electrode model and R_{sr} is the spreading resistance of the reference electrode model. Note that V_0 (equation (2.8)) is different from C_{dl} (near to 10 mV) and C_{dlr} (0 V), consequently relationship between C_{dl} and C_{dlr} depends on electrode area and the gap resistor (Fig. 2.4), R_{gap}, is considered equal for microelectrode model and reference electrode model. Since the A_e/A_{re} factor is repeated, the relationship between A_e and A_{re} is defined as:

$$k_e = \frac{A_e}{A_{re}} \tag{2.74}$$

Therefore, the parameters of the electric model of the reference electrode are:

$$R_{ctr} = R_{ct} \cdot k_e \qquad C_{dlr} = \frac{C_{dl}}{k_e} \qquad R_{sr} = R_s \cdot \sqrt{k_e} \tag{2.75}$$

The reference electrode model is defined as $Z_{CE}^{re}(s) = F(R_{ctr}, C_{dlr}, R_{sr}, R_{gap}, ff, s)$, then TF of the REW model with ten microelectrodes and one reference electrode is:

$$Z_{well}(s) = \frac{Z_{CE}(s)}{10} + Z_{CE}^{re}(s) \tag{2.76}$$

where $Z_{well}(s)$ is the impedance of the CE system considering the real distribution of the electrodes. Using the relationships between parameters of the microelectrodes model and reference electrodes model described in (2.75), $Z_{well}(s)$ is a Laplace function that depends on:

$$Z_{well}(s) = F(R_{ct}, C_{dl}, R_s, R_{gap}, ff, k_e, s) \tag{2.77}$$

$Z_{well}(s)$ have three poles and three zeros. The expressions of the zeros are too large to present here. In the same way which is done in section 2.1.5.2 poles, zeros and gain for $ff \rightarrow 0$ and $ff \rightarrow 1$ must be estimated to fit the model.

$$p_{ff \rightarrow 0} = \frac{-1}{C_{dl} R_{ct}} \qquad z_{ff \rightarrow 0} = -\frac{R_{ct} \cdot (1 + 10 \cdot k_e) + R_s \cdot (1 + 10 \cdot \sqrt{k_e})}{C_{dl} R_{ct} R_s \cdot (1 + 10 \cdot \sqrt{k_e})} \tag{2.78}$$

$$p_{ff \rightarrow 1} = \frac{-1}{C_{dl} R_{ct}} \qquad z_{ff \rightarrow 1} = -\frac{R_{ct} \cdot (1 + 10 \cdot k_e) + R_s \cdot (1 + 10 \cdot \sqrt{k_e}) + 11 \cdot R_{gap}}{C_{dl} R_{ct} \cdot (R_s \cdot (1 + 10 \cdot \sqrt{k_e}) + 11 \cdot R_{gap})} \tag{2.79}$$

$$k_{well}^{ff \rightarrow 0} = R_{ct} \cdot \left(\frac{1}{10} + k_e\right) + R_s \cdot \left(\frac{1}{10} + \sqrt{k_e}\right)$$

$$k_{well}^{ff \rightarrow 0} = R_{ct} \cdot \left(\frac{1}{10} + k_e\right) + R_s \cdot \left(\frac{1}{10} + \sqrt{k_e}\right) + 11 \cdot \frac{R_{gap}}{10} \tag{2.80}$$

In (2.78) are presented the pole and the zero when $ff \to 0$, and in (2.79) are presented the pole and the zero when $ff \to 1$. These expressions cannot be used to estimate the $Z_{well}(s)$ model parameters, since the approximation done in (2.59) is less accurate for zeros in (2.78) and (2.78). The best choice is to get the $R_{ct}^{ff \to 0}$ and $C_{dl}^{ff \to 0}$ expressions from (2.78) and the $R_{ct}^{ff \to 1}$ and $C_{dl}^{ff \to 1}$ expressions from (2.79). Working with the equations of poles and zeros, the following expressions are obtained:

$$R_{ct}^{ff \to 0} = -\frac{R_s \cdot (1 + 10 \cdot \sqrt{k_e}) \cdot (p_{ff \to 0} - z_{ff \to 0})}{p_{ff \to 0} \cdot (1 + 10 \cdot k_e)} \tag{2.81}$$

$$C_{dl}^{ff \to 0} = -\frac{1 + 10 \cdot k_e}{R_s \cdot (1 + 10 \cdot \sqrt{k_e}) \cdot (p_{ff \to 0} - z_{ff \to 0})} \tag{2.82}$$

$$R_{ct}^{ff \to 1} = -\frac{(R_s \cdot (1 + 10 \cdot \sqrt{k_e}) + 11 \cdot R_{gap}) \cdot (p_{ff \to 0} - z_{ff \to 0})}{p_{ff \to 0} \cdot (1 + 10 \cdot k_e)} \tag{2.83}$$

$$C_{dl}^{ff \to 1} = -\frac{1 + 10 \cdot k_e}{(R_s \cdot (1 + 10 \cdot \sqrt{k_e}) + 11 \cdot R_{gap}) \cdot (p_{ff \to 0} - z_{ff \to 0})} \tag{2.84}$$

Then, the values of R_{ct}, C_{dl}, poles and zeros when $ff \to 0$ and $ff \to 1$ can be obtained. The values of $f_{CE}^{ff \to 0}$, $f_{CE}^{ff \to 1}$, $a_{CE}^{ff \to 0}$ and $a_{CE}^{ff \to 1}$ used in the step one and the step two of the fitting process are the same of the Table 2.1. In Table 2.7 and Table 2.8 the values of poles, zeros and model parameters are summarized. Note that, as with the SEW model, $p_{ff \to 0} \approx p_{ff \to 1}$ have been considered. $R_{ct}^{ff \to 0}$ and $R_{ct}^{ff \to 1}$ values are still an order of magnitude below 13.67 $M\Omega$ expected from (2.6). Values of $C_{dl}^{ff \to 0}$ and $C_{dl}^{ff \to 1}$ are very close to the expected theoretical value 3.29 nF in (2.11). Besides that, R_s values are different from the expected value of 1 kHz in (2.13). The value of R_{gap} is studied below. f_{val} of both fitting steps for each well is shown in Table 2.9. Notice that, compared with f_{val} for SEW model (Table 2.2), 2 less orders of magnitude have been achieved.

Table 2.7 Model parameters at the beginning of the experiment $ff \to 0$ for AA8 cell line (REW model with 10 microelectrodes and one reference electrode).

Well	$R_{ct}^{ff \to 0}$ [$M\Omega$]	$C_{dl}^{ff \to 0}$ [nF]	$R_s^{ff \to 0}$ [$k\Omega$]	$p_{ff \to 0}$ [Hz]	$z_{ff \to 0}$ [kHz]
1	1.17	2.74	4.17	49.67	9.59
3	0.71	3.75	3.23	60.17	9.04
4	0.52	4.8	2.95	64.24	7.75
5	1.41	2.54	4.71	44.2	9.12
7	0.63	4.24	3.44	59.78	7.52
8	0.36	4.85	2.58	91.65	8.79

As for SEW model, cell concentration is estimated using *ff* for each moment and well. *ff* estimation is perform in the same way of SEW model, but in that case, the REW model

Table 2.8 Model parameters at the end of the experiment $ff \to 1$ for AA8 cell line (REW model with 10 microelectrodes and one reference electrode).

Well	$R_{ct}^{ff \to 1}$ $[M\Omega]$	$C_{dl}^{ff \to 1}$ $[nF]$	$R_s^{ff \to 1}$ $[k\Omega]$	R_{gap} $[\Omega]$	$z_{ff \to 1}$ $[kHz]$
1	1.28	2.5	6.08	346.6	5.12
3	0.88	3.02	7.41	383.5	3.63
4	0.69	3.61	1.6	1021.1	3.36
5	1.51	2.38	7.79	258.5	4.8
7	0.87	3.07	5.01	841.6	3.24
8	0.51	3.43	1.2	1017.4	3.73

Table 2.9 Function value (f_{val}) for each well in the two steps of model parameters estimation, for $ff \to 0$ and $ff \to 1$.

Well	1	3	4	5	7	8
$f_{val}^{ff \to 0}$ [x 10^{-5}]	0.089	0.38	0.99	0.161	0.16	0.69
$f_{val}^{ff \to 1}$ [x 10^{-5}]	0.26	0.068	1.53	0.18	1.61	0.38

of the wells is used. Limits for CF minimization are the same of Table 2.5, but the values of $R_{ct}^{ff \to 0}$, $R_{ct}^{ff \to 1}$, $C_{dl}^{ff \to 0}$ and $C_{dl}^{ff \to 1}$ used for each well are the values of Table 2.7 and Table 2.8. Table 2.10 present the values for R_{si} and ΔR_s for the REW model.

Table 2.10 Parameters to define the evolution of R_s.

Well	R_{si} $[k\Omega]$	ΔR_s $[k\Omega]$
1	4.17	1.91
3	3.23	4.18
4	2.95	-1.35
5	4.71	3.09
7	3.44	1.57
8	2.58	-1.38

In Fig. 2.25 shows the *fill-factor* evolution for each well using the parameters obtained in fitting process. As expected, wells 1 and 3 are the last ones to reach the maximum *fill-factor*, wells 4 and 5 are the second ones and the first to reach the maximum are wells 7 and 8. This is due to the initial number of cells on each well. The more the initial number of cells, the lower the time to reach the maximum *fill-factor*.

In the same way for SEW model, results of *ff* can be used to calculate cell concentration using (2.70). It is interesting to compare SEW model result with REW model results and with cell concentration of traditional counting method. Fig. 2.26 shows
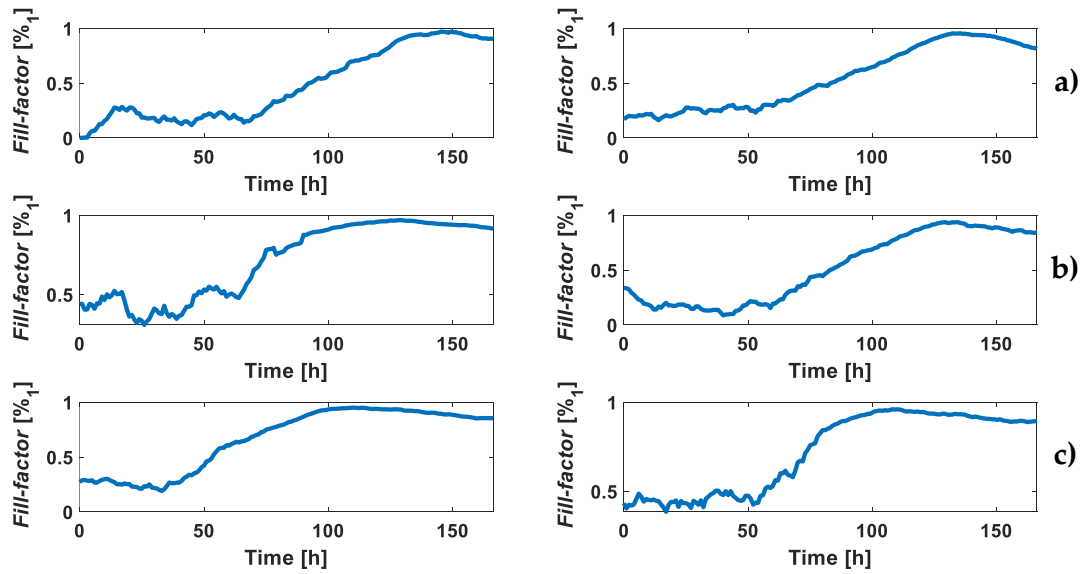
Fig. 2.25 *Fill-factor* evolution for each well of the experiment using the REW model. **a)** Initial number of cells: 2500 cells (well 1 on the left and well 3 on the right). **b)** Initial number of cells: 5000 cells (well 4 on the left and well 5 on the right). **c)** Initial number of cells: 10000 cells (well 7 on the left and well 8 on the right).

this comparison. Cell concentration evolution of REW model seems to be similar to cell concentration evolution of traditional counting method, except for the wells with an initial number of cells of 10000, where it differs slightly. In general, REW model seems to show better the behavior (or cell concentration evolution) of cell concentration (or *fill-factor*) for low values of *ff*. Like the SEW model, the REW model meets the error margins obtained from traditional optical counting.

In this subsection, it has been demonstrated that linear models can be used to know the behavior of a CC assay even if it has a clearly nonlinear behavior. Therefore, it can be concluded that it is possible to obtain the cell concentration of a CC assay using an oscillator circuit (OBT) as a measurement circuit. The errors found are relatively small, and the trend of the traditional curves and those using the OBT circuit are similar.
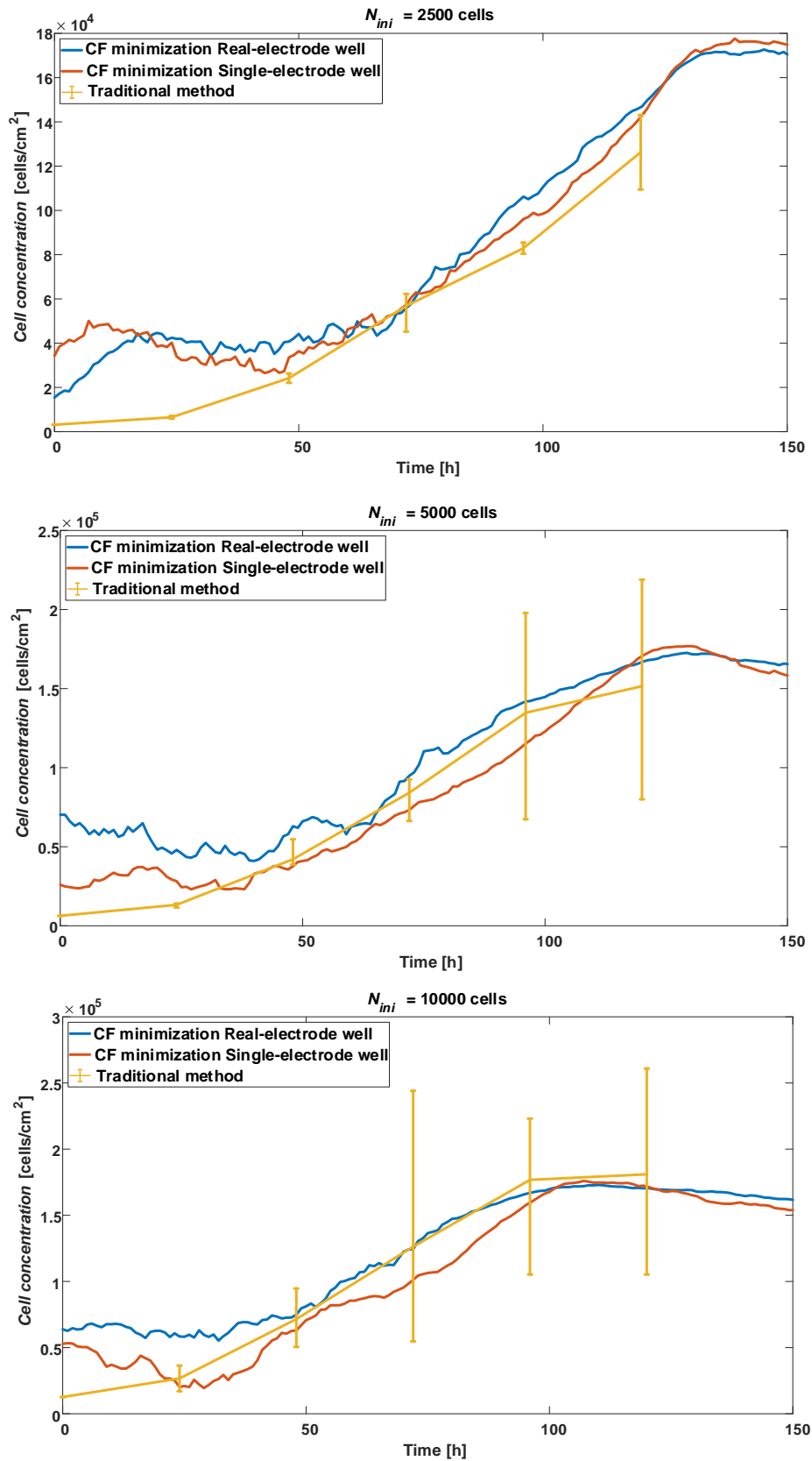
Fig. 2.26 Cell concentration comparison between CF minimizing method using SEW model (blue) and REW model (red), and traditional counting method (yellow).

2.1.5.4   Fractional order model

Integer-Order (IO) models, such as those used in the previous subsections, do not completely fit the behavior of a real system. In the case of the electrical behavior of a BS, their BDs confirm that a (relatively simple) IO model cannot capture all the dynamics of the response to an electrical stimulus. Although in the previous subsections the evolution of the growth of a CC assay has been successfully obtained using IO models (with a certain degree of complexity), it is interesting to apply Fractional Order (FO) models in the process of extracting ff from f_{osc} and a_{osc}. FO models can achieve a better fit of the CE system parameters, because they are non-linear and are closer to the real behavior. For example, in [35] a two electrode model, which contains a FO Constant Phase element (CPE) is used to is used to perform the characterization of electrodes for bioimpedance measurement of animal tissue. Authors consider that the electrodes have resistive and capacitive properties of FO (the CPE element), and that the tissue is of the resistive type. FO elements can also be used to characterize vegetal tissues, as is done in [34].

FO models are based on the premise that the order of a differential operator can be non-integer. To start learning about FO elements and their frequency behavior, the manual [64] is used as a reference document. The authors define the FO Laplace operator as follows,

$$\lambda_n = s^{\alpha_n} \qquad 0 < \alpha_n < 2 \tag{2.85}$$

where α_n is the order of the differential Laplace operator s and n is an integer such that $n = \{1, 2, 3\ldots\}$. Capacitors of the CE model (Fig. 2.5) are replaced by CPE described with FO operators,

$$X_{C_{dl1}} = \frac{1}{s^{\alpha_1} C_{dl1}} \qquad X_{C_{dl2}} = \frac{1}{s^{\alpha_2} C_{dl2}} \tag{2.86}$$

where α_1 is the order of s in reactance $X_{C_{dl1}}$ and α_2 is the order of s in reactance $X_{C_{dl1}}$.

The transfer function of the 10 electrodes FO CE model is very complex, so it is expressed as:

$$Z_{well}(s) = F(R_{ct}, C_{dl}, R_s, R_{gap}, ff, k_e, \alpha_1, \alpha_2, s) \tag{2.87}$$

From first tests, where a CF of the FO CE model was minimized to know the possible values of α_1 and α_2, a conclusion is reached: in this FO CE model, R_s does not change with ff (i.e., ΔR_s is removed from the model). The first tests have reported values of ΔR_s in the order of 10^{-3}, which does not affect the model because R_s has an order of 10^3. The explanation begins by derived the FO models of the 10 electrodes system when $ff \rightarrow 0$ and $ff \rightarrow 1$, in order to estimate the parameters in a simple way. The transfer functions obtained are as follows,

$$Z_{well}^{ff \to 0}(\lambda_1) = k_{well}^{ff \to 0} \frac{p_{ff \to 0}}{z_{ff \to 0}} \frac{\lambda_1 + z_{ff \to 0}}{\lambda_1 + p_{ff \to 0}} \tag{2.88}$$

$$Z_{well}^{ff \to 1}(\lambda_2) = k_{well}^{ff \to 1} \frac{p_{ff \to 1}}{z_{ff \to 1}} \frac{\lambda_2 + z_{ff \to 1}}{\lambda_2 + p_{ff \to 1}} \tag{2.89}$$

where poles, zeros and gains have been previously defined in equations (2.78) to (2.80). Note that, when $ff \to 0$, α_2 has no influence in the system behavior, and, when $ff \to 1$, α_1 has any influence in the system behavior. In an FO model, α changes the slope of poles and zeros, such that its magnitude curve has a slope of $\pm \alpha \cdot 20$ *dB/dec*. Furthermore, the change in phase, for single poles and zeros, is $\pm \alpha \cdot \pi/2$ º. The experimental BDs (Fig. 2.19) of the system indicate that the system has a non-linear behavior, because the slope of the magnitude curve and the changes in the phase curve do not match the general characteristics of an IO model. Considering that the fractional exponent α can modify these indicators outside the standard of an IO model, and knowing that R_s defines zeros and gains in the IO CE model, the conclusion is that small changes between α_1 and α_2 (transition from $ff \to 0$ to $ff \to 1$) produce big changes in the FO model of the system, and, therefore, ΔR_s becomes redundant and can be removed from the FO model.

The parameter estimation process is similar to the performed for the 1 electrode and 10 electrodes IO models. The BSC is used to ensure the oscillation conditions, obtaining a complex number (2.60), which must be equal to 0. Since $s = j \cdot \omega$, in FO models complex number j is replaced by j^α. Then, the FO complex number must be translated to complex number by using Moivre's formula:

$$j^\alpha = \cos\left(\alpha \cdot \frac{\pi}{2}\right) + j \cdot \sin\left(\alpha \cdot \frac{\pi}{2}\right) \tag{2.90}$$

Due to the high complexity of the model (cross products of α_1 and α_2), the model is implemented in a different way than the previous sections. IO models have been implemented (sections 2.1.5.2 and 2.1.5.3) completely to obtain its parameters, while FO models are, in this case, implemented in a transitional mode. This means that, considering that the pole is constant for any value of *ff*, a transition from $z_{ff \to 0}$ to $z_{ff \to 1}$ and from $k_{well}^{ff \to 0}$ to $k_{well}^{ff \to 1}$ is implemented using *ff*. In other words, *ff* is used to change from $Z_{well}^{ff \to 0}(\lambda_1)$ to $Z_{well}^{ff \to 1}(\lambda_2)$. Then, the implemented model is:

$$Z_{well}(\lambda_1, \lambda_2) = k_{well} \frac{p}{z} \frac{\lambda + z}{\lambda + p} \tag{2.91}$$

where $p = p_{ff \to 0} = p_{ff \to 1}$ and,

$$z = (1 - ff) \cdot z_{ff \to 0} + ff \cdot z_{ff \to 1} \tag{2.92}$$

$$k_{well} = (1 - ff) \cdot k_{well}^{ff \to 0} + ff \cdot k_{well}^{ff \to 1} \tag{2.93}$$

$$\lambda = (1 - ff) \cdot \lambda_1 + ff \cdot \lambda_2 \tag{2.94}$$

70

When $ff \to 0$, by replacing f_{osc} by $f_{CE}^{ff \to 0}$ and a_{osc} by $a_{CE}^{ff \to 0}$ (Table 2.1) in (2.91), R_{ct}, C_{dl}, R_s, p, $z_{ff \to 0}$ and α_1 can be obtained by minimizing the CF. The CF for FO model is the same of (2.66), except that during its calculation the CE model used is the FO real electrode-well (REW) model (2.91). In the same way, when $ff \to 1$, by replacing f_{osc} by $f_{CE}^{ff \to 1}$ and a_{osc} by $a_{CE}^{ff \to 1}$ (Table 2.1) in (2.91), R_{gap}, $z_{ff \to 1}$ and α_2 can be obtained by minimizing the CF (2.66). As in the previous sections, data obtained from the AA8 cell line is used.

In this case, to minimize the CF, the Matlab® function *fminsearch* [65] is used. It performs an unbounded search of the values that make the CF minimum, starting from the initial point chosen by the user. The value of the function, f_{val}, is again used as a measurement of the minimization quality. Table 2.11 shows the f_{val} values obtained for each well and *ff* limit. Notice that *fminsearch* finds parameter values for which f_{val} is very small. The results of minimizing the CF of (2.66) are shown in next tables. Table 2.12 displays the CE model parameters when $ff \to 0$ and Table 2.13 presents the CE model

Table 2.11 Function value (f_{val}) for each well in the two steps of FO model parameters estimation, for $ff \to 0$ and $ff \to 1$.

Well	1	3	4	5	7	8
$f_{val}^{ff \to 0}$ [x 10^{-15}]	0.4	0.18	0.72	0.04	0.38	0.26
$f_{val}^{ff \to 1}$	0	0	0	0	0	0

Table 2.12 Model parameters at the beginning of the experiment $ff \to 0$ for AA8 cell line (FO REW model with 10 microelectrodes and one reference electrode).

Well	R_{ct} [$M\Omega$]	C_{dl} [nF]	R_s [$k\Omega$]	p [Hz]	$z_{ff \to 0}$ [kHz]	α_1
1	0.43	1.85	0.97	200	61.1	1.05
3	0.29	2.72	0.29	199.1	137.65	1.04
4	0.47	4.1	2.39	83.05	11.2	1.02
5	0.69	2.42	0.56	94.7	80.63	1
7	0.24	3.03	0.36	222.98	98.89	1.04
8	0.84	7.2	1.21	26.24	12.52	0.95

Table 2.13 Model parameters at the end of the experiment $ff \to 1$ for AA8 cell line (FO REW model with 10 microelectrodes and one reference electrode).

Well	R_{gap} [Ω]	$z_{ff \to 1}$ [kHz]	α_2
1	501.13	12.89	1.03
3	699.81	7.58	1
4	520.64	4.37	0.98
5	686.71	8.12	0.99
7	355.63	12.32	0.99
8	412.02	3.6	0.91

parameters when $ff \rightarrow 1$. The transition from α_1 to α_2 models the effect of changes in the zero and gain. Thus, R_{ct}, C_{dl} and R_s do not change during the CC assay growth, they are obtained at $ff \rightarrow 0$ and are constant.

Fig. 2.27 shows *ff* evolution for each well using the parameters obtained in fitting process. Results are similar to the ones in subsections 2.1.5.2 and 2.1.5.3. In this case, it seems that *ff* tends to higher values in the first days of simulation. Even so, the trend and the time at which *ff* reaches value 1 is similar to the previous subsections.
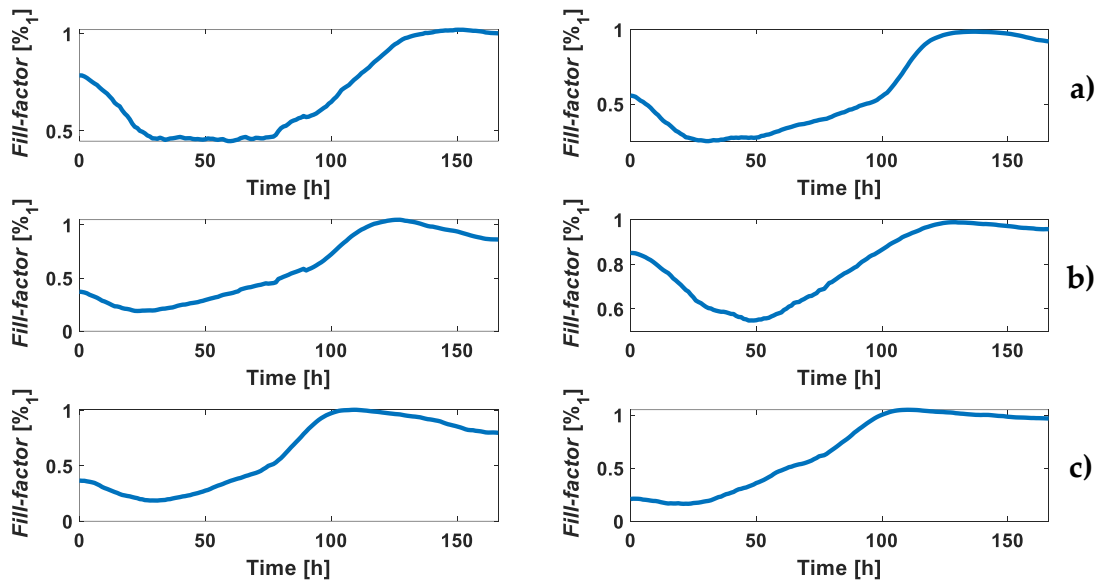
Fig. 2.27 *Fill-factor* evolution for each well of the experiment using the FO REW model.
a) Initial number of cells: 2500 cells (well 1 on the left and well 3 on the right).
b) Initial number of cells: 5000 cells (well 4 on the left and well 5 on the right).
c) Initial number of cells: 10000 cells (well 7 on the left and well 8 on the right).

As in previous sections, *ff* is used to calculate cell concentration using (2.70). Cell concentration results of FO REW model are once again compared with SEW model results and REW model results and with cell concentration of traditional counting method. Fig. 2.28 shows this comparison. Cell concentration evolution of FO REW model seems to be similar to cell concentration evolution of the previous models. The results prove that FO models can be used to track the growth of CC assays, but with a sufficiently high initial *ff* or cell concentration. For N_{ini} values of 2500 and 5000 cells, it has significant errors in the first hours and/or days of the experiment.

All three models (SEW, REW and FO REW) predict correctly the growth trend of the CC assay. However, the FO REW model, for low values of N_{ini}, fits worse than the IO models, which may be due to the high sensitivity of α_1 and α_2. When a FO is minimized, several local minima can be found, making it difficult for the algorithm to know which is the correct value. On the other hand, FO model fits better the BD of the real system,
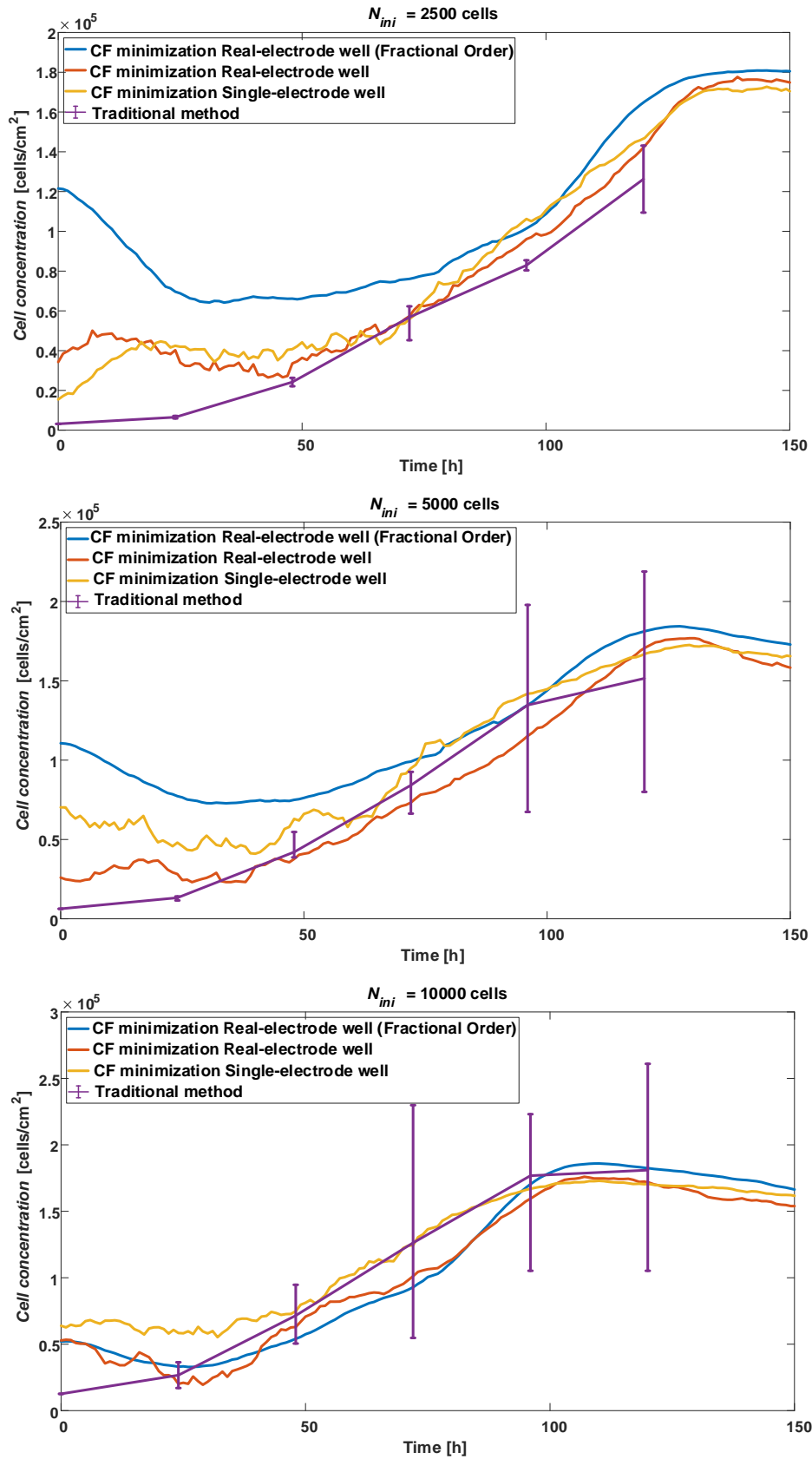
Fig. 2.28 Cell concentration comparison between CF minimizing method using FO REW model (blue), REW model (red) and SEW model (yellow), and traditional counting method (purple).

since it can be adapted to slopes of poles and zeros different from the classical ±20 *dB/dec* (also for ±90 *°/dec* phase). If the initial concentration is high or the minimization algorithm can be improved, the FO model is the best choice to simulate a BS due to its non-linear behavior.

In the current subsection the REW model has been adapted and tested to a FO model. The new model, FO REW, contains FO Laplace operators. It is shown that using an FO model it is possible to obtain the cell concentration of a CC assay from the data of an OBT to which the culture is connected. The best way to confirm these results is to test the fitting method of these models for other cell lines. In the following subsection, results obtained for the N2a and N2a-APP lines (introduced in 2.1.5.1) will be presented.

2.1.5.5   Model fitting of different cellular lines

In this section the REW model (section 2.1.5.3) and the FO REW model (section 2.1.5.4) are fitted to other cell lines than AA8. The fitting process is applied to the N2a and N2aAPP lines (introduced in section 2.1.5.1). The goal of this task is to validate the models and fitting methods with additional target cell lines. Very useful conclusions can be drawn such as the limits of the method, the influence of cell type size and morphology, etc.

The first problem found is that the values of the parameters of the FO model are not consistent. Negative results are obtained for some parameters and others are far from the expected range. This means that there are parameters, such as Rct or $z_{ff \to 0}$ and $z_{ff \to 1}$ that take negative or far out of range values when using the transitional model defined in (2.91). Therefore, from this point the REW FO model (2.87) is used to fit the other two cell lines. Then, the parameters and the procedure to obtain the cell line parameters is the same for the REW model and the FO REW model as the one used in section 2.1.5.3. The only difference between the IO and the FO is that the latter estimates α_1 for low *ff* and α_2 for high *ff*.

During the experiments with the N2a and N2aAPP cell lines the wells setup with respect to the number of cells is: wells 2 and 6 has an N_{ini} = 2500 cells, wells 3 and 7 has an N_{ini} = 5000 cells, and wells 4 and 8 has an N_{ini} = 10000 cells. As the fitting procedure is described in section 2.1.5.3, the values of the parameters obtained when $ff \to 0$ and for $ff \to 1$ are shown below.

2.1.5.5.1   Fitting results of N2a and N2aAPP cell lines

This subsection shows the fitting data of the REW model (also called IO model) and the FO REW model for the N2a and N2aAPP cell lines. In the following subsection the results obtained are discussed and explained.

Table 2.14 and Table 2.15 shows the values of the parameter fitting of REW model for N2a cell line. Table 2.16 shows the parameters that define the evolution of R_s. The

Table 2.14 Model parameters at the beginning of the experiment $ff \to 0$ for N2a cell line (REW model with 10 microelectrodes and one reference electrode).

Well	$R_{ct}^{ff \to 0}$ [$M\Omega$]	$C_{dl}^{ff \to 0}$ [nF]	$R_s^{ff \to 0}$ [$k\Omega$]	$p_{ff \to 0}$ [Hz]	$z_{ff \to 0}$ [kHz]
2	0.39	4.04	1.71	99.68	15.88
3	0.39	3.96	1.67	102.74	16.52
4	0.36	3.55	1.59	122.86	19.29
6	0.32	4.67	1.41	103.21	15.94
7	0.32	4.66	1.72	106.96	13.64
8	0.26	5.19	1.39	117.69	15.22

Table 2.15 Model parameters at the end of the experiment $ff \to 1$ for Na2 cell line (REW model with 10 microelectrodes and one reference electrode).

Well	$R_{ct}^{ff \to 1}$ [$M\Omega$]	$C_{dl}^{ff \to 1}$ [nF]	$R_s^{ff \to 1}$ [$k\Omega$]	R_{gap} [Ω]	$z_{ff \to 1}$ [kHz]
2	0.37	4.34	2.17	172.47	7.43
3	0.36	4.30	0.70	401.99	6.97
4	0.34	3.82	0.72	512.73	6.43
6	0.31	4.92	3.82	132.65	4.78
7	0.31	4.82	3.86	43.16	5.60
8	0.24	5.67	1.93	188.69	5.94

Table 2.16 Parameters to define the evolution of R_s.

Well	R_{si} [$k\Omega$]	ΔR_s [$k\Omega$]
2	1.71	0.47
3	1.67	-0.97
4	1.59	-0.88
6	1.41	2.41
7	1.72	2.13
8	1.39	0.54

first outcome observed is that both R_{ct} and C_{dl} have a very low dispersion compared to the AA8 cell line. Also, to a lesser extent, this happens for $p_{ff \to 0}$, $z_{ff \to 0}$ and, $z_{ff \to 1}$. In contrast, R_{gap}, R_{si} and ΔR_s have a similar dispersion to the AA8 line. The values of f_{val} for $ff \to 0$ and $ff \to 1$ are good or satisfactory in both cases, as shown in Table 2.17.

Table 2.17 Function value (f_{val}) for each well in the two steps of model parameters estimation of N2a, for $ff \rightarrow 0$ and $ff \rightarrow 1$.

Well	2	3	4	6	7	8
$f_{val}^{ff \rightarrow 0}$ [x 10^{-15}]	0.15	0.29	0.19	0.83	0.14	0.04
$f_{val}^{ff \rightarrow 1}$ [x 10^{-5}]	0.04	0.08	0.18	0.43	0.47	5.08

Table 2.18 and Table 2.19 shows the values of the parameter fitting of FO REW model for N2a cell line. In this case, the transitional model is not considered, but the REW complete FO model is used. Therefore, $R_{ct}^{ff \rightarrow 0}$, $C_{dl}^{ff \rightarrow 0}$, R_s, $p_{ff \rightarrow 0}$, $z_{ff \rightarrow 0}$ and α_1 are estimated for $ff \rightarrow 0$. For $ff \rightarrow 1$, $R_{ct}^{ff \rightarrow 1}$, $C_{dl}^{ff \rightarrow 1}$, R_{gap}, $z_{ff \rightarrow 1}$ and α_2 are obtained. Note that, in this case, in the FO REW model, the values of R_{ct} and C_{dl} changes with *ff*. In addition, R_s is fixed (estimated when $ff \rightarrow 0$), since the effect that was observed and modeled with ΔR_s is achieved with α_1 and α_2.

Table 2.18 Model parameters at the beginning of the experiment $ff \rightarrow 0$ for N2a cell line (FO REW model with 10 microelectrodes and one reference electrode).

Well	$R_{ct}^{ff \rightarrow 0}$ [$M\Omega$]	$C_{dl}^{ff \rightarrow 0}$ [nF]	R_s [$k\Omega$]	$p_{ff \rightarrow 0}$ [Hz]	$z_{ff \rightarrow 0}$ [kHz]	α_1
2	0.90	6.21	1.36	28.49	12.90	0.95
3	1.44	6.65	1.57	16.63	10.43	0.94
4	1.13	6.46	1.24	21.80	13.55	0.93
6	0.37	4.97	1.81	87.05	12.15	0.99
7	0.36	5.19	1.55	85.83	13.59	0.99
8	0.26	5.41	1.22	111.76	16.60	0.99

Table 2.19 Model parameters at the end of the experiment $ff \rightarrow 1$ for N2a cell line (FO REW model with 10 microelectrodes and one reference electrode).

Well	$R_{ct}^{ff \rightarrow 1}$ [$M\Omega$]	$C_{dl}^{ff \rightarrow 1}$ [nF]	R_{gap} [Ω]	$z_{ff \rightarrow 1}$ [kHz]	α_2
2	3.75	1.49	1.46	6.07	1.13
3	2.14	4.47	0.65	3.84	0.99
4	3.59	2.03	1.47	4.45	1.08
6	0.63	2.92	0.92	4.43	1.06
7	0.84	2.22	1.11	5.14	1.09
8	0.54	2.64	0.92	5.29	1.09

Parameters of FO model for N2a have more dispersion than IO model, but have similar values to those obtained with the transitional FO model for the AA8 cell line.

Table 2.20 shows the values of f_{val} for $ff \to 0$ and $ff \to 1$, which are similar to those in the Table 2.17.

Table 2.20 Function value (f_{val}) for each well in the two steps of FO model parameters estimation, for $ff \to 0$ and $ff \to 1$.

Well	1	3	4	5	7	8
$f_{val}^{ff \to 0}$ [x 10^{-15}]	0.34	0.32	0.11	0.23	0.23	0.22
$f_{val}^{ff \to 1}$ [x 10^{-5}]	1.72	0.35	1.94	0.42	0.44	1.55

Fig. 2.29 shows the cell concentration comparison of N2a cell line. Cell concentration obtained by using parameters values of IO and FO models, is compared with the cell concentration obtained from the traditional optical cell count. The first noticeable point is that the cell concentration obtained by traditional methods takes longer to initiate growth and to reach its maximum. This was not the case with the AA8 cell line. If the time of the cell concentration obtained by traditional methods is advanced, it is observed that the trends of the curves match (Fig. 2.30). This figure shows that the trend is similar, but for N_{ini} = 2500 cells, the fit is very unsatisfactory with both the IO model and the FO model. For the other two values of N_{ini}, the trend is similar and close to the margins of error. Note that the IO model, for low concentrations, does not perform as well as it should. This may be because it does not properly understand the initial perturbations due to temperature, humidity, CO_2, and the initial time that the cells take to adhering to the bottom of the well.
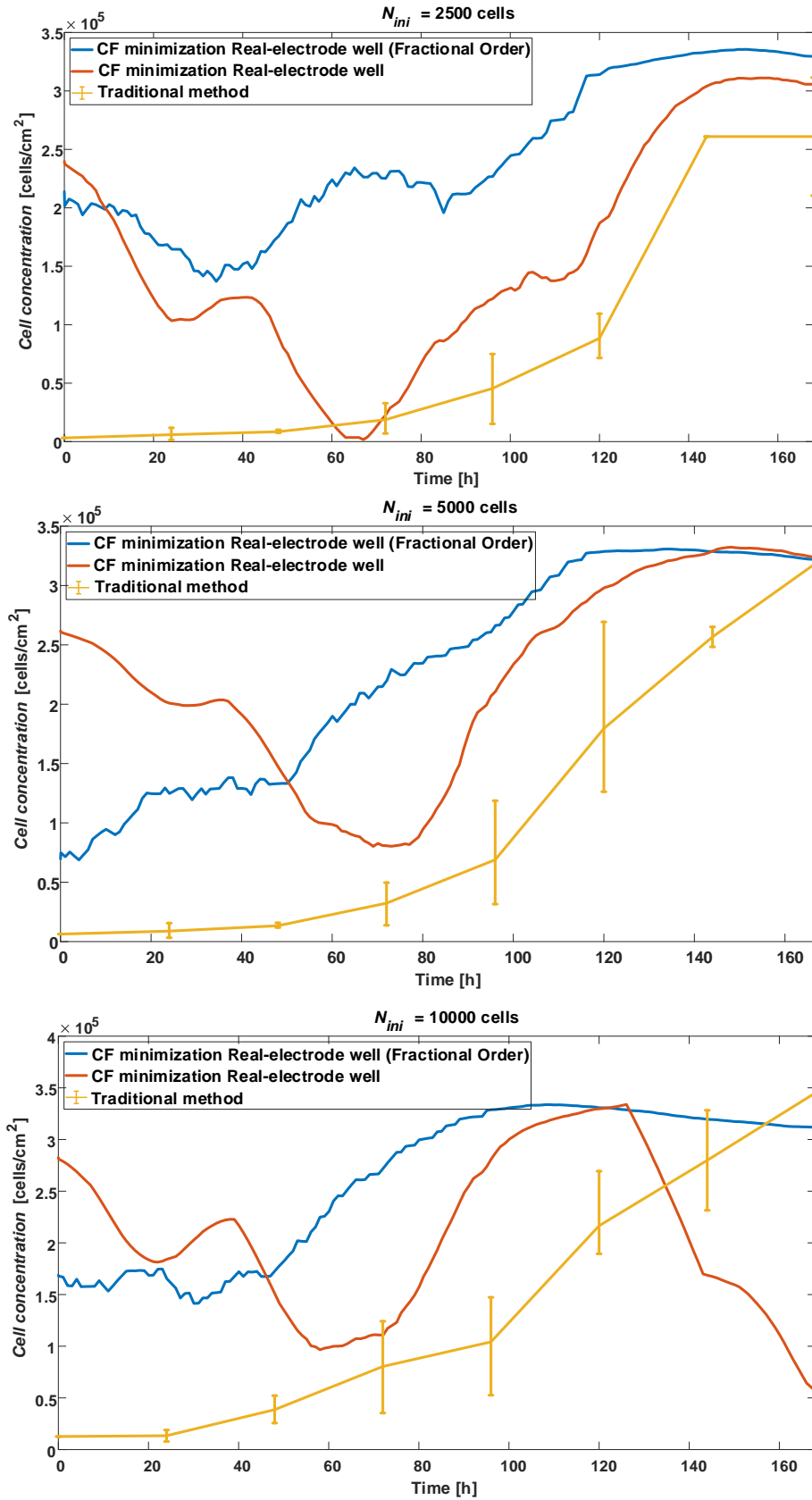
Fig. 2.29 N2a cell line cell concentration comparison between CF minimizing method using FO REW model (blue) and REW model (red), and traditional counting method (yellow).
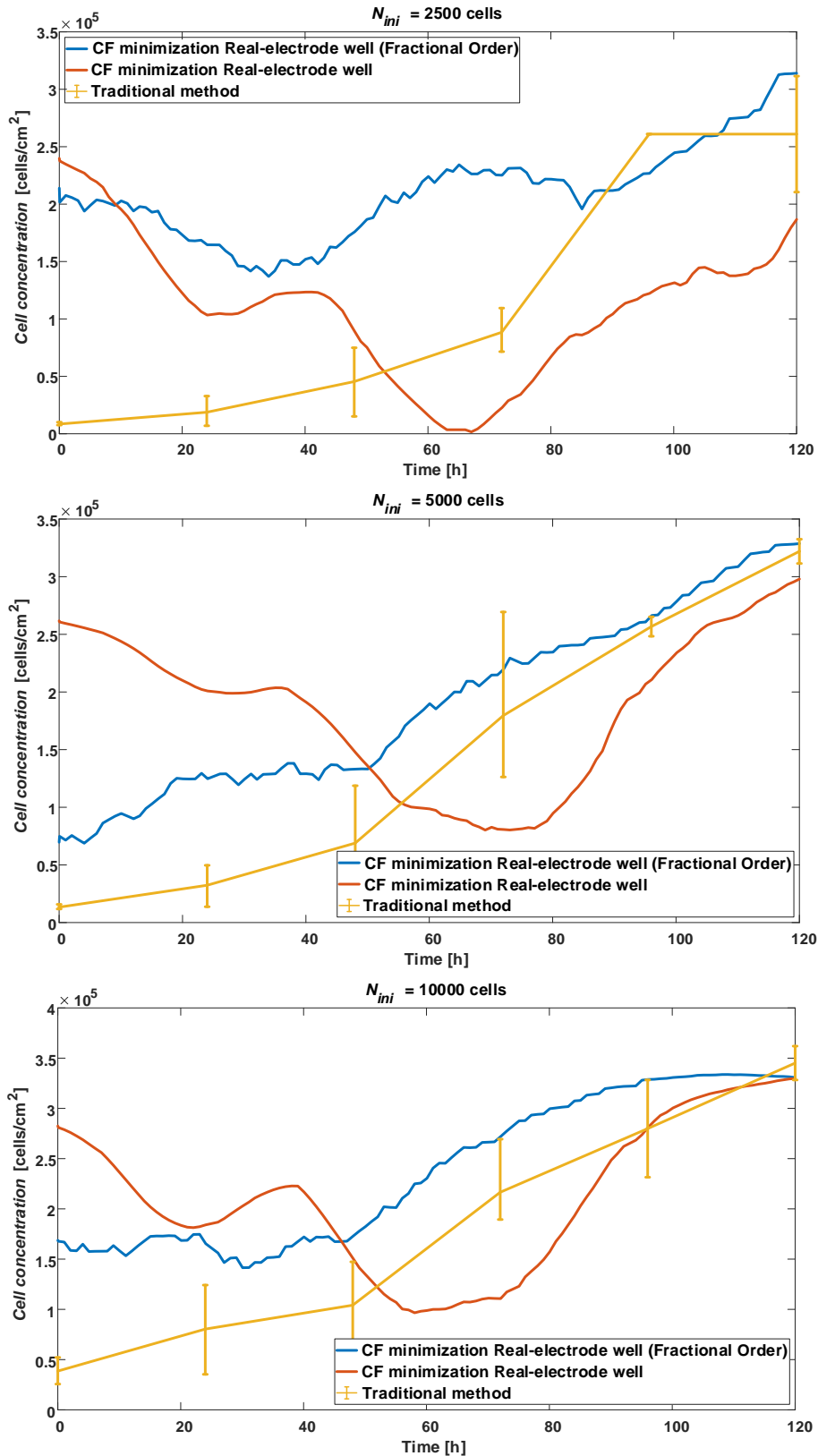
Fig. 2.30 N2a cell line cell concentration comparison between CF minimizing method using FO REW model (blue) and REW model (red), and traditional counting method (yellow). The time vector has been advanced by 48 hours to match the lines.

In Table 2.21 to Table 2.24 are shown the results of fitting the N2aAPP cell line with the REW model. The results are similar to those obtained for N2a, with a few more dispersion in some parameters.

Table 2.21 Model parameters at the beginning of the experiment $ff \rightarrow 0$ for N2aAPP cell line (REW model with 10 microelectrodes and one reference electrode).

Well	$R_{ct}^{ff \rightarrow 0}$ $[M\Omega]$	$C_{dl}^{ff \rightarrow 0}$ $[nF]$	$R_s^{ff \rightarrow 0}$ $[k\Omega]$	$p_{ff \rightarrow 0}$ $[Hz]$	$z_{ff \rightarrow 0}$ $[kHz]$
2	0.61	3.20	2.38	81.24	14.35
3	0.43	3.07	1.48	119.55	24.09
4	0.35	3.99	1.67	115.30	16.42
6	0.47	3.65	1.58	93.19	18.86
7	0.43	3.75	1.62	97.81	17.94
8	0.32	4.33	1.91	114.08	13.26

Table 2.22 Model parameters at the end of the experiment $ff \rightarrow 1$ for N2aAPP cell line (REW model with 10 microelectrodes and one reference electrode).

Well	$R_{ct}^{ff \rightarrow 1}$ $[M\Omega]$	$C_{dl}^{ff \rightarrow 1}$ $[nF]$	$R_s^{ff \rightarrow 1}$ $[k\Omega]$	R_{gap} $[\Omega]$	$z_{ff \rightarrow 1}$ $[kHz]$
2	0.66	2.96	1.75	417.65	7.67
3	0.48	2.78	0.49	628.83	7.76
4	0.39	3.57	2.23	384.32	6.17
6	0.39	4.39	4.72	69.89	4.91
7	0.47	3.45	2.66	162.74	8.35
8	0.29	4.71	3.14	415.53	3.87

Table 2.23 Parameters to define the evolution of R_s.

Well	R_{si} $[k\Omega]$	ΔR_s $[k\Omega]$
1	2.38	-0.63
3	1.48	-0.99
4	1.67	0.56
5	1.58	3.14
7	1.62	1.04
8	1.91	1.22

Table 2.24 Function value (f_{val}) for each well in the two steps of model parameters estimation of N2a, for $ff \rightarrow 0$ and $ff \rightarrow 1$.

Well	2	3	4	6	7	8
$f_{val}^{ff \rightarrow 0}$ [x 10^{-15}]	0	0.11	0.56	0	0	0
$f_{val}^{ff \rightarrow 1}$ [x 10^{-5}]	0.35	0.31	1.44	0.15	0.28	0.51

In the same way, the results of the FO REW model fit for the N2aAPP cell line are similar to those obtained for the N2a line, and are shown in Table 2.25 to Table 2.27. All the data will be discussed in the following section in which an explanation of the dispersions will be proposed by relating them to various parameters of cell morphology and the oscillation waveforms (f_{CE} and a_{CE}).

Table 2.25 Model parameters at the beginning of the experiment $ff \to 0$ for N2aAPP cell line (FO REW model with 10 microelectrodes and one reference electrode).

Well	$R_{ct}^{ff \to 0}$ [$M\Omega$]	$C_{dl}^{ff \to 0}$ [nF]	R_s [$k\Omega$]	$p_{ff \to 0}$ [Hz]	$z_{ff \to 0}$ [kHz]	α_1
2	0.90	6.21	1.36	28.49	12.90	0.95
3	1.44	6.65	1.57	16.63	10.43	0.94
4	1.13	6.46	1.24	21.80	13.55	0.93
6	0.37	4.97	1.81	87.05	12.15	0.99
7	0.36	5.19	1.55	85.83	13.59	0.99
8	0.26	5.41	1.22	111.76	16.60	0.99

Table 2.26 Model parameters at the end of the experiment $ff \to 1$ for N2a cell line (FO REW model with 10 microelectrodes and one reference electrode).

Well	$R_{ct}^{ff \to 1}$ [$M\Omega$]	$C_{dl}^{ff \to 1}$ [nF]	R_{gap} [$k\Omega$]	$z_{ff \to 1}$ [kHz]	α_2
2	3.75	1.49	1.46	6.07	1.13
3	2.14	4.47	0.65	3.84	0.99
4	3.59	2.03	1.47	4.45	1.08
6	0.63	2.92	0.92	4.43	1.06
7	0.84	2.22	1.11	5.14	1.09
8	0.54	2.64	0.92	5.29	1.09

Table 2.27 Function value (f_{val}) for each well in the two steps of FO model parameters estimation, for $ff \to 0$ and $ff \to 1$.

Well	1	3	4	5	7	8
$f_{val}^{ff \to 0}$ [x 10^{-15}]	0.34	0.32	0.11	0.23	0.23	0.22
$f_{val}^{ff \to 1}$ [x 10^{-5}]	1.72	0.35	1.94	0.42	0.44	1.55

Fig. 2.31 and Fig. 2.32 shows the cell concentration comparison of N2aAPP cell line. Cell concentration obtained by using parameters values of IO and FO models, is compared with the cell concentration obtained from the traditional optical cell count. As for the N2a line, the cell growth time of the traditional methods is longer than that obtained from the prototype data (Fig. 2.31). Therefore, in Fig. 2.32, the time of cell concentration obtained by traditional optical counting is advanced in order to compare the evolution of the concentrations. For low concentrations, the model also does not

properly reflect the real behavior of the CC assay. The trend of the curves is similar for medium and high concentration values, but like the N2a line, the fit is not sufficiently accurate, as it exceeds the error margins at many points.

The data from the OBT oscillation connected to the CC assays of the N2a and N2aAPP cell lines have provided evidence that the method of model fitting and subsequent cell concentration estimation works. Notice that, both cell lines present a worse match than the AA8 line, and therefore this point should be analyzed.
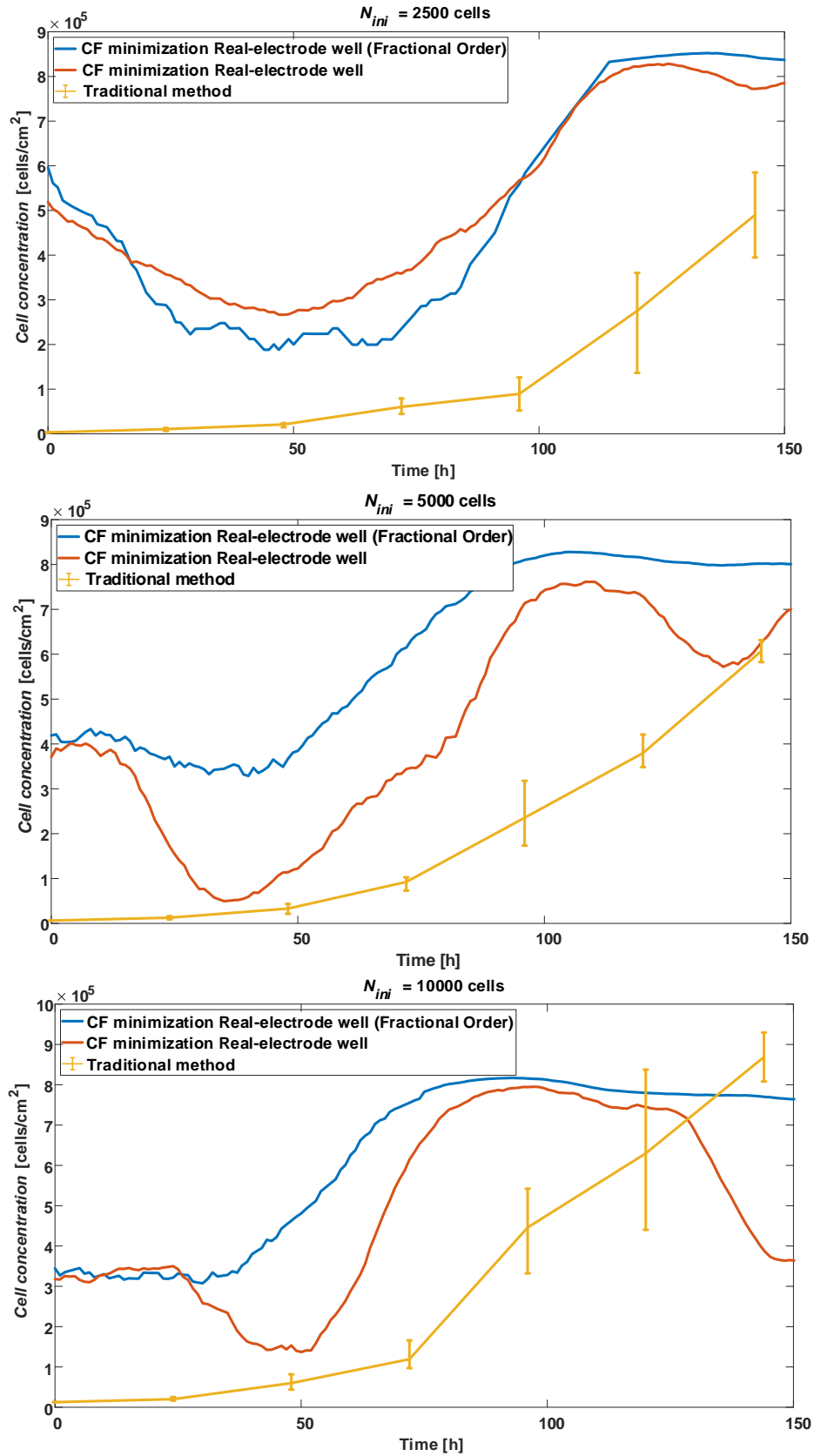
Fig. 2.31 N2aAPP cell line cell concentration comparison between CF minimizing method using FO REW model (blue) and REW model (red), and traditional counting method (yellow).
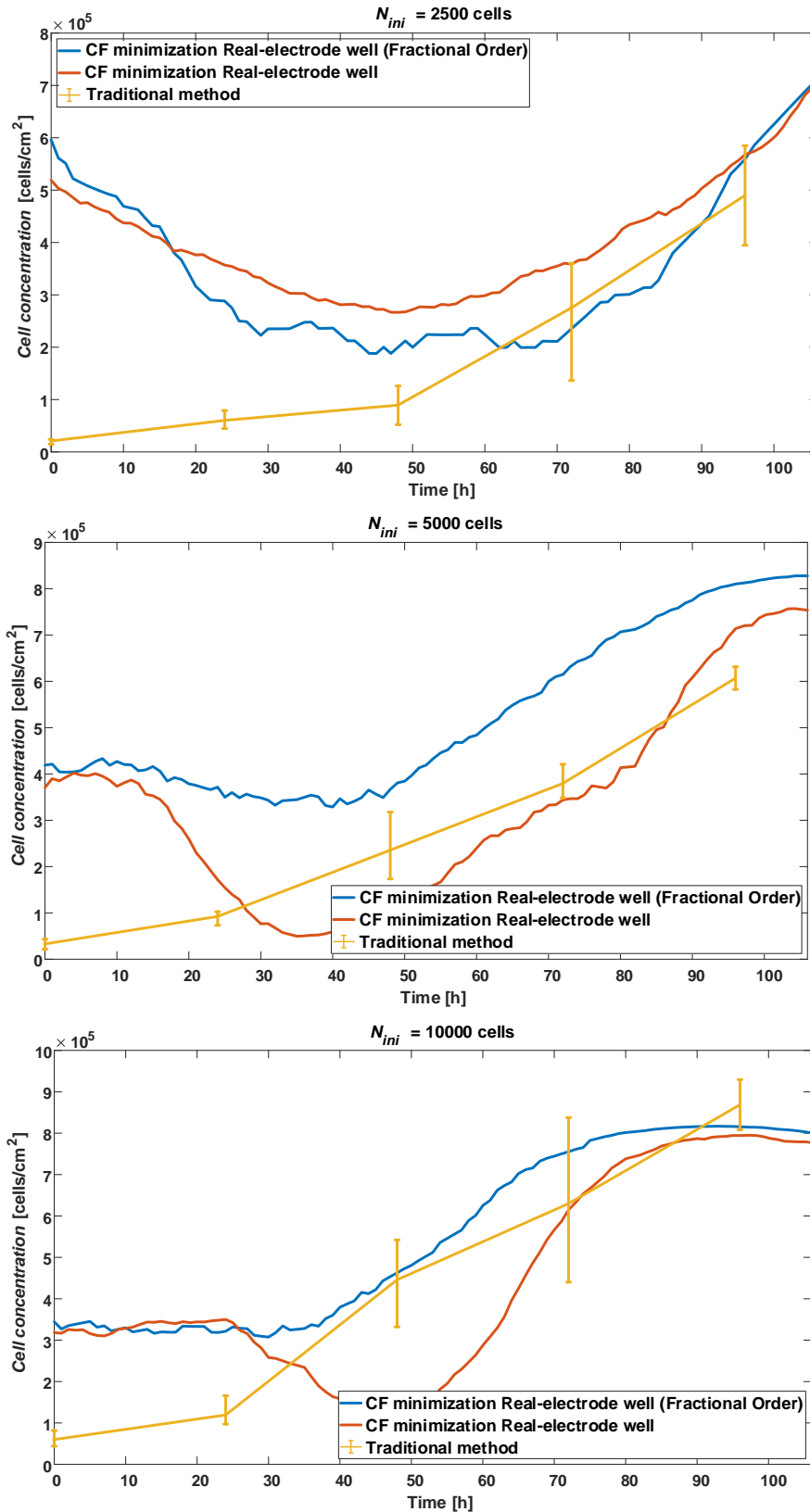
Fig. 2.32 N2aAPP cell line cell concentration comparison between CF minimizing method using FO REW model (blue) and REW model (red), and traditional counting method (yellow). The time vector has been advanced by 48 hours to match the lines.

2.1.5.5.2   Results comparison between cellular lines

The previous sections show that the results obtained, using cell concentration as a metric, are better for the AA8 cell line than for N2a and N2aAPP. In this section, an explanation for this will be discussed, as it is interesting to know the reason for future experiments.

The first factor to consider is the frequency and amplitude of oscillation. The metrics to be used are f_{CE} and a_{CE}. Concretely, it is observed that the difference between f_{CE} and a_{CE} between $ff \to 0$ and $ff \to 1$ is greater in the AA8 line than in the other cell lines fitted. If $f_{CE}^{ff \to 0}$ and $a_{CE}^{ff \to 0}$ are defined as the frequency and amplitude when $ff \to 0$, and $f_{CE}^{ff \to 1}$ and $a_{CE}^{ff \to 1}$ are defined as the frequency and amplitude when $ff \to 1$, the variations of f_{CE} and a_{CE} can be defined as

$$\Delta f_{CE} = f_{CE}^{ff \to 1} - f_{CE}^{ff \to 0}$$
$$\Delta a_{CE} = a_{CE}^{ff \to 1} - a_{CE}^{ff \to 0}$$

$$(2.95)$$

where Δf_{CE} and Δa_{CE} are the difference in frequency and amplitude, respectively, between the time when $ff \to 1$ and $ff \to 0$. Table 2.28 and Table 2.29 shows the values of Δf_{CE} and Δa_{CE}, respectively, of the three cell lines. The tables reveal a greater difference in amplitude variation between the AA8 cell line and the other two than in frequency.

Table 2.28 Δf_{CE} values of AA8, N2a and N2aAPP cell lines [Hz]

N_{ini}	2500		5000		10000	
AA8	83.57	90.51	91.45	110.39	116.15	123.28
N2aAPP	52.15	70.26	53.37	104.92	60.95	111.64
N2a	56.15	69.99	61.22	75.14	67.22	103.40

Table 2.29 Δa_{CE} values of AA8, N2a and N2aAPP cell lines [mV]

N_{ini}	2500		5000		10000	
AA8	4.23	4.61	7.20	7.63	7.73	9.17
N2aAPP	2.04	3.65	2.27	3.66	2.41	3.80
N2a	0.96	1.92	1.10	1.98	1.27	2.97

To find a relationship with the BI, the magnitude and phase variation of the BI from $ff \to 0$ to $ff \to 1$ is calculated. As for frequency and amplitude, the magnitude and phase variation can be defined as

$$\Delta Mag_{CE} = Mag_{CE}^{ff \to 1} - Mag_{CE}^{ff \to 0}$$
$$\Delta Ph_{CE} = Ph_{CE}^{ff \to 1} - Ph_{CE}^{ff \to 0}$$

$$(2.96)$$

where ΔMag_{CE} and ΔPh_{CE} are the difference in magnitude and phase, respectively, between the time when $ff \rightarrow 0$ and $ff \rightarrow 1$. Table 2.30 and Table 2.31 show the values of ΔMag_{CE} and ΔPh_{CE} sorted by cellular line and N_{ini}. ΔMag_{CE} has different values depending on the cell line, whereas ΔPh_{CE} takes close values for different cell lines.

Table 2.30 ΔMag_{CE} values of AA8, N2a and N2aAPP cell lines [V/V]

N_{ini}	2500		5000		10000	
AA8	30.16	654.77	993.03	-209.67	1288.03	1381.04
N2aAPP	166.03	-1374.60	329.02	180.28	271.68	-621.72
N2a	-577.87	-372.62	-650.96	-384.35	-643.13	509.08

Table 2.31 ΔPh_{CE} values of AA8, N2a and N2aAPP cell lines [°]

N_{ini}	2500		5000		10000	
AA8	4.57	8.72	8.17	5.10	9.06	7.22
N2aAPP	2.63	7.42	3.72	2.87	4.68	9.04
N2a	3.26	7.22	3.59	5.20	4.58	4.83

Due to the highest differences in the oscillation parameters between cell lines, ΔMag_{CE} and ΔPh_{CE} are presented versus to the Δa_{CE} for each cell line (note that the data are sorted in ascending order of Δa_{CE}). In this way, Fig. 2.33 shows these relationships, where data of Table 2.30 and Table 2.31 is displayed versus data of Table 2.29.

In the figures there are three clearly defined zones, one for each cell line. This clearly suggests that the cells (size, shape, composition, etc.) influence the accuracy of the fitting method. A useful parameter, known from experiments by traditional methods (optical counting), is the mean area of the CC assay cells. The area of the cells affects 2 main parameters: R_{gap} and R_s. The Table 2.32 shows the mean area of each cell line and the ranges of R_{gap} and R_s obtained for each cell line for the REW model.

In [55] the author of the present thesis shown how both parameters influence a_{CE} and f_{CE} when $ff \rightarrow 0$ to $ff \rightarrow 1$. On the other hand, looking at Fig. 2.4, it is concluded that R_{gap} and R_s (R_{gap} in a stronger degree) depend on the size and morphology of the cells. So, these facts indicate that the cell area influences Δa_{CE} and Δf_{CE}, which results in a loss of accuracy in the model fitting method when the cell area is low.

Table 2.32 Values of A_{cell}, and ranges of R_{gap} and R_s of the cell lines under study for REW model.

Cell line	A_{cell} [μm^2]	R_{gap} [Ω]	$R_s^{ff \rightarrow 0}$ [$k\Omega$]
AA8	552.5	258.5 – 1021.1	2.58 – 4.71
N2aAPP	118	69.9 – 628.8	1.48 – 2.38
N2a	184	43.1 – 512.7	1.39 – 1.72
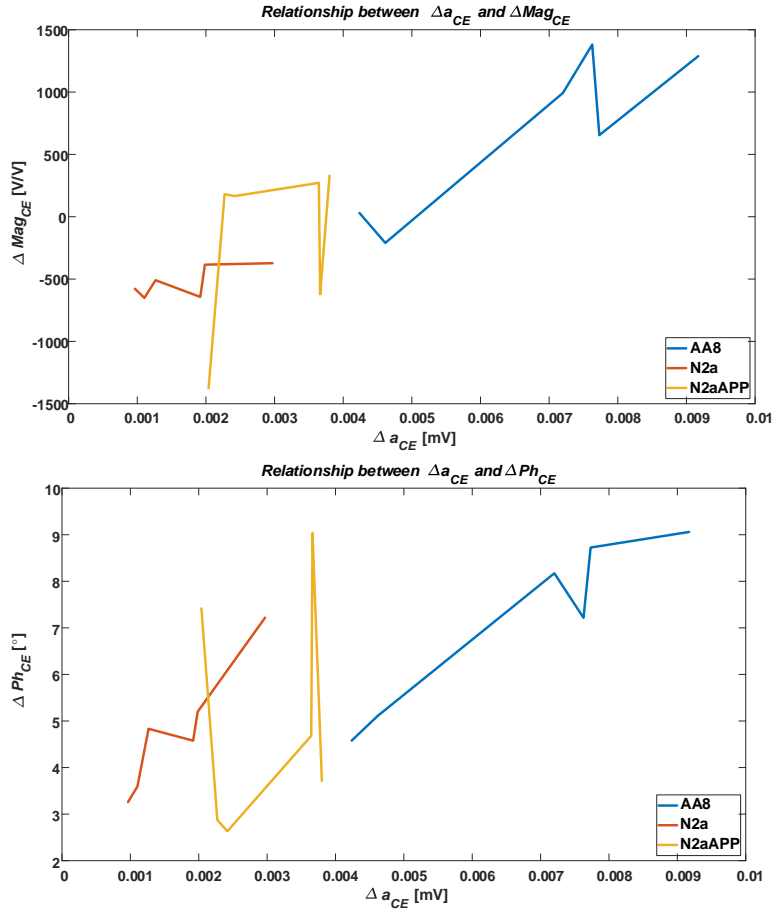
Fig. 2.33 Relationship between Δa_{CE} and oscillation parameters. Top figure shows the relationship Δa_{CE} - ΔMag_{CE}, and bottom figure shows the relationship Δa_{CE} - ΔPh_{CE}.

Table 2.33 shows the same comparison of Table 2.32, but for FO REW model. As can be seen in the cell concentration figures (Fig. 2.28 for AA8, Fig. 2.30 for N2a and Fig. 2.32 for N2aAPP), FO model fits better to the results obtained by traditional counting than the IO model.

Table 2.33 Values of A_{cell}, and ranges of R_{gap} and R_s of the cell lines under study for FO REW model

Cell line	A_{cell} [μm^2]	R_{gap} [Ω]	R_s [$k\Omega$]
AA8	552.5	355.6 – 699.8	0.29 – 2.39
N2aAPP	118	493.8 – 2010.6	1.12 – 1.98
N2a	184	653 – 1474.2	1.22 – 1.81

It can be concluded that, for this particular case, the FO model captures better the growth of a CC assay, since the model parameters are closer to the real ones because
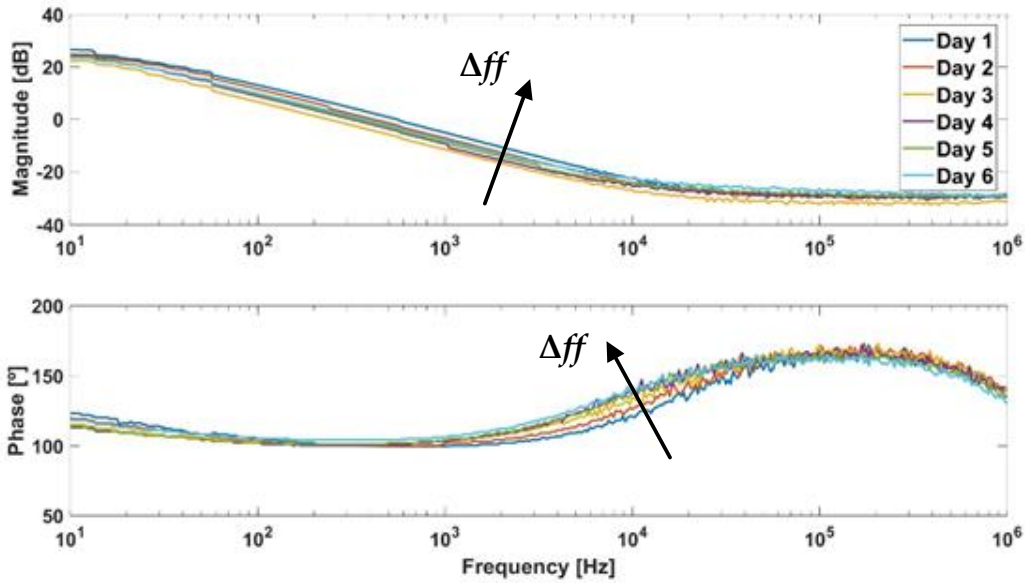
Fig. 2.34 BD of a well in AA8 cell line experiment. The range of the magnitude and phase changes with the oscillation frequency.

they should not compensate for the nonlinearities modeled by the FO Laplace operator exponent (2.85).

Comparing the three cell lines, it can be seen that while AA8 cells are easily fitted, the other two lines are not. This is mostly due to the range of the oscillation amplitude. The (2.35) shows the dependence between the oscillation amplitude and the BI of the CE system. The simplest solution to this problem is to tune the oscillator to a different frequency than 1 *kHz*. The BD of the AA8 cellular line is very useful to know the optimum frequency. Fig. 2.34 shows the BD of well in a AA8 cell line experiment. Magnitude and phase changes with *ff*, but for the tunned frequency (1 *kHz*) the variation is much smaller than for higher frequencies (10 kHz). In the absence of experimental BDs of the N2a and N2aAPP lines, the optimal frequency to maximize the range cannot be known, but the BD of Fig. 2.34 suggests that the accuracy of the tuning method improves greatly when the range (which depends on *ff*) is higher. Therefore, for future experiments the bandpass filter will be tuned to higher frequencies.

The second problem faced during the fitting of the N2a and N2aAPP cell lines is the growth rate of the CC assay. While the culture of the AA8 line grows at the same rate as the traditional parallel experiment, the other two lines seem to grow much faster than the traditional experiment performed for the N2a and N2aAPP lines. Taking into account that the conditions of the traditional experiments and using the OBT are the same, that the initial cells have the same origin, and the experiments have been performed in parallel, the only possible explanation is electrostimulation. Since the current through the cells is similar for all cell lines (close to 7 μA), the only difference is the cells themselves. Table 2.32 shows the average cell sizes for each cell line. The hypothesis proposed in this work is that the current increases the growth rate, depending on the size of the cells. Therefore, the AA8 cell line, having a considerably

larger size (on average) than the other two lines, is not affected by the current levels used, while the N2a and N2aAPP lines are accelerated in growth due to the currents used. This is only a hypothesis, which is still under study, whose results will be studied in the future.

2.2 Conclusions

This chapter has explained in detail how to model the behavior of the growth of a CC assay using OBT data. The oscillator changes its amplitude and frequency of oscillation as a function of the cell concentration from the cell culture which is connected as a load. Some conclusions and questions arising from the modeling work are detailed below:

- It is possible to measure the growth of a CC assay using an oscillator. The BS is connected as a load, which by varying its BI, changes the amplitude and frequency of oscillations. In addition, using the oscillation frequency and amplitude, and the BSC, the electrical model of the BS can be known, while injecting a signal of a given frequency through a CC assay, only its impedance at the frequency of the injected signal is known, so it would be necessary to make a sweep in frequency to obtain the BI model.

- The DF method is a very accurate approach to linearize a non-linear element, which allows to use the BSC to obtain the theoretical (mathematically) oscillation frequencies and amplitudes.

- A CC assay can be modeled by its BI, which is highly non-linear. Therefore, the theoretical value of a parameter of a CE electrical model should be considered as a nominal value with a certain margin of error.

- Experience with the three cell lines used in this work suggests that a tunable BPF is necessary in order to be able to adapt the oscillation frequency to the most suitable zone according to the electrical behavior of the BS.

- The SEW model allows easy fitting of a CC assay. On the other hand, it does not work sufficiently robust for low N_{ini}, or in case the oscillation parameters have low ranges (e.g., the N2a and N2aAPP lines).

- The experimental BD is very useful to configure the measurement circuit (OBT), since it provides the optimum oscillation frequency for each BS.

- Choosing an appropriate CF is important, as the minimization of CF must meet all the objectives required. For that reason, the module of an imaginary number is perfect as a CF for the fitting which use the BSC.

- The FO model is more robust than the IO model (also called REW model) because it captures the non-linearities and makes use of the FO coefficients to predict them. If the IO model is used, the model parameters must compensate for the non-linearities of the real system (CE system), so their values may differ from the nominal theoretical value.

- The size of the cells impacts the accuracy of the measurements. In addition, if they are too small for the applied current, this can stimulate the CC assay and influence the measurements, so they would not be valid and reliable data (as with the N2a and N2aAPP lines).

- A method has been developed to obtain the electrical model of a CC assay from the oscillation data of the OBT circuit. This one provides the value of the cell concentration at each time point, which is a very important step in the field of cell biology. Notice that, although it has been shown that the cell concentration can be obtained from the oscillation parameters, this fitting method has considerable error and needs to be improved. From the work performed in this dissertation, the required knowledge to improve the fitting method, from the changes in the measurement prototype to the algorithms of the method, is available. In future work, all these changes will be added, expecting a significant improvement in the accuracy of the results.

- The estimation of the cell concentration has been performed after the completion of the cell growth experiments with the three lines. The goal of this work is to develop a method to obtain the cell concentration in real-time during an experiment. Therefore, in the following chapter, simulations of real-time experiments will be performed to obtain the cell concentration without knowing the following values of amplitude and frequency. That is, for each amplitude and frequency measurement performed by the OBT, the cell concentration should be estimated in real-time, which, up to now, has not been achieved, being this one of the best and main contributions of this thesis.

Chapter 3   Simulations of real experiments of biological systems

System modeling is the starting point for understanding and predicting a system behavior. The simulation of systems based on its models, helps to know its current state and future behavior. The information extracted from a simulation can be used in several ways:

- To apply a control on a system to regulate its outputs or to restrict the behavior of some of its internal states. For example, the rotational speed of an electric motor can be controlled using a PI (proportional-integral) control at the input voltage. Another example is to apply predictive control with constraints to an electrical circuit to limit the maximum and minimum currents flowing through its nodes.

- To know the behavior of a system when some of its parameters are changed. For example, obtain the consumption and speed curves of a mobile robot when modifying its dimensions.

- To ensure the robustness of a system against different conditions, such as temperature changes, potential failures, ... A good example is the simulations of an electronic circuit varying the working temperature.

These are just a few examples of the benefits of system simulation. This chapter focuses on the simulation of the oscillator-electronic circuit, including the cell-electrode (CE) block. The oscillator circuit, coupled with the CE system as a load, will be mathematically simulated using the Barkhausen stability criterion (BSC), to test the feasibility of estimating the on-line cell concentration in a real experiment. Additionally, the same system will be simulated using the Ngspice [61] electrical simulator. It is a very useful tool, which can be used from Matlab to optimize circuit design processes.

3.1   Real-time estimation of cell-concentration growth

In the Chapter 2 the parameters of the electrical models of the cell-electrode (CE) system have been found. In sections 2.1.5.2 to 2.1.5.4 values have been searched for the integral order (IO) electrical models called single-electrode well (SEW) well model and

real-electrode well (REW) model, and for the fractional order (FO) REW electrical model. These values have been fitted to the AA8 cell line. Since the SEW well model is not enough real, its use has been discarded for the 2.1.5.5, where the values of the other two models (REW and FO REW) for the N2a and N2aAPP cell lines have been searched.

Model fitting, the use of the Oscillation-Based Test (OBT) as a sensor, the minimization of a cost function (CF) to predict *ff* values, etc., have as final goal to predict in real-time (RT), i.e., during a real growth experiment of a cell-culture (CC) assay, the cell concentration in the well at each moment. In this section a routine will be designed (based on the previous work [66]) in which a real experiment is simulated and the value of *ff* is predicted at each moment, as well as the cell concentration. This routine will be tested using the REW and FO REW electrical models for the three cell lines used in Chapter 2: AA8, N2a and N2aAPP.

3.1.1 Fitting routine

The key problem of knowing *ff* at each time of a real experiment is that the values of f_{CE} and a_{CE} when well is totally covered by cells ($ff \rightarrow 1$) are not available. That is, you can estimate the parameters of the models at the beginning of the experiment, where there is any cell in the well ($ff \rightarrow 0$), but there are certain parameters that have no influence on the behavior of the system at this point. These parameters are R_{gap}, $z_{ff \rightarrow 1}$, ΔR_s (for the REW model), and also α_2 (for the FO REW model). The designed routine is as follows:

1. **Estimate initial values of f_{CE} and a_{CE}**: Fig. 3.2 shows the block diagram of the step 1, where the initial routine is presented in graphic form. During the first hours or days of the experiment, the mean of the last 5 values of f_{CE} and a_{CE} measured is calculated ($\overline{f_{CE}}$ and $\overline{a_{CE}}$). As the sampling time (time between measurements) is 1 *h*, the average of the last 4 hours is taken together with the values just obtained. After each measurement, after calculating the mean, a check is performed to verify whether the values obtained are greater than the mean of the new measurement plus a margin ($k_m = 1.005$). If this condition is met, showed in (3.1), the lowest $\overline{f_{CE}}$ and $\overline{a_{CE}}$ are stored as minimum values. Fig. 3.2 also defines the initial value of R_{gap} and the value of the constant k_m. Note that the index *j* is the time index, and goes from 1 to j_{max}. During the calculation of $\overline{f_{CE}}$ and $\overline{a_{CE}}$ *j* is incremented from 1 until (3.1) is satisfied. j_{max} is the maximum value of *j*, and its value is defined by the number of measurements taken during the real experiment.

$$\left(f_{CE}(j) > \overline{f_{CE}(j-1)} \cdot k_m \right) \& \left(a_{CE}(j) > \overline{a_{CE}(j-1)} \cdot k_m \right) \tag{3.1}$$
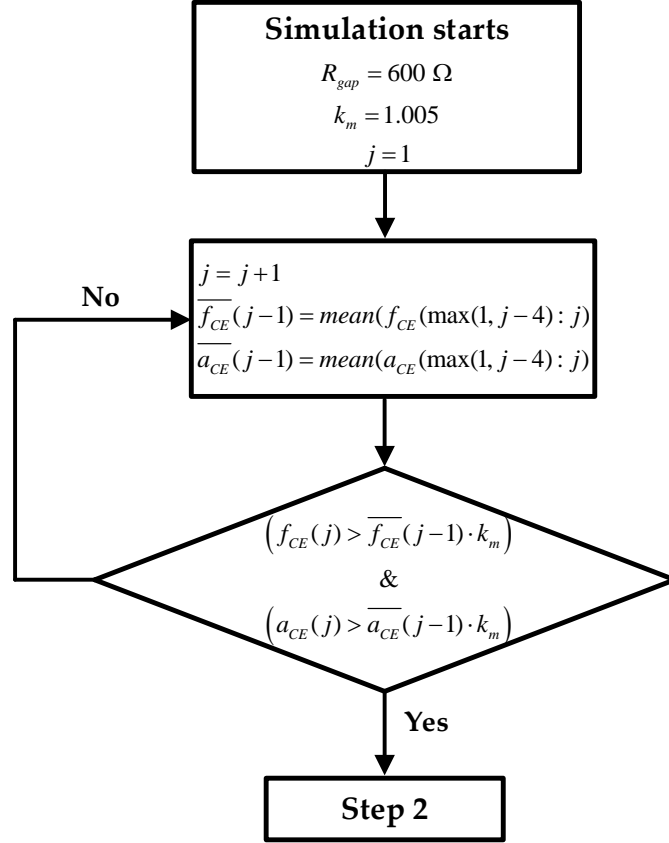
Fig. 3.1 Block diagram of step 1 of RT simulation, whose target is to find the mean around the f_{CE} and a_{CE} minimums.

2. **Computation of the initial parameters of the electrical models:** Using the minimum $\overline{f_{CE}}$ and $\overline{a_{CE}}$ estimated in the previous step, the initial parameters of the electrical models are fitted. The prediction is performed using the method of CF minimization, as in Chapter 2 (sections 2.1.5.3 and 2.1.5.4). For the REW model the parameters $p_{ff\to1}$ (which met that $p_{ff\to0} \approx p_{ff\to1}$), R_{si} and $z_{ff\to0}$ are calculated, and the values of $R_{ct}^{ff\to0}$ and $C_{dl}^{ff\to0}$ can be derived from these using (2.81) and (2.82). For the FO REW model the parameters $p_{ff\to1}$ (which met that $p_{ff\to0} \approx p_{ff\to1}$), R_s, $z_{ff\to0}$ and α_1 are calculated, and the values of $R_{ct}^{ff\to0}$ and $C_{dl}^{ff\to0}$ can be derived from these using (2.81) and (2.82). The initial parameters calculated are the same for all $t(j)$, and therefore they are not re-estimated during the simulation. The whole process of estimating the initial parameters is illustrated in the Fig. 3.2 block diagram, which starts from the results of Step 1 and ends at the beginning of the third and last step.
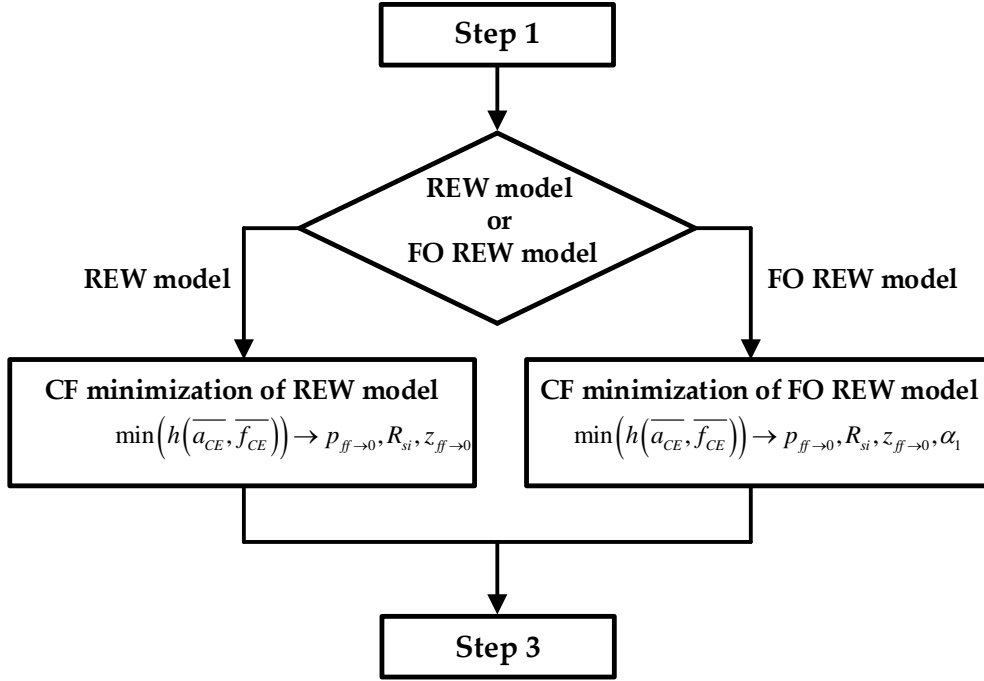
Fig. 3.2 Block diagram of step 2 of RT simulation, whose target is to find the initial parameters ($ff \rightarrow 0$) using the values of $\overline{f_{CE}}$ and $\overline{a_{CE}}$.

3. **Real-time estimation of *ff*:** The last step and the goal is to predict in RT the parameter *ff*. The computation of *ff*, once the initial parameters of the models are obtained (previous step), is performed for all the previous measurements and for all the measurements that will be performed until the end of the experiment. The Fig. 3.3 describes the whole prediction process. First, the time index *j* is initialized to start the estimation of *ff* from *j* = 1 to *j* = *jmax*. The CF minimization is different from the one performed in Chapter 2, since it must be more robust in order to obtain the parameters as accurately as possible. The minimization attempts to obtain the values for each *j*-measure of the parameters: *ff*, R_{gap}, $z_{ff \rightarrow 1}$ and ΔR_s (for the REW model), : *ff*, R_{gap}, $z_{ff \rightarrow 1}$ and α_2 (for the FO REW model). For this purpose, a loop is used to increment the index *j* from 1 to *jmax*. Inside the loop, for each value of *j*, the CF minimization function is used to obtain the candidate values of the parameters to be calculated that obtain a lower *fval* value. These candidate values are indexed by the indices *m* (from 1 to *mmax*) and *n* (from 1 to *nmax*). *m* and *n* index are internal to the CF minimization function, so the parameters computed inside the function (*ff*, R_{gap}, etc.) indexed with *m* and *n* are not the same as the parameters outside the function. When the parameters with the best *fval* (minimum *fval* values) are obtained, among all, the ones with the lowest *fval* are chosen and assigned as the values taken by the parameters for time *j*. Inside CF minimization function, the first step is to define the bounds of these parameters, which are shown in (3.2). *ff* bounds changes for each *j*-estimations, but the bounds of the others parameters remain constant for all

94
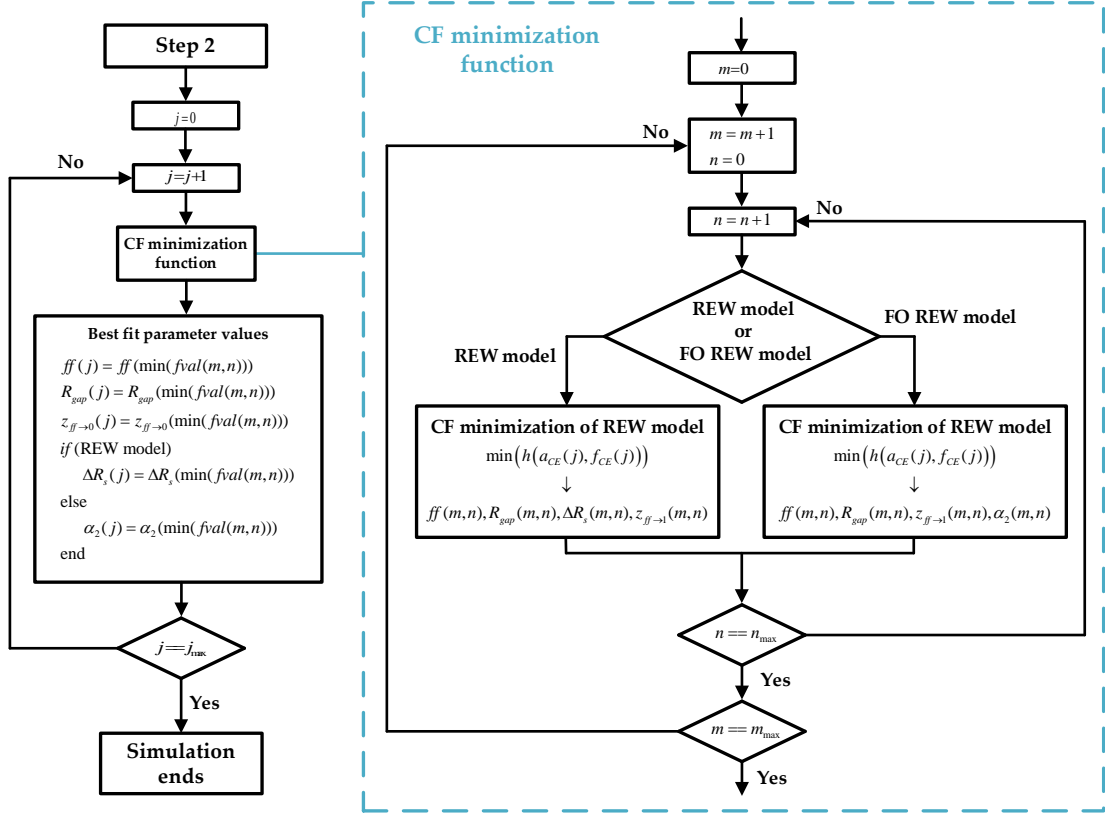
Fig. 3.3 Block diagram of step 3 of RT simulation. Describe, after obtaining the initial parameters, the simulation process from $j = 1$ to $j = j_{max}$.

j-estimations depending on the experience collected in the previous sections of this work.

$$ff^{bounds}(j) = \begin{bmatrix} f(j-1) - 0.2 & ff(j-1) + 0.2 \end{bmatrix}$$
$$R_{gap}^{bounds} = \begin{bmatrix} 0.1 & \infty \end{bmatrix} \quad z_{ff \to 1}^{bounds} = \begin{bmatrix} 10^3 & 10^5 \end{bmatrix} \tag{3.2}$$
$$\Delta R_s^{bounds} = \begin{bmatrix} -R_s^{ff \to 0} & 4 \cdot R_s^{ff \to 0} \end{bmatrix} \quad \alpha_2^{bounds} = \begin{bmatrix} 0.9 & \alpha_1 \end{bmatrix}$$

CF minimization is performed using as initial values those shown in (3.3). As can be seen, R_{gap}^{ini} and $z_{ff \to 1}^{ini}$ have four and two initial values, respectively. The index m moves along the vector R_{gap}^{ini} (from 1 to $m_{max} = 4$) and the index n moves along $z_{ff \to 1}^{ini}$ (from 1 to $n_{max} = 2$). This is due to the fact that for each j-estimation several minimizations of the CF are performed, as many as possible combinations of the initial values, i.e., eight minimizations. The main purpose of this approach is to find the point that achieves the lowest f_{val}, in a robust and computationally time efficient way. As a result, a matrix of values is obtained at each time j for each of the estimated parameters. This process is performed for each value of j, after which, when exiting the function and as already explained, the values of the parameters for which f_{val} is minimum are chosen (note that there is an f_{val} for each value of the matrix $m \times n$, and there is a matrix $m \times n$ for each value of j).

$$ff^{ini}(j) = ff(j-1)$$

$$R_{gap}^{ini} = \begin{bmatrix} 10 & 100 & 10^3 & 10^4 \end{bmatrix}$$

$$z_{ff \to 1}^{ini} = \begin{bmatrix} 10^3 & 10^4 \end{bmatrix} \tag{3.3}$$

$$\Delta R_s^{ini} = 0$$

$$\alpha_2^{ini} = 1$$

The steps described above are applied for each value of j for each well of each cell line, performing simulations that do not consider the future values of f_{CE} and a_{CE}, using the REW and FO REW models. The following subsection shows the results of this simulation procedure of the real CC assay experiments, which predicts the cell concentration in RT.

3.1.2   Real-time simulation results

The RT simulation method is finally designed to be implemented in a prototype to report the *ff* and cell concentration values after each measurement. As the required sampling time is 1 *h*, the time to perform all the necessary mathematical operations is not a critical point. This means that the computation time of the initial parameters, and of the *ff* and other parameters for each measurement, is not a critical problem.

Two metrics will be used to determine the level of accuracy of the method. The first is the error in the estimation of *ff*, and the second is the error in the calculation of the cell concentration. The error in the estimation of the fill factor will be measured with respect to the deviation from its ideal final value. It is considered that for the maximum *ff* obtained in the simulation, the error is the difference between the maximum value obtained and the maximum value that *ff* should reach, i.e., a value of 0.99. Thus, it is possible to calculate the real *ff* curve that should have been obtained for each well using the following equation,

$$ff_i(j) = k_{ff} \cdot ff_{sim}(j)$$

$$k_{ff} = \frac{0.99}{\max\left(ff_{sim}\right)} \tag{3.4}$$

where ff_{sim} is the vector of *ff* values obtained from RT simulation, ff_i is the vector of theoretically real values of *ff* and k_{ff} is the factor applied to ff_{sim} to obtain ff_i. The metrics for measuring accuracy are the mean relative error in the fill factor and the mean relative error in cell concentration, both in percent (%). The results for each of the cell lines are presented in the next three subsections.

3.1.2.1   AA8 results

This cell line is the one that should obtain better results, considering the Chapter 2, where the best results of modelling CE block were achieved with the AA8 cell line. The

following tables show the values of the initial parameters of the simulation in RT, i.e., when the simulator detects that the minimum f_{CE} and a_{CE} have been reached. Table 3.1 shows the values obtained using the REW model, while Table 3.2 shows the values obtained using the FO REW model. Large differences are observed between some of the parameter values of the two models, for example, between the parameters $R_{ct}^{ff \to 0}$, $p_{ff \to 0}$ and $z_{ff \to 0}$ of both models. This effect may be due to the fact that by introducing α_1, the other parameters do not have to adjust for the nonlinear behavior of the real CE system.

Table 3.1 Model parameters estimated at the beginning of the RT simulation ($ff \to 0$) for AA8 cell line (REW model with 10 microelectrodes and one reference electrode).

Well	$R_{ct}^{ff \to 0}$ [$M\Omega$]	$C_{dl}^{ff \to 0}$ [nF]	$R_{s}^{ff \to 0}$ [$k\Omega$]	$p_{ff \to 0}$ [Hz]	$z_{ff \to 0}$ [kHz]	ff_i
1	0.61	2.66	1.27	98.56	32.19	0.02
3	0.44	3.71	1.56	98.08	18.81	0.01
4	0.34	4.76	1.88	97.29	12.28	0.02
5	0.72	2.56	2.01	86.37	21.20	0.02
7	0.35	4.17	1.73	107.95	15.22	0.02
8	0.26	4.78	1.43	129.08	16.05	0.02

Table 3.2 Model parameters estimated at the beginning of the RT simulation ($ff \to 0$) for AA8 cell line (FO REW model with 10 microelectrodes and one reference electrode).

Well	$R_{ct}^{ff \to 0}$ [$M\Omega$]	$C_{dl}^{ff \to 0}$ [nF]	R_{s} [$k\Omega$]	$p_{ff \to 0}$ [Hz]	$z_{ff \to 0}$ [kHz]	α_1	ff_i
1	2.34	4.21	1.71	16.16	15.15	0.95	0.01
3	2.67	6.60	1.44	9.04	14.69	0.93	0.02
4	0.33	4.92	1.56	98.02	14.25	0.99	0.02
5	1.64	3.56	2.09	27.20	14.64	0.96	0.01
7	0.45	5.75	0.71	61.13	26.59	0.96	0.03
8	0.32	5.94	1.16	83.21	15.86	0.97	0.02

If the obtained values for the REW model (Table 3.1) are compared with the values obtained for the same model during the modeling (Table 2.7), it is observed that the new values have less dispersion. The differences during the estimation of the initial parameters are that $f_{CE}^{ff \to 0}$ and $a_{CE}^{ff \to 0}$ are obtained automatically, and that the value of ff parameter is estimated at the same time as the other parameters. The value of ff when f_{CE} and a_{CE} reach its minimum is named as ff_i. The fact that ff_i is estimated, gives more freedom to the other parameters to get closer to their correct value.

A similar situation appears with the parameters of the FO REW model of the Table 3.2 if they are compared with the Table 2.12. The values obtained for $ff \to 0$ in the RT simulation present less spread than those obtained during the modeling.

Fig. 3.4 and Fig. 3.5 illustrate the evolution of ff_{sim} and ff_i during the RT simulation of a RT simulation experiment for AA8 cells using the REW and FO REW models, respectively. As can be seen in the figures, the accuracy is considerably high, considering that the values of $f_{CE}^{ff \to 1}$ and $a_{CE}^{ff \to 1}$ are not known. Note also that the simulation performed with the REW model seems to be more accurate than the one performed with the FO REW model. The mean relative error (e_{rm}) is calculated using the following expression,

$$e_{rm} = \sum_j \frac{\left| ff_{sim}(j) - ff_i(j) \right|}{ff_i(j)}$$ (3.5)

where the sum of j is the sum of the expression for each calculated value of ff. Table 3.3 shows the mean relative errors per well using both models. This table confirms what was previously observed in the Fig. 3.4 and Fig. 3.5, by simulating in RT, more accurate results are obtained, in terms of ff, using the REW (IO) model than the FO REW model. Considering that the FO REW model should fit better to the behavior of the real CE system, the most likely explanation for its lower accuracy is that it is more complex, implying the estimation of more parameters, which can greatly change the other parameters. These parameters that are introduced in the FO REW model are the FO coefficients α_1 and α_2, which with a small change produce a considerable change in the other parameters, since in terms of bode diagrams (BD) they configure the slope of the magnitude and phase lines, as well as the degrees per pole or zero.

Table 3.3 Mean relative error (e_{rm}) per well for AA8 cell line. e_{rm} is shown for REW and FO REW models.

Well	1	3	4	5	7	8
e_{rm}^{REW} [%]	11.44	5.76	5.72	11.79	5.11	6.26
$e_{rm}^{FO\ REW}$ [%]	16.23	6.79	24.73	30.41	9.98	17.65

The final target of this work is the simulation of a RT experiment to know the cell concentration of a CC assay at each moment. In the following figures and tables, the level of accuracy of the cell concentration will be analyzed compared to the traditional optical counting method. Fig. 3.6 shows the cell concentration estimated in the RT simulation for N_{ini} of 2500, 5000 and 1000 cells. Lines blue and red present the cell concentration obtained by using the FO REW model using ff_{sim} and ff_i respectively. Lines yellow and purple present the cell concentration obtained by using the REW model using ff_{sim} and ff_i respectively. The last line, in green, present the cell concentration obtained using the traditional optical counting method. As can be seen, as for the ff curves (Fig. 3.4 and Fig. 3.5) the FO REW model performs a little worse than the REW model on the final point (t
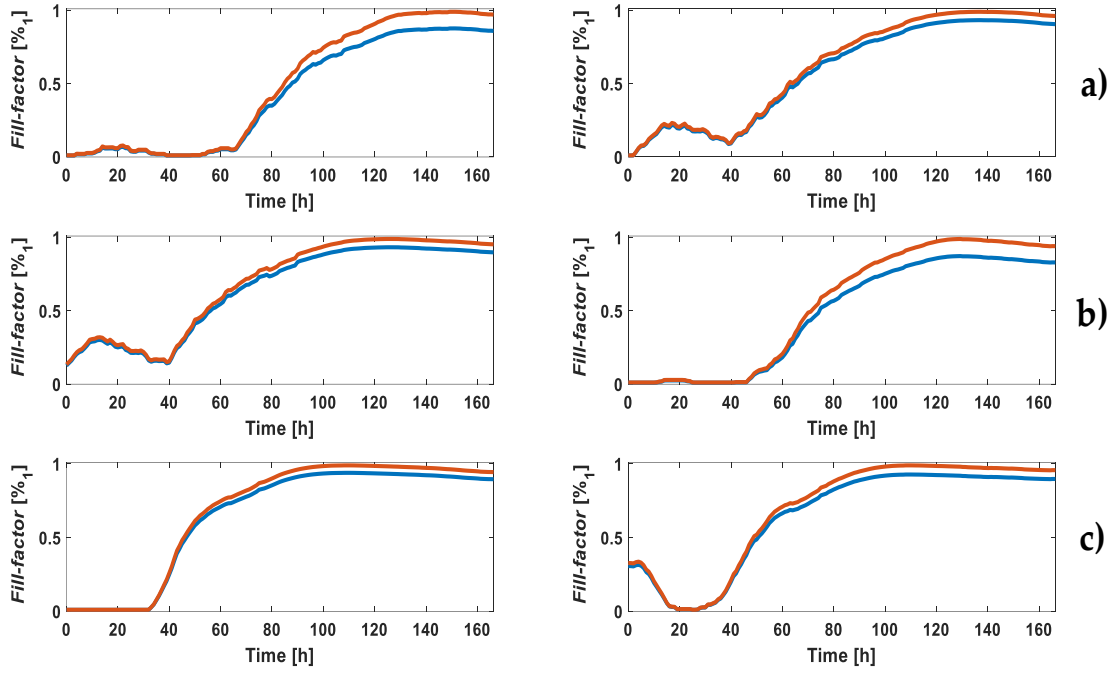
Fig. 3.4 *Fill-factor* evolution for each well of the experiment using the REW model in the RT simulation. *ff$_{sim}$* in blue and *ff$_i$* in red **a)** N_{ini}: 2500 cells (well 1 on the left and well 3 on the right). **b)** N_{ini} : 5000 cells (well 4 on the left and well 5 on the right). **c)** N_{ini} : 10000 cells (well 7 on the left and well 8 on the right).

Fig. 3.5 *Fill-factor* evolution for each well of the experiment using the FO REW model in the RT simulation *ff$_{sim}$* in blue and *ff$_i$* in red **a)** N_{ini}: 2500 cells (well 1 on the left and well 3 on the right). **b)** N_{ini} : 5000 cells (well 4 on the left and well 5 on the right). **c)** N_{ini} : 10000 cells (well 7 on the left and well 8 on the right).
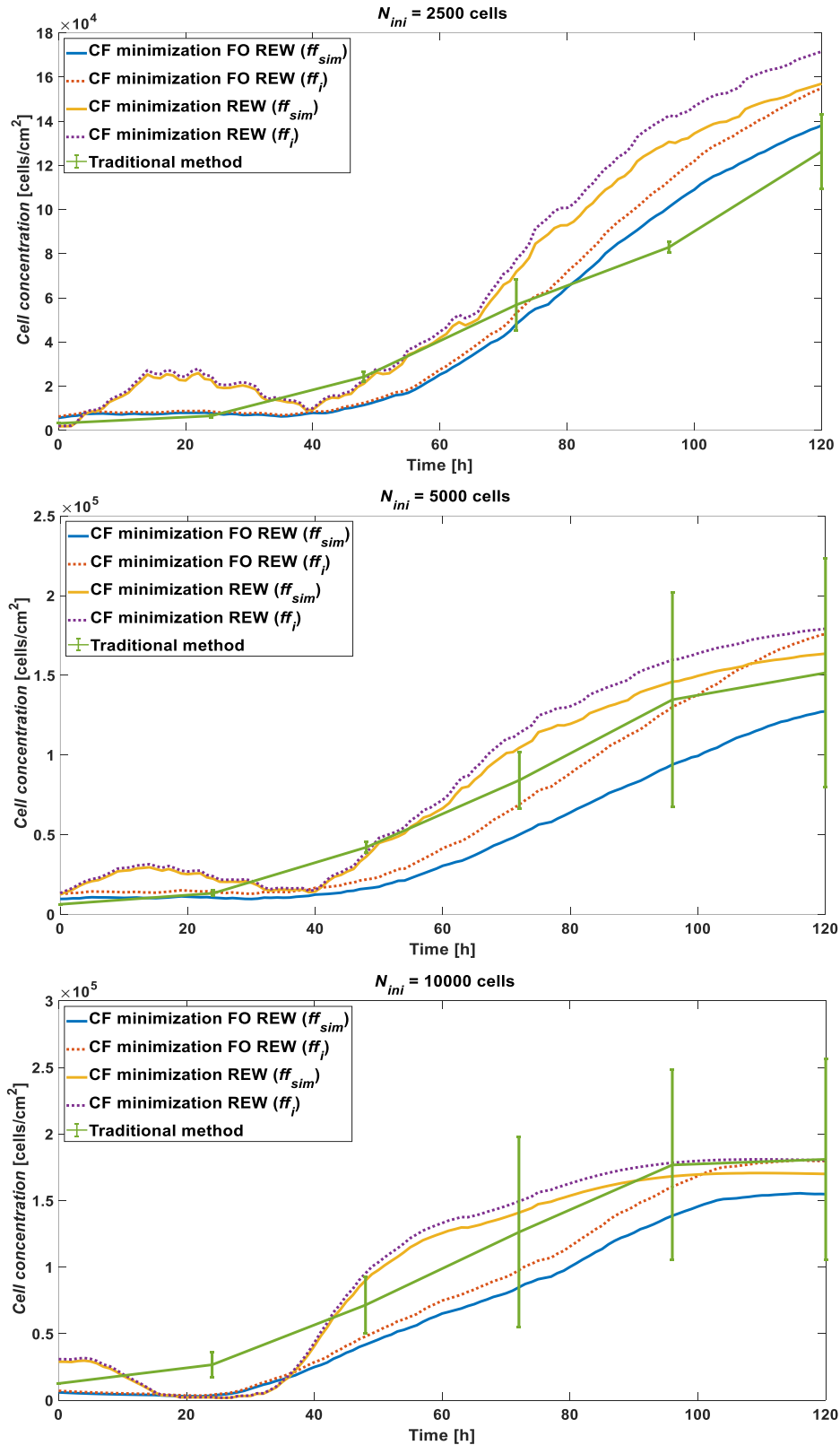
Fig. 3.6 AA8 cell line cell concentration comparison between RT simulation using FO REW model (obtained from ff_{sim} in blue and ff_i in red) and REW model (obtained from ff_{sim} in yellow and ff_i in purple), and traditional counting method (green).

= 120 h). In addition, the graphs also show that the higher the initial concentration, the more accurate the cell concentration estimation method. As a final point, notice that the RT experiment estimation method calculates the fill factor (and consequently the cell concentration) better at the beginning of the experiment than the estimation of the model parameters carried out in the Chapter 2. Therefore, it is concluded that the estimation of all parameters for each measurement of f_{CE} and a_{CE} is more accurate than using the parameter values calculated at the end of the experiment.

Finally, the mean relative error of the cell concentration (e_{rm}) will be calculated using the formulas as follows,

$$
\begin{aligned}
e_{rm.sim} &= \sum_{j_{trad}} \frac{\left|C_{sim}(j_{trad}) - C_{trad}(j_{trad})\right|}{C_{trad}(j_{trad})} \\
e_{rm.i} &= \sum_{j_{trad}} \frac{\left|C_i(j_{trad}) - C_{trad}(j_{trad})\right|}{C_{trad}(j_{trad})}
\end{aligned}
\tag{3.6}
$$

where j_{trad} is the index of the cell concentration obtained by traditional optical method (defined as C_{trad}), C_{sim} is the cell concentration calculated using ff_{sim}, and C_i is the cell concentration estimated using ff_i. Since the cell concentration vectors obtained in the RT simulation have many more points than the one obtained by the traditional method (sampling times of 1 h versus 1 day respectively), the error is estimated using the point j closest in time to the j_{trad} point. Table 3.4 contains the e_{rm} calculated from C_{sim} and C_i for the REW and FO REW model. The first point to note is that the average e_{rm} is high. However, note that the C_{sim} and C_i curves are closer to or in the error margins of Ctrad. Moreover, the tendency is similar. Therefore, the values are acceptable. On the other hand, although the graphs show that the FO REW model is less accurate at the end than the REW for the RT simulation, the e_{rm} values are lower for the FO REW model.

Table 3.4 Cell concentration mean relative error (e_{rm}) per N_{ini} for AA8 cell line. e_{rm} is shown for REW and FO REW models. The e_{rm} obtained from C_{sim} and C_i is calculated for each model.

N_{ini}	2500	5000	10000
$e_{rm.sim}^{REW}$ [%]	59.37	37.56	46.40
$e_{rm.i}^{REW}$ [%]	68.47	46.70	49.79
$e_{rm.sim}^{FO\ REW}$ [%]	33.34	36.79	40.70
$e_{rm.i}^{FO\ REW}$ [%]	41.04	31.61	31.19

The differences between $e_{rm.sim}$ and $e_{rm.i}$ are almost negligible considering the e_{rm} values. Although the e_{rm} values of Table 3.4 are better for FO REW model, the graph shows that at the end the REW model gives better results. Finally, note that the FO REW model returns better results in terms of the trend of the curve (first hours of the experiment), as it is similar to that obtained by traditional methods. This may be due to

the greater complexity of the model, which better describes the real dynamics of the growth of a CC assay.

In the conclusions of Chapter 2, it was discussed that the electrical model of the CE block can be fitted using the OBT values of f_{CE} and a_{CE} at the beginning $(ff \to 0)$ and at the end $(ff \to 1)$ of the experiment. In the current chapter, it has been found that, at least for the best performing cell line (AA8), it is possible to determine the cell concentration in RT during a laboratory experiment. By implementing the algorithm in the OBT prototype (which includes a microcontroller [47]), it is possible to calculate the cell concentration in RT (each time a measurement of f_{CE} and a_{CE} is taken) in an experiment with a CC assay. This is a significant improvement in the field of biology, because the time and economic savings are very large. It is one of the main contributions of this thesis, with which biological and medical research processes can be optimized, and go further with the research or invest the saved resources in another research.

3.1.2.2 N2a results

In this section the results of the RT simulation for the N2a line will be presented. The simulation is performed in the same way as for the AA8 cell line (3.1.2.1). Then, the first data to report are the initial parameters derived during the first hours of the RT simulation. Table 3.5 and Table 3.6 shows the initial parameters from simulations using both models, REW and FO REW model. As is the case for the AA8 cell line, the $R_{ct}^{ff \to 0}$ and $p_{ff \to 0}$ parameters have a higher dispersion using the FO REW model. This is mainly due to the estimation of $p_{ff \to 0}$, which directly influences the calculation of $R_{ct}^{ff \to 0}$ (equation (2.78)). The values of $p_{ff \to 0}$, in some cases, are much lower (almost an order of magnitude) for the FO REW model than for the REW model. A small fluctuation of α_1 can produce these changes, since it changes the slope of the BD of the model. Moreover, taking into account that this cell line has a low Δa_{CE}, and knowing that the value of $p_{ff \to 0}$ is largely determined by $f_{CE}^{ff \to 0}$ and $a_{CE}^{ff \to 0}$ [55], it is expected that more deviations can be seen in the FO REW model as it is more sensible.

Table 3.5 Model parameters estimated at the beginning of the RT simulation $(ff \to 0)$ for N2a cell line (REW model).

Well	$R_{ct}^{ff \to 0}$ [$M\Omega$]	$C_{dl}^{ff \to 0}$ [nF]	$R_{s}^{ff \to 0}$ [$k\Omega$]	$p_{ff \to 0}$ [Hz]	$z_{ff \to 0}$ [kHz]	ff_i
2	0.41	3.95	1.68	98.88	16.53	0.004
3	0.38	3.86	1.66	107.94	17.04	0.006
4	0.36	3.69	1.68	121.68	17.67	0.006
6	0.32	4.87	1.43	102.68	15.67	0.004
7	0.32	4.66	1.74	106.60	13.54	0.001
8	0.30	5.49	2.00	95.19	10.00	0.040

Table 3.6 Model parameters estimated at the beginning of the RT simulation
($ff \rightarrow 0$) for N2a cell line (FO REW).

Well	$R_{ct}^{ff \rightarrow 0}$ [$M\Omega$]	$C_{dl}^{ff \rightarrow 0}$ [nF]	R_s [$k\Omega$]	$p_{ff \rightarrow 0}$ [Hz]	$z_{ff \rightarrow 0}$ [kHz]	α_1	ff_i
2	1.57	6.56	1.58	15.47	10.49	0.94	0.007
3	0.48	4.30	1.88	77.93	13.52	0.99	0.010
4	1.09	6.70	1.28	21.75	12.73	0.93	0.020
6	0.37	4.97	1.81	87.05	12.15	0.99	0.001
7	0.38	5.48	1.45	76.30	13.74	0.98	0.017
8	0.23	5.04	1.45	137.59	15.00	1.01	0.044

Table 3.7 displays the e_{rm} of the ff_{sim} using as reference ff_i. As can be seen, e_{rm} in terms of ff is much larger for N2a cell line than for AA8. This was expected, since worse results were obtained in Chapter 2 for the N2a and N2aAPP lines than for AA8, as explained in 2.1.5.5.2. Notice that the e_{rm} of the ff does not follow a pattern as a function of N_{ini}. An interesting fact is that the e_{rm} of the ff generated from the FO REW model in the simulation is larger than the e_{rm} of the ff generated from the REW model.

Table 3.7 Mean relative error (e_{rm}) per well for N2a cell line. e_{rm} is shown for REW and FO REW models.

Well	2	3	4	6	7	8
e_{rm}^{REW} [%]	19.51	19.00	12.68	7.73	11.87	13.48
$e_{rm}^{FO\ REW}$ [%]	28.13	52.81	19.29	29.55	33.23	39.82

The e_{rm} values shown in the table above are obtained from Fig. 3.7 and Fig. 3.8. Figures clearly show very large differences between ff_{sim} and ff_i. The hypothesis to explain such high errors is the same as in 2.1.5.5.2, the differences in Δa_{CE}. And the solution, in the same way, is still to tune the BPF to a higher frequency (around 10 kHz).

Table 3.8 Cell concentration mean relative error (e_{rm}) per N_{ini} for N2a cell line. e_{rm} is shown for REW and FO REW models. The e_{rm} obtained from C_{sim} and C_i is calculated for each model.

N_{ini}	2500	5000	10000
$e_{rm.sim}^{REW}$ [%]	372.52	154.33	83.80
$e_{rm.i}^{REW}$ [%]	430.92	173.84	91.49
$e_{rm.sim}^{FO\ REW}$ [%]	205.13	100.82	56.00
$e_{rm.i}^{FO\ REW}$ [%]	275.54	129.35	55.11

While the Fig. 3.9 presents the evolution of C_{sim} and C_i versus C_{trad} for the N2a cell line, the Table 3.8 shows the errors of these concentrations. Of course, the C_{trad} time vector had to be advanced 48 h to match the dynamics, as discussed in 2.1.5.5.1. The figure shows that, in terms of the final value of cell concentration ($t = 120\,h$), C_{sim} is always more distant than C_i from C_{trad}. This does not necessarily mean that it is a worse fit, since the table shows slightly worse e_{rm} values for C_i than for C_{sim} for any N_{ini}. On the other hand, note that C_i in the figure fits much better to C_{trad} if the first hours of the simulation are excluded. Finally, although the cell concentration obtained from the FO REW model achieves significantly lower e_{rm}, notice that it is closer to the real dynamics at the beginning of the experiment but from the middle to the end of the simulation, the FO REW model does not produce as good results as the REW model.
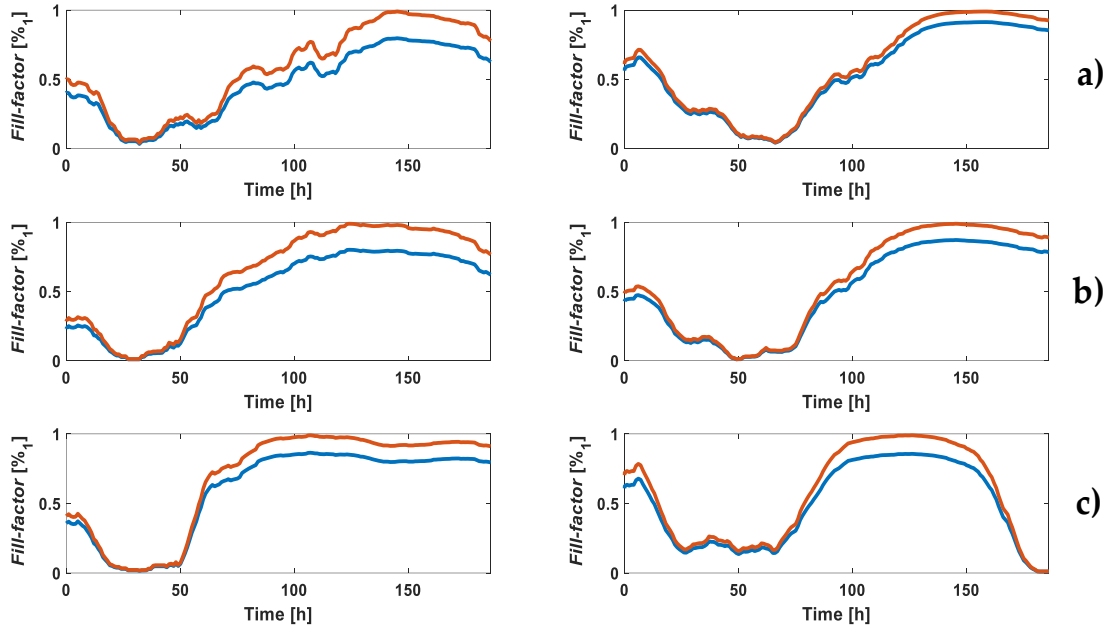
Fig. 3.7 *Fill-factor* evolution for each well of the experiment using the REW model in the RT simulation. *ff*$_{sim}$ in blue and *ff*$_i$ in red **a)** N_{ini}: 2500 cells (well 2 on the left and well 6 on the right). **b)** N_{ini} : 5000 cells (well 3 on the left and well 7 on the right). **c)** N_{ini} : 10000 cells (well 4 on the left and well 8 on the right).
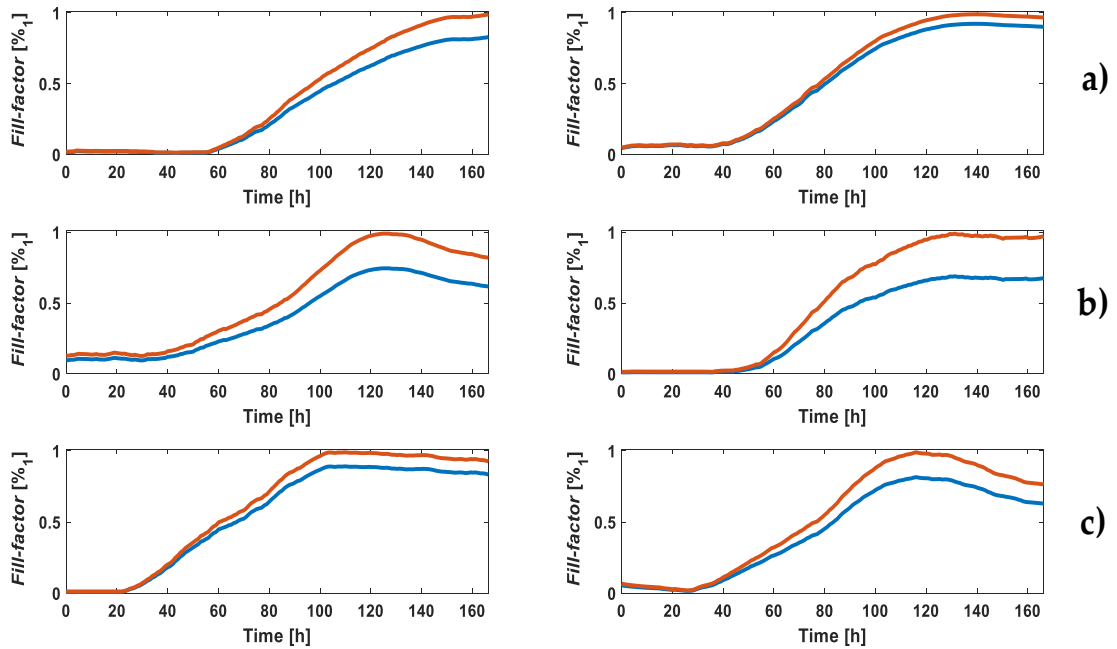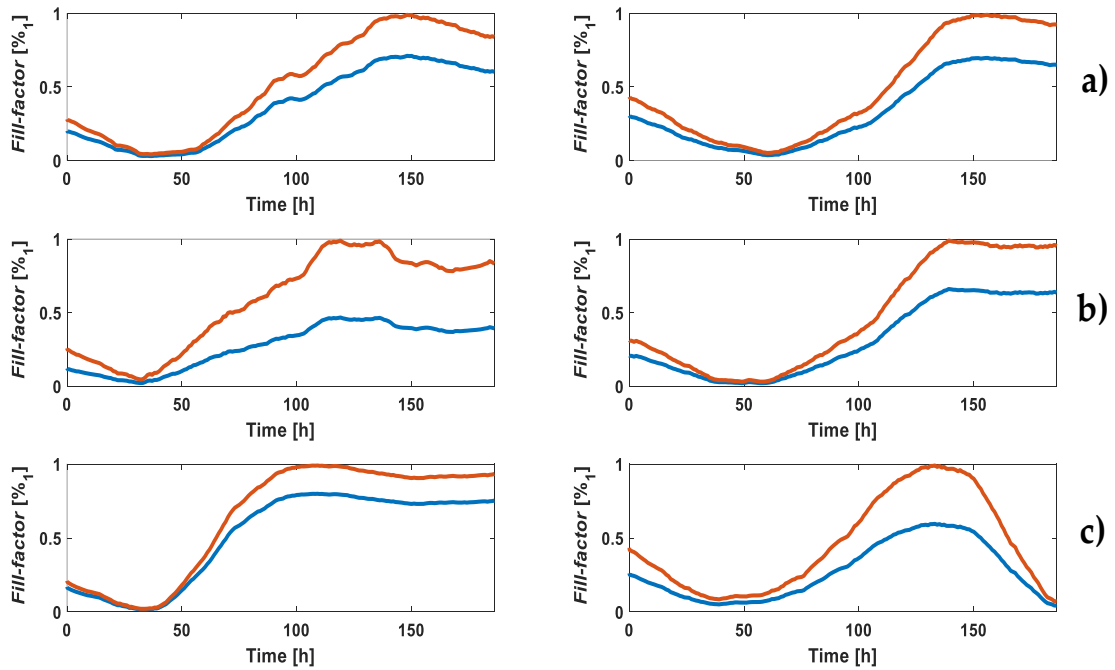

Fig. 3.8 *Fill-factor* evolution for each well of the experiment using the FO REW model in the RT simulation *ff*$_{sim}$ in blue and *ff*$_i$ in red **a)** N_{ini}: 2500 cells (well 1 on the left and well 3 on the right). **b)** N_{ini} : 5000 cells (well 4 on the left and well 5 on the right). **c)** N_{ini} : 10000 cells (well 7 on the left and well 8 on the right).
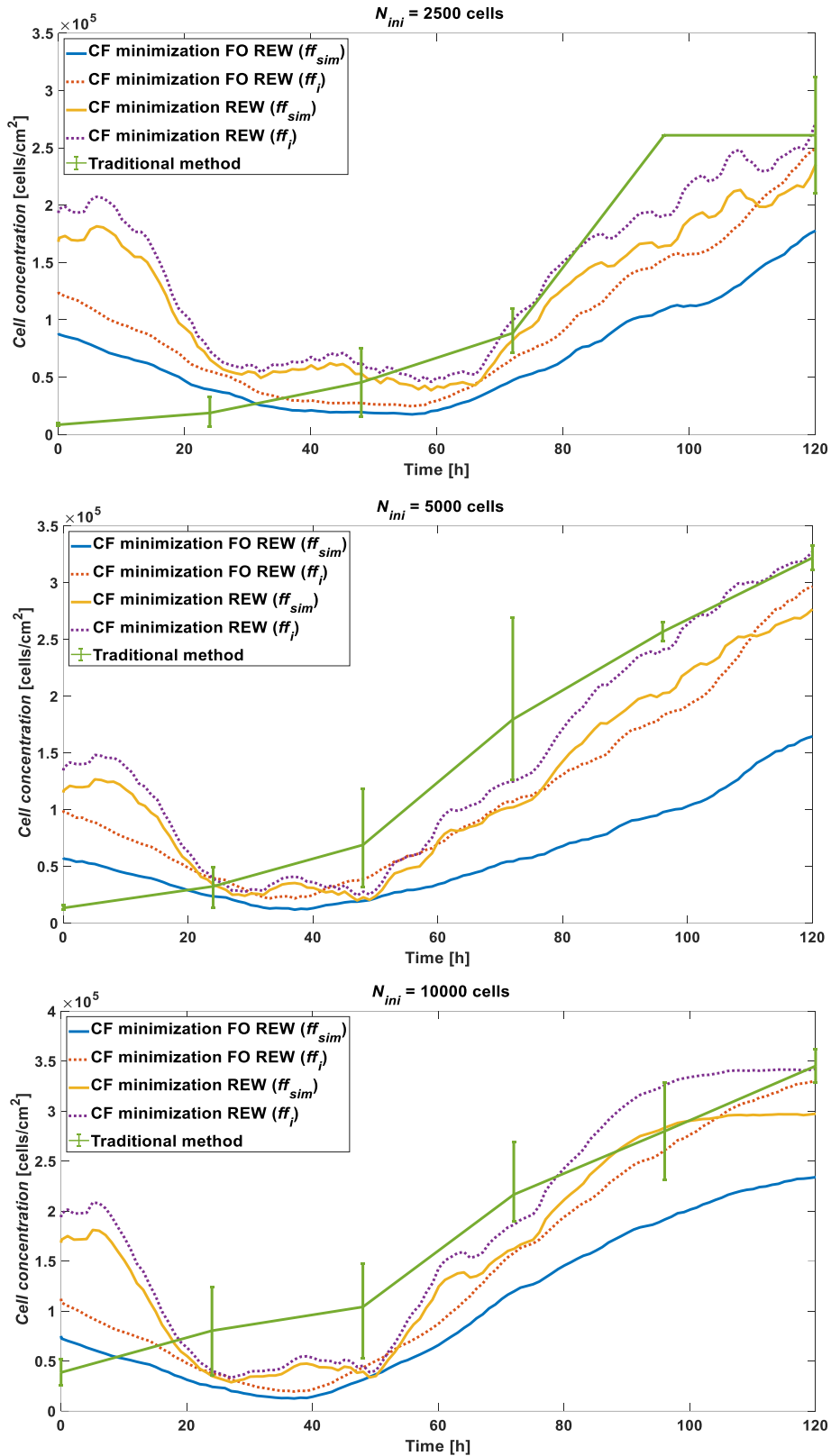
Fig. 3.9 N2a cell line cell concentration comparison between RT simulation using FO REW model (obtained from *ff*$_{sim}$ in blue and *ff*$_i$ in red) and REW model (obtained from *ff*$_{sim}$ in yellow and *ff*$_i$ in purple), and traditional counting method (green).

A RT experiment has been simulated based on the f_{CE} and a_{CE} data obtained in a real experiment. The error data from the simulation suggest that it is possible to estimate the cell concentration of this cell line using an oscillator circuit (OBT). To improve the accuracy of the cell concentration, the OBT prototype must be reconfigured, in particular, the cutoff frequency of the BPF. If the frequency response of the CE block of the AA8 line is observed (Fig. 2.19), the $1\,kHz$ zone has less variation between $ff \to 0$ and $ff \to 1$. Therefore, it would be easier to obtain measurements in a zone with a larger range.

3.1.2.3   N2aAPP cell line results

In this section the results of RT simulation of the N2aAPP cell line are presented. As in the previous subsections, the values of the initial parameters, the *ff* and cell concentration graphs, as well as the erm of each well in terms of *ff* and concentration in terms of N_{ini} will be presented. The results presented include the simulation using the REW model and the FO REW model. Table 3.9 and Table 3.10 present the values of the initial parameters using the REW model and the FO REW model, respectively. Both the range of values and the dispersion of some parameters of the FO REW model are as expected after analyzing the AA8 and N2a cell lines previously. Therefore, these results will not be discussed again in this section.

Table 3.9 Model parameters estimated at the beginning of the RT simulation
($ff \to 0$) for N2aAPP cell line (REW model).

Well	$R_{ct}^{ff \to 0}$ [$M\Omega$]	$C_{dl}^{ff \to 0}$ [nF]	$R_{s}^{ff \to 0}$ [$k\Omega$]	$p_{ff \to 0}$ [Hz]	$z_{ff \to 0}$ [kHz]	ff_i
2	0.61	3.20	2.38	81.65	14.35	0.003
3	0.48	3.04	1.74	110.17	20.65	0.011
4	0.35	4.00	1.67	114.96	16.39	0.003
6	0.45	3.45	1.35	102.68	23.38	0.004
7	0.44	3.50	1.44	103.01	21.73	0.006
8	0.23	4.73	1.57	143.89	14.79	0.005

Table 3.10 Model parameters estimated at the beginning of the RT simulation
($ff \to 0$) for N2aAPP cell line (FO REW).

Well	$R_{ct}^{ff \to 0}$ [$M\Omega$]	$C_{dl}^{ff \to 0}$ [nF]	R_{s} [$k\Omega$]	$p_{ff \to 0}$ [Hz]	$z_{ff \to 0}$ [kHz]	α_1	ff_i
2	2.32	5.19	1.81	13.20	11.61	0.94	0.003
3	1.50	5.11	1.60	20.78	13.30	0.94	0.001
4	1.03	6.80	1.52	22.63	10.57	0.94	0.012
6	2.69	6.24	1.29	9.49	13.50	0.93	0.004
7	2.55	6.32	1.34	9.89	12.89	0.93	0.007
8	0.28	5.59	1.43	103.03	13.73	0.98	0.001
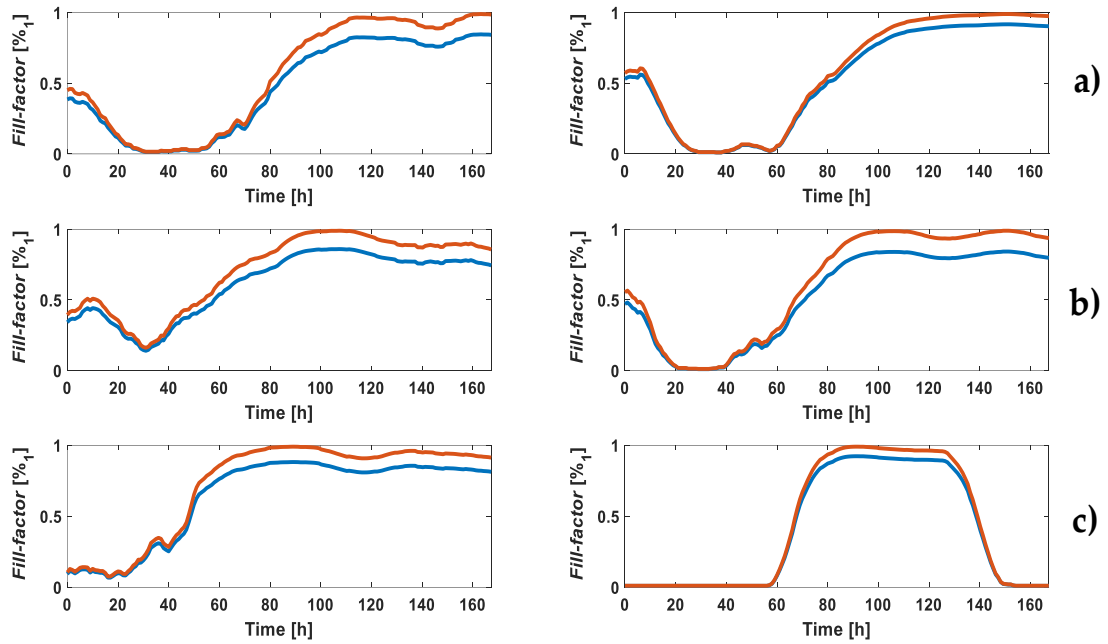
Fig. 3.10 *Fill-factor* evolution for each well of the experiment using the REW model in the RT simulation. *ff*$_{sim}$ in blue and *ff*$_i$ in red **a)** N_{ini}: 2500 cells (well 2 on the left and well 6 on the right). **b)** N_{ini} : 5000 cells (well 3 on the left and well 7 on the right). **c)** N_{ini} : 10000 cells (well 4 on the left and well 8 on the right).
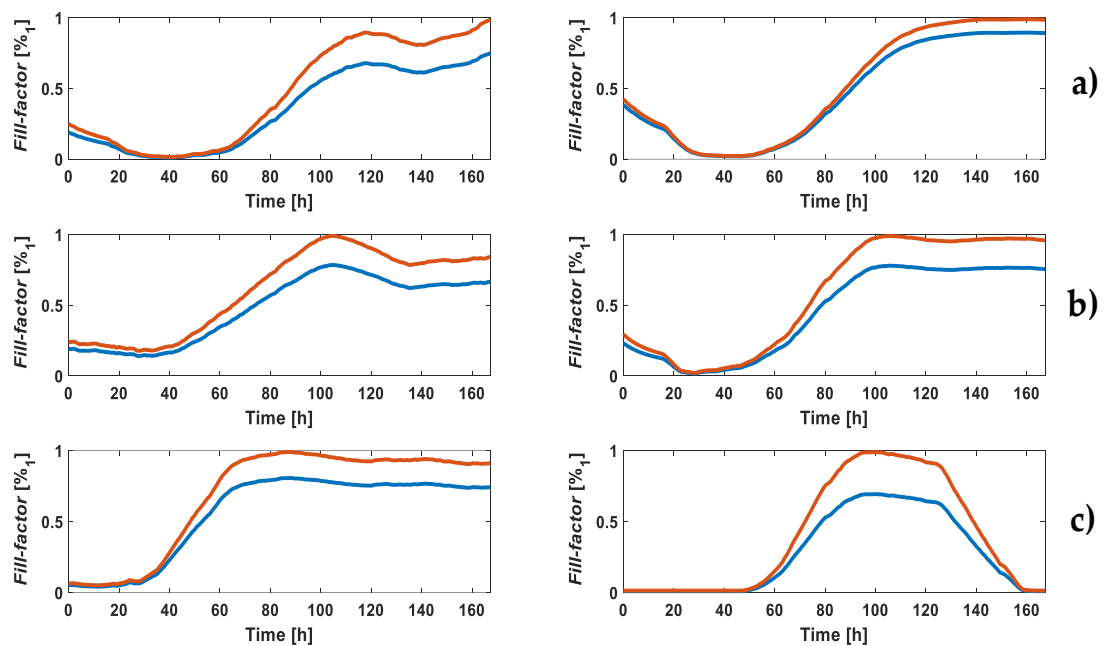
Fig. 3.11 *ff* evolution for each well of the experiment using the FO REW model in the RT simulation *ff*$_{sim}$ in blue and *ff*$_i$ in red **a)** N_{ini}: 2500 cells (well 1 on the left and well 3 on the right). **b)** N_{ini} : 5000 cells (well 4 on the left and well 5 on the right). **c)** N_{ini} : 10000 cells (well 7 on the left and well 8 on the right).

Fig. 3.10 and Fig. 3.11 shows show the *ff* (*ff*$_{sim}$ and *ff*$_i$) using the REW and FO REW models, respectively. As with the AA8 line, the FO REW model predicts the cell culture

growth dynamics better than the REW model. This means that the RT simulation works better for the N2aAPP cell line than for the N2a line. As discussed in the 2.1.5.5.2, this may be due to the Δa_{CE} and the A_{cell}. Even so, as expected, the results do not reach a level of accuracy similar to those of the AA8 cell line. To know the degree of accuracy, the e_{rm} of ff is used, which is illustrated for both models used in Table 3.11. The e_{rm} in terms of ff obtained for the N2aAPP line is similar to that obtained for the N2a cell line, and worse than that of the AA8 line.

Table 3.11 Mean relative error (e_{rm}) per well for N2aAPP cell line. e_{rm} is shown for REW and FO REW models.

Well	2	3	4	6	7	8
e_{rm}^{REW} [%]	14.53	13.13	10.93	7.34	14.89	6.80
$e_{rm}^{FO\ REW}$ [%]	24.20	20.78	18.47	9.58	21.25	29.93

The cell concentration graphs generated during the RT simulation of the N2aAPP cell line are shown in Fig. 3.12. The same details as in Fig. 3.9 of line N2a can be observed: The REW model gives better results in the final half of the experiment, while the FO REW model fits better to the initial dynamics. Actually, contrary to the N2a line, the graph of N_{ini} = 10000 *cells* manages to match the growth dynamics in a similar way as the AA8 line does. This could be due to the cells of the N2aAPP cell line would take less time to adhere to the bottom of the well, or some other characteristic of this cell line. It should be studied in depth in future work.

Table 3.12 shows the e_{rm} of the cell concentration, in the same way as in the analysis of the results of cell lines AA8 and N2a. In this case the errors are very large for N_{ini} values of 2500 and 5000 cells compared to the other two lines. This is due, mostly, to the fact that at the beginning of the experiment (first hours and/or days) the errors are very high. In the following subsection the results of the three lines will be analyzed, compared and some conclusions will be presented. As in the previous subsections, a RT estimation (simulation) of the cell concentration of the N2aAPP cell line has been achieved using an oscillator. The method of minimizing a CF seems to work, although it needs to be improved, both the algorithm and the OBT measurement prototype.

Table 3.12 Cell concentration mean relative error (e_{rm}) per N_{ini} for N2aAPP cell line. e_{rm} is shown for REW and FO REW models. The e_{rm} obtained from C_{sim} and C_i is calculated for each model.

N_{ini}	2500	5000	10000
$e_{rm.sim}^{REW}$ [%]	396.43	219.13	25.51
$e_{rm.i}^{REW}$ [%]	443.78	271.15	22.31
$e_{rm.sim}^{FO\ REW}$ [%]	238.65	102.22	45.56
$e_{rm.i}^{FO\ REW}$ [%]	276.67	135.65	30.58
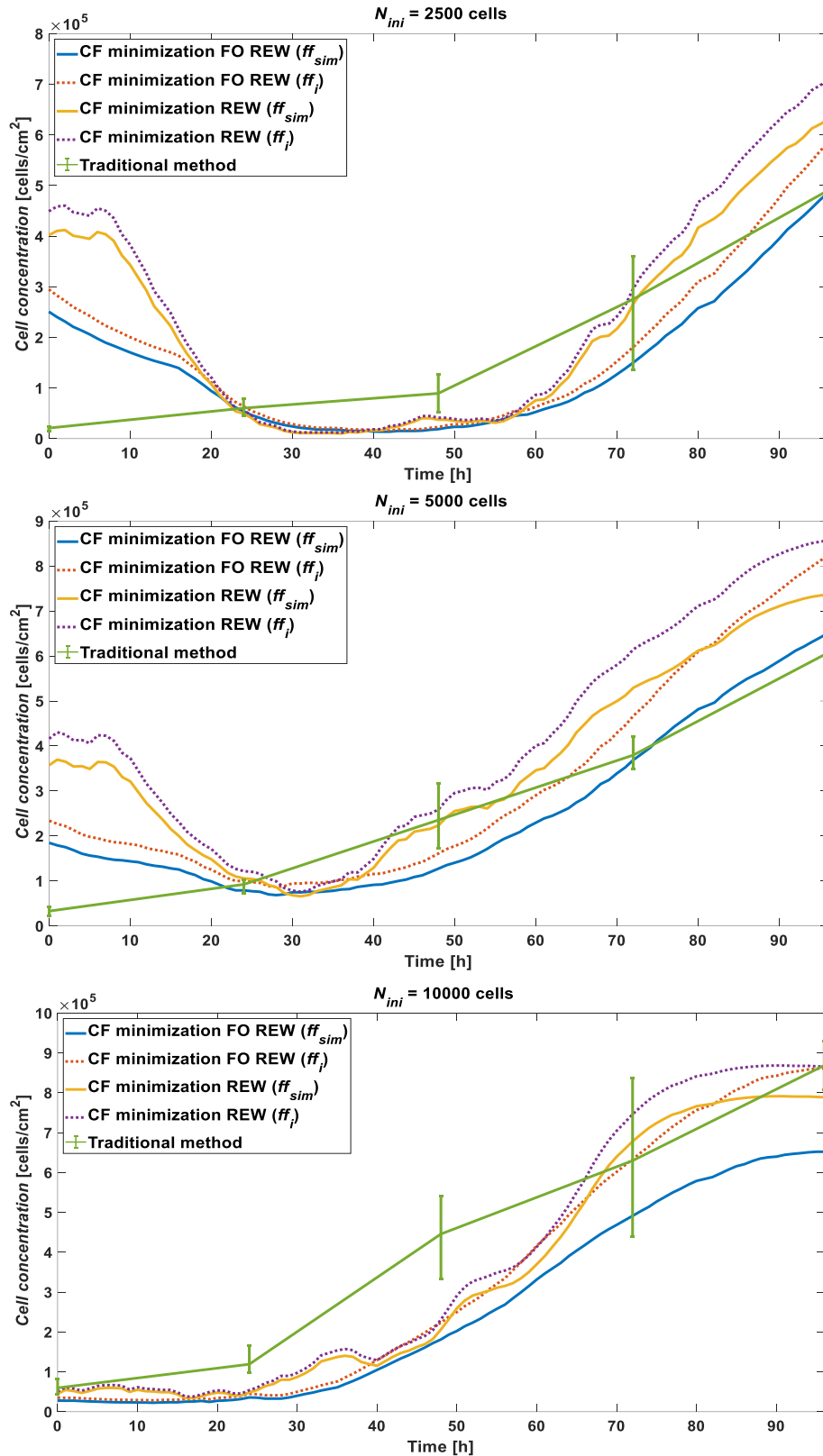
Fig. 3.12 N2aAPP cell line cell concentration comparison between RT simulation using FO REW model (obtained from ff_{sim} in blue and ff_i in red) and REW model (obtained from ff_{sim} in yellow and ff_i in purple), and traditional counting method (green).

3.1.2.4   Comparison of cell line results

In this subsection, the RT simulation results of the three cell lines used in this thesis (AA8, N2a and N2aAPP) are compared. The data will be analyzed and compared, as well as divided into sections of the experiment. There are two main sections of interest: the initial section, where the cells adapt to the culture medium and adhere to the bottom of the well, and the section from the beginning of growth (exponential phase) to the saturation phase of the well ($ff \rightarrow 1$).

The Table 3.13 shows the e_{rm} of the cell concentration for the three cell. The error shown is the e_{rm} of the cell concentration curves during the first hours and/or days of the experiment, i.e., from the time the CC assay is seeded until the moment when it starts to grow significantly (beginning of the exponential phase).

Table 3.13 Cell concentration mean relative error, in %, before the beginning of CC assay growth ($t < 40\ h$).

N_{ini}	2500			5000			10000		
Line	AA8	N2a	Na2APP	AA8	N2a	Na2APP	AA8	N2a	Na2APP
$e_{rm.sim}^{REW}$	120.6	1082.9	946.0	88.8	390.4	515.9	111.1	200.2	31.4
$e_{rm.i}^{REW}$	128.9	1252.4	1056.6	101.1	472.5	616.7	118.6	230.6	25.6
$e_{rm.sim}^{FO\ REW}$	52.5	518.6	535.4	38.5	176.4	229.2	69.7	78.9	62.2
$e_{rm.i}^{FO\ REW}$	68.3	771.4	629.5	55.2	327.9	295.9	64.1	117.4	52.5

As expected from the cell concentration plots the e_{rm} in the first simulation period are larger than the total erm. Specifically, the REW model returns much larger errors than the FO REW, since it does not obtain good results for low *ff*, as previously discussed. The opposite case is the e_{rm} for the second part of the simulation, which are detailed in the Table 3.14.

Table 3.14 Cell concentration mean relative error, in %, after the beginning of CC assay growth ($t > 40\ h$).

N_{ini}	2500			5000			10000		
Line	AA8	N2a	Na2APP	AA8	N2a	Na2APP	AA8	N2a	Na2APP
$e_{rm.sim}^{REW}$	28.7	17.3	30.0	11.9	36.3	21.3	14.0	25.6	21.6
$e_{rm.i}^{REW}$	38.3	20.2	35.2	19.5	24.5	40.8	15.4	21.9	20.1
$e_{rm.sim}^{FO\ REW}$	23.8	48.4	40.8	35.9	63.0	17.6	26.2	44.5	34.5
$e_{rm.i}^{FO\ REW}$	27.4	27.6	41.4	19.8	30.1	28.8	14.8	23.9	15.9

As expected, the e_{rm} in the second half of the simulation is much lower than in the first half. The most notable difference is found in the simulations using the REW model, since there is a large difference in error between the first and second frame, with the

second one providing much better results (at the accuracy level of FO REW model). Another point to note is that, in general, better results are obtained at higher Nini. Finally, it should be pointed out that the first section of the simulation is not as important in terms of predicting *ff* and cell concentration. Therefore, these data are quite acceptable, and provide a useful starting point for an improvement in the models and the method of simulation and parameter computation.

Separate analysis of the two zones of the experiment has provided interesting results. The cell concentration of a CC assay can be estimated in RT by connecting the CC assay as a load to an OBT. The errors are still large, but with some improvements of the algorithm, and of the OBT measurement prototype, the error should be greatly reduced.

3.2 Electrical simulation of the Bio-Oscillator

In the previous sections and chapters, the cell concentration in a CC assay has been obtained from the oscillation data of the electronic system where the CE block is connected as a load to the OBT circuit. Apparently, the results are acceptable as the obtained cell concentration has been compared with the measured cell concentration obtained by traditional optical counting method. Oscillation amplitude and frequency are the key parameters to achieve the main goal: provide the cell concentration of a CC assay experiment in RT. On the other hand, the oscillator must be designed to produce self-sustained oscillations. This point requires to perform electrical simulations (ES) of the oscillator, which should consider similar load values to the CE block. In this way it is possible to know the response of the system to different values of *ff* and other parameters of the electrical model. Prior to performing the experiments to obtain the experimental amplitude and frequency values, electrical simulations of the oscillator were carried out considering values of the model parameters obtained theoretically. In future work, the oscillator prototype will be modified, so it is crucial to have very accurate values of the model parameters, so that the prototype and the results obtained are as optimal and accurate as possible. Therefore, because of the relevance of the electrical simulations, it should be ensured that the values of the model parameters calculated in the previous sections can be used in future electrical simulations.

In the current subsection ES of the oscillator will be performed, using the values of the model parameters previously obtained. The simulations will be performed using the electrical simulator Ngspice [61], but with the difference that all the electrical simulations are launched from Matlab. As a comparison metric, the amplitude and frequency data will be obtained using the method of minimization of a CF, and the error with respect to the amplitudes and frequencies obtained in a real experiment will be calculated. The same error will be estimated for the results of the electrical simulations and the error of both methods will be compared. As in the previous subsections, tests will be performed using data from cell lines AA8, N2a and N2aAPP.

3.2.1 Electrical simulator and its integration in Matlab

The electrical simulator used is Ngspice, which is an open-source Spice simulator for electric and electronic circuits. All its documentation can be found at [61]. Ngspice is used in this work due to the fact that it can be launched from Matlab using commands through the *system* function.

To simulate the oscillator circuit in order to reproduce each point of the experiments performed, it is necessary to perform as many simulations as amplitude and frequency measurements have been taken in each of the experiments with the different cell lines. Considering that the time between each sample taken is 1 *h*, and that the experiments have a duration of between 6 and 9 days, at least 170 simulations must be performed for each cell line. This is unmanageable, since editing each of the components of the electrical model of the CE block one by one would be too laborious. All this without considering that exporting the results to Matlab for processing becomes really impractical. For these reasons, Matlab and Ngspice are connected to each other to edit, simulate and process the data automatically.

Section 3.1.1 presents the simulation routine of the system under test using mathematical methods of a CF minimization. These simulations emulate a RT experiment in which the future values of f_{CE} and a_{CE} are not known, recalculating certain model parameters for each measurement of f and a. In this way, acceptable results were achieved in predicting the behavior of the cell concentration of a CC assay. The initial parameters calculated in mentioned section, together with the parameters that are reevaluated for each measurement of f_{CE} and a_{CE}, will be introduced in the electrical simulator to reproduce the frequency and amplitude values obtained experimentally.

The whole circuit (oscillator plus the electrical model of the CE block has been implemented in Spice language with the same topology and characteristics as described in section 2.1.4. Notice that the file which contains the electrical model of the CE block can be easily replaced to switch between the different electrical models (SEW, REW and FO REW). The details, step by step, of the electrical simulation using Matlab in combination with Ngspice are described below:

1. **Edit the model netlist.** The oscillator circuit is not modified from one measurement to another. Therefore, the part of the circuit to be edited is the CE block model. This block, composed of passive components, is defined by the model used, which can be SEW, REW and FO REW. There is a text file in Spice language defining the structure of the CE model to be used in the simulations. For each actual measurement of f_{CE} and a_{CE}, the CF minimization method obtained the values of the model parameters. Matlab edits the Spice file that contain the model to include the values of the passive components of the CE model. Matlab does it automatically, using string replacement. In this way it is not necessary to edit the values one by one before each electrical simulation.

2. **Run the simulation.** As previously mentioned, an electrical simulation with Ngspice can be executed from Matlab using commands. The simulation is run in a single command line, choosing certain options, the Spice file to be simulated and the files where the results are stored. Using commands, it is not possible to choose the analysis time to be performed (DC, transient, AC, etc.), neither the variables to be displayed and saved at the end of the simulation. All this is included in the Spice file to be simulated. For this reason, a script has been designed to which the Spice file to be simulated, the analysis to be performed, the necessary parameters for the analysis and the variables to be saved at the end of the simulation are provided. This Matlab script or function works as a mask to automate the process of editing the type of analysis and the results to be shown, since for a user not used to the use of Spice, it can be useful to launch in a simple way from Matlab some electrical simulations in Spice (for example, for educational purposes). As in step 1, the script inserts the necessary code into the Spice file to perform the required analysis.

3. **Results generation.** After finishing the simulation, the script described in step 2 extracts the variables to be saved from a text file generated by Ngspice. This file contains the information of the variables that have been requested to be saved. These variables are stored in a Matlab struct variable that contains their names and values, as well as other variables that may be necessary for their interpretation (e.g., time).

Using the mixed electrical simulation technique which involves Matlab and Ngspice, it is possible to automate the process of CE block configuration, electrical simulation and data analysis, which is much more efficient than performing the simulations one by one. All the scripts to perform the simulations using Matlab are in **Appendix B**. The function *simOBTngspice* is the main function, managing the whole simulation. Function *editBioZngspice* edits automatically the netlist of the CE model used. *ngspiceSim* is the function that manages the simulation of a spice circuit, launching Ngspice from Matlab and processing the results. The function *getfA* obtains the frequency and amplitude of a sine wave without using the Fast Fourier Transform.

3.2.2 Electrical simulation using REW electric model

Due to the fact that the SEW model is less accurate, responds worse to possible perturbations (an example is the values of f_{CE} and a_{CE} at the beginning of an experiment) and the parameter values obtained are not close to those theoretically expected (because it is not the real model), it is decided to implement the REW model for the electrical simulations. These electrical simulations are performed as explained in the previous subsection and using the data from the three cell lines. As an example of the result of the electrical simulation, Fig. 3.13 shows the V_{CE} voltage waveform (at the bottom of the
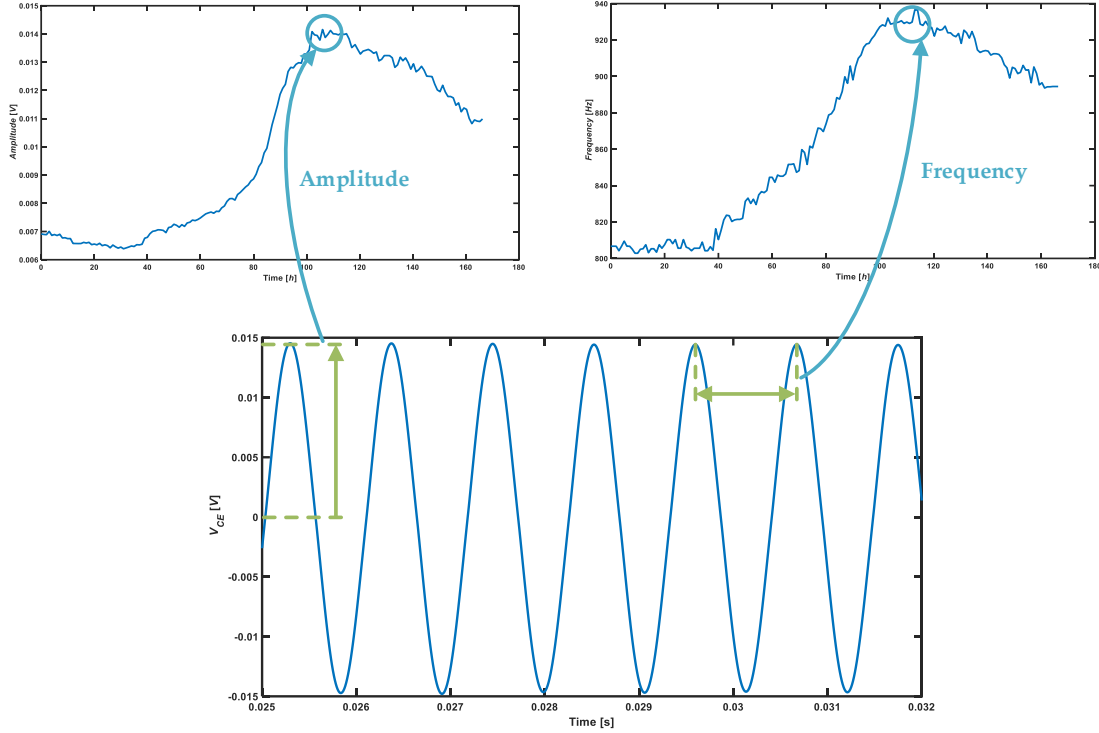
Fig. 3.13 Voltage V_{CE} waveform (bottom graph) obtained from a Ngspice electrical simulation of the oscillator circuit (including the CE block).From the wave,f_{CE} and a_{CE} are extracted for each time $t(j)$ (top graphs).

figure) obtained in that simulation. A waveform is obtained for each time of the simulation (for each $t(j)$), from which values of f_{CE} and a_{CE} are extracted for each $t(j)$ (top of the figure).

The value of R_{si} obtained at the beginning of the RT simulation (AA8 in Table 3.1, N2a in Table 3.5 and N2aAPP in Table 3.9), and the values of *ff*, R_{ct}, C_{dl}, ΔR_s and R_{gap} obtained for each measure of f and a are used. Since there is a value of each parameter for each measure of f_{CE} and a_{CE}, they are not shown because of the space requirement in this document. In addition, using the CF minimization method, the values of f_{CE} and a_{CE} will be estimated from these same parameters. As a comparison metric, the e_{rm} in terms of frequency and amplitude is used in relation to the real values measured experimentally for each cell line. e_{rm} is calculated as follows,

$$
\begin{aligned}
e_{rm}^{f} &= 100 \cdot \frac{\left| f_{CEmeas} - f_{CEestim} \right|}{f_{CEmeas}} \\
e_{rm}^{a} &= 100 \cdot \frac{\left| a_{CEmeas} - a_{CEestim} \right|}{a_{CEmeas}}
\end{aligned}
\tag{3.7}
$$

where e_{rm}^{f} and e_{rm}^{a} are the mean relative error in terms of frequency and amplitude respectively, f_{CEmeas} and a_{CEmeas} are the values of f_{CE} and a_{CE}, respectively, measured in a real experiment, and $f_{CEestim}$ and $a_{CEestim}$ are the values of f_{CE} and a_{CE}, respectively, obtained by one of the both methods (CF minimization and electrical simulation).

In the following subsections, the frequency and amplitude e_{rm} data for the three cell lines obtained using the REW model will are presented.

3.2.2.1 AA8

In this subsection the e_{rm} values, in terms of frequency and amplitude, obtained with CF minimization and by electrically simulating the oscillator using REW model and AA8 cell line data are presented. In Table 3.15 and Table 3.16 e_{rm} values are shown. $e_{rm.f}^{CF}$ and $e_{rm.a}^{CF}$ are the mean relative errors of the frequency and amplitude estimated by using the CF minimization method. On the other hand, $e_{rm.f}^{ES}$ and $e_{rm.a}^{ES}$ are the mean relative errors of the frequency and amplitude obtained from the electrical simulation (ES).

Table 3.15 Mean relative error (e_{rm}) per well for AA8 cell line in terms of frequency.

Well	1	3	4	5	7	8
$e_{rm.f}^{CF}$ [%]	0.34	0.31	0.27	0.25	0.28	0.16
$e_{rm.f}^{ES}$ [%]	1.34	0.55	1.84	1.77	1.30	1.26

Table 3.16 Mean relative error (e_{rm}) per well for AA8 cell line in terms of amplitude.

Well	1	3	4	5	7	8
$e_{rm.a}^{CF}$ [%]	1.14	1.25	1.24	0.82	1.01	0.84
$e_{rm.a}^{ES}$ [%]	6.36	9.14	8.62	6.46	8.55	7.85

The frequency error is smaller than the amplitude error, which may be due to the smaller amplitude ranges. On the other hand, as expected, the error using the CF minimization method is lower than that obtained for the ESs. Larger errors were expected for ES because the model parameter values are calculated for CF minimization, not for ES. Therefore, it is reasonable to expect bigger errors due to tolerances and computational methods. For the AA8 cell line, it is concluded that the errors found during the ES are acceptable. In the future, simulations will be performed based on this data to redesign or improve the oscillator prototype, since the errors are acceptable and do not imply a problem. Perhaps, if the circuit were to be integrated, more accurate data would be needed, since smaller voltage ranges would be used.

3.2.2.2 N2a

As in the previous subsection, the e_{rm} values, in terms of frequency and amplitude, obtained with CF minimization and by electrically simulating the oscillator using REW model and N2a cell line data are presented. Table 3.17 and Table 3.18 show the values of the e_{rm} for the N2a cell line. The conclusions reached for the error data of the AA8 cell line are applicable to the N2a cell line. In addition, it should be added that the errors of the N2a line are slightly higher than the AA8. This fact may be due, as explained in previous sections, to the difference in the ranges of f and a between the different cell lines. However, the errors are also acceptable, which means that these data can be used in future ESs.

Table 3.17 Mean relative error (e_{rm}) per well for N2a cell line in terms of frequency.

Well	2	3	4	6	7	8
e_{rm}^{CF} [%]	0.51	0.36	0.30	0.37	0.28	0.33
e_{rm}^{ES} [%]	2.21	1.97	1.65	2.08	2.01	2.47

Table 3.18 Mean relative error (e_{rm}) per well for N2a cell line in terms of amplitude.

Well	2	3	4	6	7	8
e_{rm}^{CF} [%]	1.94	1.59	1.48	1.55	1.27	1.39
e_{rm}^{ES} [%]	10.58	9.06	9.25	9.70	8.84	10.11

3.2.2.3 N2aAPP

The e_{rm} values, in terms of frequency and amplitude, obtained from CF minimization and electrical simulation using REW model and N2aAPP cell line data are presented in the current subsection. Table 3.19 and Table 3.20 show the frequency and amplitude e_{rm} values respectively. All comments and conclusions given for the two previous cell lines are applicable to the N2aAPP cell line. The error of both parameters is similar to the error values of the previous cell lines. All three cell lines have acceptable error values. The

Table 3.19 Mean relative error (e_{rm}) per well for N2aAPP cell line in terms of frequency.

Well	2	3	4	6	7	8
e_{rm}^{CF} [%]	0.39	0.36	0.37	0.25	0.24	0.90
e_{rm}^{ES} [%]	2.20	1.69	1.58	1.67	1.76	1.09

values of the REW model parameters obtained are valid for performing ESs, which allows testing of future improvements of the prototype.

Table 3.20 Mean relative error (e_{rm}) per well for N2aAPP cell line in terms of amplitude.

Well	2	3	4	6	7	8
e_{rm}^{CF} [%]	1.43	1.53	1.68	0.93	0.90	3.33
e_{rm}^{ES} [%]	9.58	8.60	9.06	9.44	10.25	8.21

3.3 Conclusions

The main target of Chapter 3 is to simulate in RT a CC assays growth real experiment connected to an OBT as a load and make predictions. The simulation has the goal to estimate the cell concentration in the wells in RT, i.e., when a measurement of f_{CE} and a_{CE} is performed, calculating the cell concentration at that time. In order to perform this task, the parameters of the electrical model used to predict the electrical behavior of the CE block must be estimated. Keeping in mind that future values are not known, so parameters such as R_{gap}, which has more influence at the end of the simulation ($ff \rightarrow 1$), must be calculated for each measurement taken. The method of minimization of a CF has been used to obtain the optimal values of the model parameters that meet the BSC for each value of f_{CE} and a_{CE}. Due to the complexity of the used models (REW and FO REW) it is hard to obtain good results, since there is a considerable number of parameters to calculate at each moment, and small variations in one of them can make the value of the parameter *ff* differs from its real value. In addition, the f_{CE} and a_{CE} data for some cell lines are worse than the data for others, as the prototype measurement is still in the experimental phase. Even with these difficulties, it has been possible to successfully estimate the RT cell concentration present in a CC assay, although with a certain margin of error. Considering the variability of cell concentration, and the studies performed up to now, it can be considered that the results are good. It is a very useful method, but should be improved in future works. Some conclusions have been derived from these simulations, which are discussed below:

- Cell concentration of a CC assay can be measured using an oscillator as a measuring circuit to which the CC is connected as a load. The oscillator circuit (OBT) must be configured to oscillate at the frequencies at which the most robust measurements are obtained taking into account the frequency response (BD) of the CC assay (CE block).

- The optimum oscillation frequency depends on the cell line. In this work, all measurements have been performed with the cut-off frequency of the BPF of the OBT set at 1 *kHz*, i.e., the circuit oscillates at frequencies somewhat lower than the filter cut-off frequency. The cell lines used as subject of study in this

work (AA8, N2a and N2aAPP) have provided relatively good results in terms of oscillation parameters. However, after observing the BD of other different cell lines, in future works, the cut-off frequency of the BPF should be increased to obtain larger ranges of frequency and amplitude (Δf_{CE} and Δa_{CE}).

- The e_{rm} obtained, in terms of cell concentration, depends on the cell line, because the lines with a lower A_{cell} (N2a and N2aAPP) reach much larger error values than the cell line with a higher A_{cell} (AA8).

- More generally, it has been demonstrated that the cell concentration can be obtained in RT during the performance of a cell growth experiment. The errors found, while significant, can be reduced by improving the measurement circuit and the algorithm for calculating the cell concentration.

The other purpose of Chapter 3, derived from the main goal, is to obtain the values of the parameters of the CE model of the CE block. Although it is considered secondary in this work, it is crucial for the development of the measurement prototype, since it allows to perform ES with real data of the CE model. The ES are very important to improve and test the OBT before implementing improvements to the current prototype or designing a new one. For this reason, ES have been performed with the CE model data using the Ngspice electrical simulator. Routines have been created in Matlab to automatically edit the Spice files of the CE model and to launch simulations with Ngspice in an automated and much easier way than using the Ngspice software's own command window. The results of the electrical simulations are very promising, as the error margins are acceptable, so the CE model data obtained can be used as a starting point to improve the OBT circuit and obtain more robust and accurate measurements of the RT cell concentration of a CC assay.

Chapter 4   Conclusions and future works

The goal of this thesis is to find a method to estimate in real-time (RT) the cell concentration in a cell culture (CC) assay real experiment using bioimpedance (BI) measurements. For this purpose, an electronic oscillator circuit (OBT) has been used which ensures the measurement of BI in a non-invasive, fast and safe way for the cells. Some conclusions have been reached after finishing this thesis:

- The BI of a biological sample (BS) is usually obtained by injecting a signal of a specific frequency and amplitude through the BS. This is a limitation, because although it is possible to calculate the impedance of the BS at a particular frequency or frequencies, it is very complex to obtain an electrical model of these averages. In this thesis an indirect BI measurement technique has been used. The CC is connected to an OBT circuit, which oscillates by itself at an amplitude and frequencies determined by all the elements that compose the circuit, including the CC. The oscillation frequency and amplitude depend, therefore, on the BI of the CC. From the two oscillation parameters, it is possible to obtain the electrical model of the cell-electrode (CE) block.

- Although the models tested in this work consider the contribution of the cells to the electrical behavior of the CE block to be negligible (not including capacitance or intracellular resistance), these models are reasonably accurate at predicting the electrical response of the block by selecting the adequate frequency. This is because at some frequencies the cells impedance achieves very high values (short circuit). The fill-factor (ff) parameter can measure, with high precision, the fill percentage of the bottom of the well, which means that the cell concentration can be obtained in an approximate range. This means that it is possible to perform a RT monitoring of the CC assay growth from $ff = 0$ to $ff = 1$, which is a key contribution of this work (only applicable to a monolayer CC assay).

- The electrode model used has been widely employed in the BI field, and in this work, it has provided good results. Although some parameters differ a little from the theoretical calculated values, this is not a problem, because there are many variables during the theoretical calculation whose values are still under study.

- Three variants of the same model have been tested: single-electrode well (SEW), real-electrode well (REW) and fractional order (FO) real-electrode well (FO REW). In general, the SEW model offers less accuracy than the other two, since it contains the effects of eleven electrodes in one. Therefore, although the SEW model has been used as a starting point, tests should be performed with the other two models, since they are more accurate.

- The method for fitting the models has been to minimize a cost function (CF). The chosen CF ensures the fulfillment of the Barkhausen stability criterion (BSC), which guarantees the OBT oscillations. The BSC is the key to the mathematical estimation of the electrical models, because it would be impossible to translate the oscillation parameters to the models without it.

- The CF minimization has been applied, firstly to the initial ($ff \to 0$) and final ($ff \to 1$) points of the experiments. This is because it was found that there are certain parameters that only influence the model for low *ff*, and there are also other parameters that only influence the model when *ff* is high. It is a way to calculate model parameters that, although successfully, does not allow RT estimation of cell concentration.

- An algorithm has been designed to estimate the cell concentration in a CC assay in RT. It is based on the use of the minimization of a CF that meets the BSC. In addition, it can determine the minimum points of the oscillation parameters to estimate the initial parameters with the lowest possible *ff*.

- RT estimation of cell concentration is computationally expensive. However, this is not a problem because one measurement is taken per hour in the experiments performed for this thesis. In terms of computation time, the bottle neck could be below 30 seconds from measurement to measurement, which is not realistic, since such a level of precision is not necessary and would introduce a lot of noise in the amplitude and frequency curves (and consequently in the *ff* curve).

- Although in previous works, other authors have used R_{gap} (resistor that models the gap region between cells and between cells and the electrode) values of the order of 10^4 and 10^5 Ω, in this thesis the R_{gap} values obtained are of the order of 10^3 Ω. This suggests that the R_{gap} value may depend on the estimation method or on the cell line.

- The first hours of a CC assay are not important in predicting cell concentration growth. In these hours, the cells adapt to the medium and adhere to the bottom of the well. Therefore, in this work, somewhat inaccurate measurements are obtained during these hours. The RT cell concentration has a much larger error in the first hours than in the growth and saturation phase of the well. Therefore, the results are considered

acceptable due to the low density of the cells (or the low area occupied by cells in the bottom of the well).

- The three used models seem to predict correctly the growth dynamics of a CC. The SEW model, although computationally lighter, is the least accurate of all, finding its largest errors in the first hours of the experiments. REW model is much more accurate than SEW, but it is still slightly unstable in the first hours of the experiments. On the other hand, the FO REW model has a much better knowledge of the electrical behavior of the CE block. This model, being an FO model, can fit the nonlinear effects with the fractional coefficients, without the need for the other parameters of the model to compensate for the nonlinearities. Although, in general, the FO REW model is more accurate, during RT estimation of cell concentration, the REW model returns more accurate results in the final region of the experiment ($ff \rightarrow 1$).

- Similar tests have been performed using 3 different cell lines: AA8, N2a and N2aAPP. The AA8 line shows better results than the others. One of the possible hypotheses is that, since the morphology and size of the cells is different for each line, and the N2a and N2aAPP lines have a mean area five times smaller than AA8, it is possible that this factor results in lower amplitude and frequency ranges. This fact makes harder the model fitting and estimation of *ff* and cell concentration.

- The cell growth data of the AA8 line obtained by traditional methods are similar to those obtained using the BI data. In contrast, this is not the case for the other two lines, which seem to take longer to start growing during a traditional experiment.

- To perform electrical simulations of the system from Matlab, some scripts have been developed that automatically edit the CE block model, launch the electrical simulation and process the data. The electrical simulation is performed with Ngspice, an open-source software, which can perform electrical simulations of Spice files. Part of the toolbox developed in Matlab can be very useful in the educational field, since it allows to launch simulations of Spice files from Matlab and easily save, process and display the data.

- The electrical simulations present an acceptable error in terms of frequency and amplitude of oscillation (the maximum errors are found in the amplitude curves of the N2a and N2aAPP lines, reaching levels of 10 %) . Therefore, while the first prototype of the OBT circuit was designed, designers did not have experimental real BI data to perform the electrical simulations (simulations required before building the first prototype), the model data obtained from the RT simulations can be used, in the future, to simulate modifications and improvements of the OBT circuit.

- Although the error margins of RT simulations are still large, it has been shown that the objective of estimate the cell concentration using an indirect measure of BI via an OBT is possible and feasible. The center frequency of the band-pass filter (BPF), according to the bode diagrams of the CCs, could be increasing in order to obtain more accurate results with the N2a and N2aAPP line and improve the results obtained with the AA8 line. In addition, the RT cell concentration calculation algorithm can be improved. Therefore, although data acquisition prototype and estimation algorithm in RT should be improved, the results can be considered promising.

- After the completion of this thesis, several clearly differentiated sources of error are found: the first is the BPF cut-off frequency that defines around which frequency the circuit oscillates; the second is the difference in cell size between the cell lines (which leads to differences in the electrical model), which can be solved with a BPF circuit whose cut-off frequency is variable (by software or hardware); and the third is the complexity to know the electrical behavior of the CE block during the first hours of an experiment (research on this topic should be carried out).

Based on the above conclusions, certain questions and future work to be performed are suggested:

- The OBT circuit should be improved. The circuit will be modified in order to make the cut-off frequency of the BPF tunable in a suitable range of frequencies, which will allow to work with different types of cells.

- A detailed study on the influence of cell size and morphology on the model parameters should be carried out. This should allow RT corrections during RT estimation. In other words, the perturbation model that introduces the size difference between one cell line and another must be found.

- The growth rate of cells of the N2a and N2aAPP lines is different in the presence of electric current and in its absence. The causes and the relationship between cell size and electric current will be studied to determine if electrostimulation has been produced.

- Electrical simulations are very slow compared to simulations using CF minimization. On the other hand, electrical simulations should be more accurate and closer to reality. Therefore, it is planned to implement the OBT measurement circuit in a nonlinear semi-analytical simulation toolbox, which has been developed in [67]. This work could find a more equilibrated point between the accuracy of an electrical simulation and the speed of a semi-analytical solution.

- The RT cell concentration estimation method will be applied to other cell lines. It will also be tested in toxicology or radiation experiments to check if it can overcome such challenges. In addition, cell identification is planned to be applied to viruses and bacteria, as well as to the stem cell differentiation process.

- Designing and building a CAD tool for the electrical simulation of cell cultures using the toolbox developed with Ngspice and Matlab, similar to [68].

References

[1] G. Huertas, D. Vázquez, A. Rueda, and J. L. Huertas, *Oscillation-Based Test in Mixed-Signal Circuits*. The Netherlands: Dordrecht: Springer-Verlag, 2006.

[2] L. D. Rojas, G. Martinez, and T. Scheper, "Cell counting based on local intensity maxima grouping for in-situ microscopy," *2014 IEEE 11th Int. Symp. Biomed. Imaging, ISBI 2014*, pp. 1344–1347, Jul. 2014.

[3] J. Lou, M. Zhou, Q. Li, C. Yuan, and H. Liu, "An automatic red blood cell counting method based on spectral images," *Proc. - 2016 9th Int. Congr. Image Signal Process. Biomed. Eng. Informatics, CISP-BMEI 2016*, pp. 1391–1396, Feb. 2017.

[4] A. Adan, G. Nel Alizada, Y. ˇ Mur Kiraz, Y. Baran, and A. Nalbant, "Flow cytometry: basic principles and applications," *Crit Rev Biotechnol*, vol. 37, no. 2, pp. 163–176, 2017.

[5] I. Giaever and C. R. Keese, "Use of Electric Fields to Monitor the Dynamical Aspect of Cell Behavior in Tissue Culture," *{IEEE} Trans. Biomed. Eng.*, vol. {BME}-33, no. 2, pp. 242–247, Feb. 1986.

[6] P. Perez, A. Yufera, J. A. Serrano, and G. Huertas, "Designing bioimpedance based sensors for cell cultures test," *2020 35th Conf. Des. Circuits Integr. Syst. DCIS 2020*, Nov. 2020.

[7] C. Hildebrandt, H. Büth, S. Cho, Impidjati, and H. Thielecke, "Detection of the osteogenic differentiation of mesenchymal stem cells in 2D and 3D cultures by electrochemical impedance spectroscopy," *J. Biotechnol.*, vol. 148, no. 1, pp. 83–90, Jul. 2010.

[8] P. Pérez, J. A. Serrano, and A. Olmo, "3D-printed sensors and actuators in cell culture and tissue engineering: Framework and research challenges," *Sensors (Switzerland)*, vol. 20, no. 19, 2020.

[9] B. Arredondo-Vega and D. Voltolina, "Concentración, recuento celular y tasa de crecimiento," in *Métodos y herramientas analíticas en la evaluación de la biomasa microalgal*, Centro de Investigaciones Biologicas del Noroeste S.C., 2007.

[10] H. P. Schwan, "Electrical Properties of Tissue and Cell Suspensions," *Adv. Biol. Med. Phys.*, vol. 5, pp. 147–209, Jan. 1957.

[11] J. Li, T. Igbe, Y. Liu, Z. Nie, W. Qin, L. Wang, and Y. Hao, "An Approach for Noninvasive Blood Glucose Monitoring Based on Bioimpedance Difference Considering Blood Volume Pulsation," *IEEE Access*, vol. 6, pp. 51119–51129, Aug. 2018.

[12] F. Zhu, P. Kotanko, and N. W. Levin, "Estimation of peripheral blood volume and interstitial volume in hemodialysis patients using bioimpedance techniques," *Proc. Annu. Int. Conf. IEEE Eng. Med. Biol. Soc. EMBS*, pp. 1389–1392, Sep. 2017.

[13] C. I. Guerrero-Robles, G. J. Vazquez-Zapien, M. M. Mata-Miranda, J. E. Noriega-Gonzalez, and C. A. Gonzalez-Diaz, "Electrical bioimpedance spectroscopy as biosensor technique to identify cells lineages and cell differentiation process," *Proc. Annu. Int. Conf. IEEE Eng. Med. Biol. Soc. EMBS*, pp. 3568–3571, Sep. 2017.

[14] S. Khalil, M. Mohktar, and F. Ibrahim, "The Theory and Fundamentals of Bioimpedance Analysis in Clinical Status Monitoring and Diagnosis of Diseases,"

Sensors, vol. 14, no. 6, pp. 10895–10928, Jun. 2014.

[15] Y.-Y. Lu, J.-J. Huang, and K.-S. Cheng, "The design of electrode-array for monitoring the cellular bioimpedance," in *2009 {IEEE} Symposium on Industrial Electronics & Applications*, Oct. 2009.

[16] K. Lei, "Review on Impedance Detection of Cellular Responses in Micro/Nano Environment," *Micromachines*, vol. 5, no. 1, pp. 1–12, 2014.

[17] D. A. Borkholder, "Cell based biosensors using microelectrode," Stanford University, 1998.

[18] R. Pradhan, M. Mandal, A. Mitra, and S. Das, "Monitoring cellular activities of cancer cells using impedance sensing devices," *Sensors Actuators B Chem.*, vol. 193, pp. 478–483, Mar. 2014.

[19] P. Daza, A. Olmo, D. Cañete, and A. Yúfera, "Monitoring living cell assays with bio-impedance sensors," *Sensors Actuators B Chem.*, vol. 176, pp. 605–610, 2013.

[20] M. Abdolahad, H. Shashaani, M. Janmaleki, and S. Mohajerzadeh, "Silicon nanograss based impedance biosensor for label free detection of rare metastatic cells among primary cancerous colon cells, suitable for more accurate cancer staging," *Biosens. Bioelectron.*, vol. 59, pp. 151–159, Sep. 2014.

[21] C. F. Lourenço, A. Ledo, J. Laranjinha, G. A. Gerhardt, and R. M. Barbosa, "Microelectrode array biosensor for high-resolution measurements of extracellular glucose in the brain," *Sensors Actuators B Chem.*, vol. 237, pp. 298–307, 2016.

[22] A. Dibao-Dina, J. Follet, M. Ibrahim, A. Vlandas, and V. Senez, "Electrical impedance sensor for quantitative monitoring of infection processes on {HCT}-8 cells by the waterborne parasite Cryptosporidium," *Biosens. Bioelectron.*, vol. 66, pp. 69–76, 2015.

[23] S. Reitinger, J. Wissenwasser, W. Kapferer, R. Heer, and G. Lepperdinger, "Electric impedance sensing in cell-substrates for rapid and selective multipotential differentiation capacity monitoring of human mesenchymal stem cells," *Biosens. Bioelectron.*, vol. 34, no. 1, pp. 63–69, 2012.

[24] S. Grimnes and O. G. Martinsen, *Bioimpedance and Bioelectricity Basics*, 3rd Ed. Oslo: Elsevier, 2015.

[25] X. Huang, D. Nguyen, D. W. Greve, and M. M. Domach, "Simulation of Microelectrode Impedance Changes Due to Cell Growth," *{IEEE} Sensors J.*, vol. 4, no. 5, pp. 576–583, Oct. 2004.

[26] A. Olmo and A. Yúfera, "Computer simulation of microelectrode based bio-impedance measurements with COMSOL," in *Third International Conference on Biomedical Electronics and Devices*, 2010, pp. 178–182.

[27] X. Zhang, W. Wang, and S. Jang, "The Modeling, Design, Fabrication, and Application of Biosensor Based on Electric Cell-Substrate Impedance Sensing (ECIS) Technique in Environmental Monitoring," *Biosens. Environ. Monit.*, Dec. 2018.

[28] I. Giaever and C. R. Keese, "Micromotion of mammalian cells measured electrically," *Proc. Natl. Acad. Sci. U. S. A.*, vol. 88, no. 17, pp. 7896–7900, 1991.

[29] G. T. A. Kovacs, "Microelectrode models for neural interfaces," in *Enabling*

technologies for cultured neural networks, D. A. Stenger and T. M. McKenna, Eds. New York: Academic Press, 1994, pp. 121–165.

[30] J. A. Serrano, P. Pérez, A. Maldonado, M. Martín, A. Olmo, P. Daza, G. Huertas, and A. Yúfera, "Practical characterization of cell-electrode electrical models in bio-impedance assays," in *BIODEVICES 2018 - 11th International Conference on Biomedical Electronics and Devices, Proceedings; Part of 11th International Joint Conference on Biomedical Engineering Systems and Technologies, BIOSTEC 2018*, 2018, vol. 1, pp. 100–108.

[31] A. Yúfera, P. Daza, and D. Cañete, "Using microelectrode models for real time cell-culture monitoring," in *Proceedings of the Annual International Conference of the IEEE Engineering in Medicine and Biology Society, EMBS*, 2011, vol. 2011, pp. 3983–3986.

[32] F. Liu, S. M. Arifuzzaman, A. N. Nordin, D. Spray, and I. Voiculescu, "Characterization of endothelial cells using electrochemical impedance spectroscopy," *IEEE Asia-Pacific Conf. Circuits Syst. Proceedings, APCCAS*, pp. 252–255, 2010.

[33] N. Goda, N. Kataoka, J. Shimizu, S. Mohri, Y. Yamamoto, and F. Kajiya, "Evaluation of micromotion of vascular endothelial cells with estrogen in electrical cell-substrate impedance sensing (ECIS) method using a mathematical model - Cell-to-cell distance and cell-to-substrate distance," *2005 3rd IEEE/EMBS Spec. Top. Conf. Microtechnology Med. Biol.*, vol. 2005, pp. 211–214, 2005.

[34] J. J. Cabrera, "Electrical Characterization of Vegetable Tissues Based on Fractional- Order Models," 2020.

[35] A. Maldonado, P. Perez, G. Huertas, A. Yufera, A. Rueda, and J. L. Huertas, "Monitoring tissue evolution on electrodes with bio-impedance test," *2016 Conf. Des. Circuits Integr. Syst. DCIS 2016 - Proc.*, pp. 213–218, Feb. 2017.

[36] J. O. Bockris and A. K. N. Reddy, *Modern Electrochemistry: Volume 1*. Boston, MA: Springer US, 1970.

[37] D. A. Robinson, "The Electrical Properties of Metal Microelectrodes," *Proc. IEEE*, vol. 56, no. 6, pp. 1065–1071, 1968.

[38] H. P. Schwan, "Determination of biological impedance," in *Physical in Biological Research*, W. L. Nastuk, Ed. New York: Academic Press, 1963.

[39] S. R. W, B. J. G, and S. H. P, "Nonlinear AC and DC polarization of platinum electrodes.," *IEEE Trans Biomed Eng*, vol. 27, no. 3, pp. 166–171, 1980.

[40] H. P. Schwan, "Linear and nonlinear electrode polarization and biological materials," *Ann. Biomed. Eng. 1992 203*, vol. 20, no. 3, pp. 269–288, May 1992.

[41] J. J. Ackmann, "Complex bioelectric impedance measurement system for the frequency range from 5 Hz to 1 MHz," *Ann. Biomed. Eng. 1993 212*, vol. 21, no. 2, pp. 135–146, Mar. 1993.

[42] P. R and W. JG, "Bioelectric impedance measurements using synchronous sampling," *IEEE Trans. Biomed. Eng.*, vol. 40, no. 8, pp. 824–829, 1993.

[43] G. Huertas, A. Maldonado, and A. Yúfera, "Electrical Cell-substrate Impedance Spectroscopy (ECIS) measurements based on Oscillation-Based Test techniques," *Lect. Notes Impedance Spectrosc.*, pp. 109–118, Jan. 2015.

[44] R. Bragós, E. Sarró, A. Fontova, A. Soley, J. Cairó, A. Bayés-Genís, and J. Rosell, "Four versus two-electrode measurement strategies for cell growing and differentiation monitoring using electrical impedance spectroscopy," *Annu. Int. Conf. IEEE Eng. Med. Biol. - Proc.,* pp. 2106–2109, 2006.

[45] R. D. Beach, R. W. Conlan, M. C. Godwin, and F. Moussy, "Towards a miniature implantable in vivo telemetry monitoring system dynamically configurable as a potentiostat or galvanostat for two- and three-electrode biosensors," *IEEE Trans. Instrum. Meas.,* vol. 54, no. 1, pp. 61–72, Jan. 2005.

[46] "Applied Biophysics." http://www.biophysics.com/ (accessed Nov. 05, 2020).

[47] P. Pérez, "Circuit design for biomedical laboratories based on impedance measurement," Universidad de Sevilla, 2019.

[48] R. N. Bracewell, *The Fourier Transform and Its Applications (3rd ed.).* Boston: McGraw-Hill, 2000.

[49] J. Wegener, C. R. Keese, and I. Giaever, "Electric cell-substrate impedance sensing (ECIS) as a noninvasive means to monitor the kinetics of cell spreading to artificial surfaces," *Exp. Cell Res.,* vol. 259, no. 1, pp. 158–166, Aug. 2000.

[50] O. Stern, "Zur Theorie der Elektrolytischen Doppelschicht," *Zeitschrift fur Elektrochemie,* vol. 30, no. 21-22, pp. 508–516, Nov. 1924.

[51] H. Helmholtz, "Studien über electrische Grenzschichten," *Ann. Phys.,* vol. 243, no. 7, pp. 337–382, Jan. 1879.

[52] M. Gouy, "Sur la constitution de la charge électrique à la surface d'un électrolyte," *J. Phys. Théorique Appliquée,* vol. 9, no. 1, pp. 457–468, 1910.

[53] D. L. Chapman, " LI. A contribution to the theory of electrocapillarity ," *London, Edinburgh, Dublin Philos. Mag. J. Sci.,* vol. 25, no. 148, pp. 475–481, Apr. 1913.

[54] H. J. Lewerenz, "On the Structure of the Helmholtz Layer and its Implications on Electrode Kinetics," *ECS Trans.,* vol. 50, no. 52, pp. 3–20, Apr. 2013.

[55] J. Serrano, G. Huertas, A. Maldonado-Jacobi, A. Olmo, P. Pérez, M. Martín, P. Daza, and A. Yúfera, "An Empirical-Mathematical Approach for Calibration and Fitting Cell-Electrode Electrical Models in Bioimpedance Tests," *Sensors,* vol. 18, no. 7, p. 2354, Jul. 2018.

[56] P. Pérez, A. Maldonado-Jacobi, A. J. López, C. Martínez, A. Olmo, G. Huertas, and A. Yúfera, "Remote Sensing of Cell-Culture Assays," in *New Insights into Cell Culture Technology,* InTech, 2017, pp. 135–155.

[57] P. Pérez, G. Huertas, A. Maldonado-Jacobi, M. Martín, J. A. Serrano, A. Olmo, P. Daza, and A. Yufera, "Sensing Cell-Culture Assays with Low-Cost Circuitry," *Sci. Rep.,* vol. 8, no. 1, p. 11, 2018.

[58] P. Pérez, G. Huertas, A. Olmo, A. Maldonado-Jacobi, J. Serrano, M. Martín, P. Daza, and A. Yúfera, "Remote Cell Growth Sensing Using Self-Sustained Bio-Oscillations," *Sensors,* vol. 18, no. 8, p. 2550, Aug. 2018.

[59] G. Huertas, A. Maldonado, A. Yufera, A. Rueda, and J. L. Huertas, "The Bio-Oscillator: A Circuit for Cell-Culture Assays," *IEEE Trans. Circuits Syst. II Express Briefs,* vol. 62, no. 2, pp. 164–168, Feb. 2015.

[60] "Matlab." https://es.mathworks.com (accessed Nov. 05, 2020).

[61] "Ngspice." http://ngspice.sourceforge.net (accessed Nov. 05, 2020).

[62] "Texas Instruments." https://www.ti.com/ (accessed Nov. 16, 2020).

[63] Y. Yuste, J. A. Serrano, A. Olmo, A. Maldonado-Jacobi, P. Pérez, G. Huertas, S. Pereira, F. de la Portilla, and A. Yúfera, "Monitoring muscle stem cell cultures with impedance spectroscopy," in *BIODEVICES 2018 - 11th International Conference on Biomedical Electronics and Devices*, 2018, vol. 1.

[64] C. a Monje, Y. Q. Chen, B. M. Vinagre, D. Xue, and V. Feliu, *Fractional-order Systems and Controls. Fundamentals and Applications*. 2010.

[65] "fminsearch." https://es.mathworks.com/help/matlab/ref/fminsearch.html (accessed Mar. 12, 2021).

[66] J. A. Serrano, P. Perez, G. Huertas, and A. Yufera, "Alternative General Fitting Methods for Real-Time Cell-Count Experimental Data Processing," *IEEE Sens. J.*, vol. 20, no. 24, pp. 15177–15184, Dec. 2020.

[67] J. A. Serrano, A. J. Gines, and E. Peralias, "Fast Simulation of Non-Linear Circuits using Semi-Analytical Solutions Based on the Matrix Exponential," in *IEEE International Symposium on Circuits and Systems (ISCAS)*, 2020.

[68] P. Pérez, J. A. Serrano, M. E. Martín, P. Daza, G. Huertas, and A. Yúfera, "A computer-aided design tool for biomedical OBT sensor tuning in cell-culture assays," *Comput. Methods Programs Biomed.*, vol. 200, p. 105840, Mar. 2021.

Appendix A: Scientific publications

The present thesis has contributed to the publication of some papers in important journals (Table A.1) and the attendance and publication in some international conferences (Table A.2).

Table A.1   Journal publications

Name	Journal	Year	Quartile	Reference
Sensing cell-culture assays with low-cost circuitry	Scientific reports	2018	Q1	[57]
An empirical-mathematical approach for calibration and fitting cell-electrode electrical models in bioimpedance tests	Sensors MDPI	2018	Q1	[55]
Remote cell growth sensing using self-sustained bio-oscillations	Sensors MDPI	2018	Q1	[58]
3D-printed sensors and actuators in cell culture and tissue engineering: framework and research challenges	Sensors MDPI	2020	Q1	[8]
Alternative General Fitting Methods for Real-Time Cell-Count Experimental Data Processing	IEEE Sensors Journal	2020	Q2	[66]
A computer-aided design tool for biomedical OBT sensor tuning in cell-culture assays	Computer Methods and Programs in Biomedicine	2021	Q1	[68]

Table A.2   Conference publications

Name	Conference	Year	Reference
Monitoring muscle stem cell cultures with impedance spectroscopy	11th BIODEVICES	2018	[63]
Practical characterization of cell-electrode electrical models in bio-impedance assays	11th BIODEVICES	2018	[30]
Designing bioimpedance based sensors for cell cultures test	25th DCIS	2020	[6]

Appendix B: Ngspice toolbox code

Main Function

```
function [f,A,R1,R2,C1,C2] = simOBTngspice(R,C,Rgap,Rsi,iRs,ff,n,elec,ref)
        R1  = R/(1-ff);
        R2  = R/ff;
        C1  = C*(1-ff);
        C2  = C*ff;
        Rs = Rsi+iRs*(ff^n);
        if elec==0
           ref = [];
        else
           ref.Rs = (Rsi+iRs*(ff^n))*sqrt(ref.ker);
           ref.R1  = ref.Rr/(1-ff);
           ref.R2  = ref.Rr/ff;
           ref.C1  = ref.Cr*(1-ff);
           ref.C2  = ref.Cr*ff;
        end

        % Edit circuit
        out = editBioZngspice (R1,R2,C1,C2,Rgap,Rs,elec,ref);

        % NGSpice Simulation
        netlistfilename = 'ngspice_OBT.cir';
        simType = {'tran'};
        tstep = 1e-005;
        tfinal = 0.001*32;
        tini = 0.001*25;
        maxstep = 1e-005;
        simParams = {[tstep tfinal tini maxstep]};
        outVars = {'0','vvcmp','vvbpf','vvcs','vvpa'};
        data_ngs = ngspiceSim(netlistfilename,simType,simParams,outVars);

        % Estimate amplitude and frequency
        t = data_ngs.time;
```

```matlab
        L = length(t);
        y = data_ngs.outVars(3).value;
        Lint = 2^nextpow2(L);
        tint = linspace(t(1),t(end),Lint);
        ts = tint(2)-tint(1);
        yint = interp1(t,y,tint);
        ymean = mean(yint);
        out = getFA(yint-ymean,tint,Lint);
        f = out.f;
        A = out.A;
end
```

Edit Bioimpedance to Ngspice

```matlab
function out = editBioZngspice (R1,R2,C1,C2,Rgap,Rs,elec,ref)
        fclose ('all');

        % Parameters
        flagR1 = 'R1val';
        flagR2 = 'R2val';
        flagC1 = 'C1val';
        flagC2 = 'C2val';
        flagRgap = 'Rgapval';
        flagRs = 'Rsval';
        if elec==1
           flagR1_r = 'R1val_r';
           flagR2_r = 'R2val_r';
           flagC1_r = 'C1val_r';
           flagC2_r = 'C2val_r';
           flagRgap_r = 'Rgapval_r';
           flagRs_r = 'Rsval_r';
        end

        % Copy base code of Bioimpedance circuit
        if elec==0
           circuito = 'ngspice_BioZ_sub.mod';
           circuito_base = 'ngspice_BioZ_sub_base.mod';
        else
```

```
      circuito = 'ngspice_BioZ11e_sub.mod';
      circuito_base = 'ngspice_BioZ11e_sub_base.mod';
end

fid = fopen(circuito_base);
fulltext = fread(fid,'*char')';
close = fclose(fid);
if close==-1
   out = close;
   disp('Error al cerrar durante la lectura del circuito Spice');
   return;
else
   out = close;
end

% Write parameters values
fulltext = strrep(fulltext,flagR1_r,num2str(ref.R1));
fulltext = strrep(fulltext,flagR2_r,num2str(ref.R2));
fulltext = strrep(fulltext,flagC1_r,num2str(ref.C1));
fulltext = strrep(fulltext,flagC2_r,num2str(ref.C2));
fulltext = strrep(fulltext,flagRgap_r,num2str(ref.Rgap));
fulltext = strrep(fulltext,flagRs_r,num2str(ref.Rs));
fulltext = strrep(fulltext,flagR1,num2str(R1));
fulltext = strrep(fulltext,flagR2,num2str(R2));
fulltext = strrep(fulltext,flagC1,num2str(C1));
fulltext = strrep(fulltext,flagC2,num2str(C2));
fulltext = strrep(fulltext,flagRgap,num2str(Rgap));
fulltext = strrep(fulltext,flagRs,num2str(Rs));

% Save Spice files
fid = fopen(circuito,'w');
fprintf(fid,'%s',fulltext);
close = fclose(fid);
if close==-1
   out = close;
   disp('Error al cerrar durante la escritura del circuito Spice');
   return;
else
   out = close;
```

```
        end
end
```

Ngspice simulator launcher

```
% NGSPICESIM function to simulate spice circuit
%
% out = ngspiceSim(netlistfilename,simType,simParams,outVars,options)
%
% Inputs:   netlistfilename ->  Name of netlist file (.net or .cir).
%                       File must not include the simulation code.
%         simType ->  Code of simulations to be permormance in struct
%                 format. Example of declaration for OP and
%                 transient: simType = {'op','tran'}.
%         simParams ->Necessary and optional parameters for perform
%                 the simulations declared in simType (in the same
%                 order as in simType.
%                 Example of declaration for OP and transient
%                 analysis: simParams = {[1e-9 100e-9]}
%         outVars ->  variables to show. Example for voltages 'vo' and
%                 'vi': outVars = {'0',vvo,vvi}. '0' denotes not
%                 print vars.
%         options ->  Input of simulation options. Example of options
%                 declaration: opts = {'abstol', 2e-12, 'reltol',
%                 0.001}.
%
% List of options:
%     GENERAL OPTIONS
%         'temp' -> Operating temperature of the circuit. Default is 27º.
%         'tnom' -> Nominal temperature at which device parameters are
%                 measured. Default is 27º.
%     OP AND DC OPTIONS
%         'abstol' -> Absolute current error tolerance of the program.
%                 Default is 1pA.
%         'reltol' -> Absolute current error tolerance of the program.
%                 Default is 0.001 (0.1%).
%
% Simulations codes and parameters:
%   Operatinal Point:   Code -> 'op'
%                 Parameters: No parameters needed
```

```matlab
%   Transient:       Code -> 'tran'
%               Parameters:
%                   tstep (double) ->  Printing or plotting increment
%                               for line-printer output.
%                   tstop (double) ->  Final time.
%                   tstart (double) -> Initial time. (OPTIONAL)
%                   tmax (double) ->   Maximum stepsize that ngspice
%                               use. (OPTIONAL)
%   Small-Signal AC:   Code -> 'ac'
%               Parameters:
%                   variation (char)->  Variation type: decade (1),
%                               octave (2), linear (3).
%                   np (double) ->    Number of points per decade,
%                               octave or lin.
%                   fstart (double) -> Starting frequency.
%                   fstop (double) ->  Final frequency.
%

function out = ngspiceSim(netlistfilename,simType,simParams,outVars,varargin)

    % Check input arguments
    nvarargin = length(varargin);              % Number of variable input arguments

    % Required arguments
    if ~ischar(netlistfilename)                % Check netlist filename
        error('First argument must be "char" type.');
    end
    nSim = length(simType);                    % Number of simulation to be performance
    for i=1:nSim
        if ~ischar(simType{i})                 % Check simulation type name
            error('Second argument must be "char" type.');
        end
    end

    if nSim~=length(simParams)         % Check number of simulation parameters vector
        error('Number of simulations don''t match with number of simulation …
        parameters vector.');
    end
    for i=1:nSim
```

```matlab
    if ~isnumeric(simParams{i})                % Check simulation type name
        error('Second argument must be "char" type.');
    end
end


% Variable arguments (simulation options)
if nvarargin>0
    if mod(nvarargin,2)==0
        simText{1} = '.options ';
        charFlag = 1;
        for i=1:nvarargin
            if charFlag
                if ischar(varargin{i})
                    charFlag = 0;
                    if sum(strcmp({'temp','tnom','abstol','reltol'},varargin{i}))>0
                        simText{1} = [simText{1} varargin{i} ' = '];
                    else
                        error([varargin{i} 'is not a valid option.']);
                    end
                else
                    error('%E value is not associated with any option.',varargin{i});
                end
            else
                if isnumeric(varargin{i})
                    charFlag = 1;
                    simText{1} = [simText{1} varargin{i} ' '];
                else
                    error([varargin{i} 'and ' varargin{i-1} 'options are not properly set.']);
                end
            end
        end
    else
        error('Attempt to enter option without a new value or vice versa. The …
        number of optional arguments must be even.');    % Number varargin error
    end
end


%% Simulations to be performed
for i=1:nSim
```

```matlab
    switch simType{i}
        case 'op'
            simResultsTitle{i} = 'Operating Point';
            if isempty(simParams{i})
                simText{i+1} = '.op';
            else
                error('For Operating Point ("op") Analysis length of simParams vector …
                    must be 0.');
            end


        case 'tran'
            simResultsTitle{i} = 'Transient Analysis';
            if (length(simParams{i})<=4)&&(length(simParams{i})>=2)
                simText{i+1} = ['.tran ' num2str(simParams{i})];
            else
                if length(simParams{i})>4
                    error('For Transient ("tran") Analysis simParams max length vector is 4.');
                else length(simParams{i})<2
                    error('For Transient ("tran") Analysis simParams min array length is 2.');
                end
            end
        case 'ac'
            simResultsTitle{i} = 'Small-Signal AC Analysis';
            acVariation = {'dec', 'oct', 'lin'};
            if length(simParams{i})==4
                    simText{i+1} = ['.ac ' acVariation{simParams{i}(1)} ' ' …
                    num2str(simParams{i}(2:end))];
            else
                    error('For Small-Signal AC Analysis ("ac") analysis length of array …
                    simParams must be 4.');
            end


        otherwise
            error('Simulation type not supported.');
    end
end

simText{end} = [simText{end} newline '.save '];
for j=2:length(outVars)
```

```matlab
        simText{end} = [simText{end} outVars{j}(1) '(' outVars{j}(2:end) ') '];
    end


    % Modify net file to include simulation
    netlist = fileread(netlistfilename);    % Read netlist
    tempfolder = 'tempSimFiles';          % Temp folder
    if exist([pwd '\' tempfolder])~=7
        mkdir(tempfolder);
    end
    idtemp = sprintf('%d', round(9*rand(1,3)));
    netlist_tempPath = [pwd '\' tempfolder '\' netlistfilename(1:end-4) '_' idtemp …
netlistfilename(end-3:end)];  % new temp file for temp netlist


    % Modify netlist
    netlist_temp = [netlist newline];
    for i=1:nSim+1
        netlist_temp =[netlist_temp newline simText{i}];
    end
    netlist_temp =[netlist_temp newline '.end' newline];


    % Save temp netlist
    [fid,message] = fopen(netlist_tempPath,'w');
    if fid==-1
        error(['Error open netlist temp file.' message]);
    end
    fprintf(fid,'%s',netlist_temp);
    close = fclose(fid);
    if close~=0
        error(['Error closing netlist temp file.']);
    end



    %% Spice path
    ngspicePath = char(which('ngspice.exe','-all'));


    %% Raw and log files
    savedatafolder = 'savedata';         % Temp folder
    if exist([pwd '\' savedatafolder])~=7
        mkdir(savedatafolder);
```

```matlab
    end
    rawfilename = [pwd '\' savedatafolder '\raw_' netlistfilename(1:end-4) '_' idtemp …
'.txt'];
    logfilePath = 'logfile.log';

    %% Run simulation
    command = [ngspicePath ' -b -r ' rawfilename ' -o ' logfilePath ' ' netlist_tempPath ];

    % Simulation command
    system(command, '-echo');                                    % run simulation

    % Check simulation error in logfile
    logfile = fileread(logfilePath);    % Read logfile

    if contains(lower(logfile),'error')
        error(['Simulation error.' logfile]);
    end
    delete(netlist_tempPath);   % Delete temp netlist

    %% Read rawfile (simulations results)
    rawfile = fileread(rawfilename);    % Read logfile

    % Find sim data ini
    simTitleIni = strfind(rawfile,'Title:');
    simDateIni = strfind(rawfile,'Date:');
    simPlotNameIni = strfind(rawfile,'Plotname:');
    simFlagsIni = strfind(rawfile,'Flags:');
    simNoVariablesIni = strfind(rawfile,'No. Variables:');
    simNoPointsIni = strfind(rawfile,'No. Points:');
    simValuesIni = strfind(rawfile,'Values:');


    % Read simulations data
    for i=1:nSim
        % Find simulation initial data
        datetext = char(regexp(rawfile(simDateIni(i):simPlotNameIni(i)), …
'^Date:\s*(\w.*?\w)\s*$', 'tokens', 'once', 'lineanchors'));
        data(i).date = datestr(datenum(datetext, 'ddd mmm dd HH:MM:SS  yyyy'));
```

```matlab
    data(i).plotname = char(regexp(rawfile(simPlotNameIni(i):simFlagsIni(i)), …
'^Plotname:\s*(\w.*?\w)\s*$', 'tokens', 'once', 'lineanchors'));
    data(i).flags = char(regexp(rawfile(simFlagsIni(i):simNoVariablesIni(i)), …
'^Flags:\s*(\w.*?\w)\s*$', 'tokens', 'once', 'lineanchors'));
    % Find var number
    numVariables = …
str2double(char(regexp(rawfile(simNoVariablesIni(i):simNoPointsIni(i)), '^No\. …
Variables:\s*(\d+)\s*$', 'tokens', 'once', 'lineanchors')));
    % Find var names
    simVariablesIni(i) = …
simNoPointsIni(i)+11+strfind(rawfile(simNoPointsIni(i)+12:simNoPointsIni(i)+35),' …
Variables:');
    vartext = rawfile(simVariablesIni(i)+12:simValuesIni(i)-3);
    variables = regexp(vartext, …
'^\s*(?<num>\d+)\s+(?<name>\S+)\s+(?<type>.*?)\s*$', 'names', 'lineanchors');
    if numVariables < 1
        error('The RAW file:\n\t%s\ncontains no variables.', rawfilename);
    end
    if numVariables ~= length(variables)
        error('Was expecting %d variables, but found %d in RAW file:\n\t%s', …
numVariables, length(variables));
    end
    data(i).numVariables = numVariables;

    % Tanslate vars to valid names in Matlab
    varnames = {variables.name};
    varnames = regexprep(varnames, '(', '');
    varnames = regexprep(varnames, ')', '');
    varnames = regexprep(varnames, '-', '');
    varnames = regexprep(varnames, '#', 'hash');
    varnames = regexprep(varnames, '\.', 'dot');
    varnames = regexprep(varnames, '\+', 'plus');
    varnames = regexprep(varnames, ':', ''); % Remove colons.
    data(i).varnames = varnames;
    % Find num points
    if (strcmp(simType{i},'tran'))||(strcmp(simType{i},'ac'))
        numPoints = …
str2double(char(regexp(rawfile(simNoPointsIni(i):simVariablesIni(i)), '^No\. …
Points:\s*(\d+)\s*$', 'tokens', 'once', 'lineanchors')));
        if numPoints < 1
```

```matlab
        error('The RAW file:\n\t%s\ncontains no points.', rawfilename);
    end
    data(i).numPoints = numPoints;
end


% next sim
if i==nSim
    nextSim = length(rawfile);
else
    nextSim = simTitleIni(i+1)-3;
end


% Show vars to save??
if isempty(str2num(outVars{1}))
    flagShow = 1;
    ind_oV = 1;
else
    flagShow = str2num(outVars{1});
    ind_oV = 2;
end


switch simType{i}
    case 'op'
        % Read data
        opData = sscanf(rawfile(simValuesIni(i)+10:nextSim),'%f');
        data(i).results = opData;
        if flagShow
            % Show data
            text2show = ['Results Operating Point Analysis: ' newline];
            numOutVars = length(outVars);
            for j=ind_oV:numOutVars
                index = find(strcmp(data(i).varnames,outVars{j}));
                if isempty(index)
                    warning(['Variable ' outVars{j} ' does not exist.']);
                else
                    if strcmp(variables(index).type,'current')
                        unit = 'A';
                    elseif strcmp(variables(index).type,'voltage')
                        unit = 'V';
```

```matlab
            end
            text2show =[text2show varnames{index} ' = ' ...
num2str(opData(index)) ' ' unit newline];
          end
        end
        fprintf(text2show);
      end


    case 'tran'
      % Read data
      data_matrix = zeros(numVariables, numPoints);
      tranData = sscanf(rawfile(simValuesIni(i)+9:nextSim),'%f');
      for j=1:numPoints
        for k=1:numVariables
          data_matrix(k,j) = tranData((j-1)*(numVariables+1)+1+k);
        end
      end
      data(i).time = data_matrix(1,:);
      data(i).results = data_matrix(2:end,:);
      data(i).varnames = data(i).varnames(2:end);
      % Show data
      numOutVars = length(outVars);
      for j=ind_oV:numOutVars
        index = find(strcmp(data(i).varnames,outVars{j}));
        if isempty(index)
          warning(['Variable ' outVars{j} ' does not exist.']);
        else
          if strcmp(variables(index+1).type,'current')
            unit = 'A';
          elseif strcmp(variables(index+1).type,'voltage')
            unit = 'V';
          end

          data(i).outVars(j-ind_oV+1).name = outVars{j};
          data(i).outVars(j-ind_oV+1).value = data(i).results(index,:);
          if flagShow
            figuremax;
            plot(data(i).time,data(i).results(index,:));
            ylabel([outVars{j} ' [' unit ']'])
```

```matlab
                    xlabel('Time [s]');
                end
            end
        end
    case 'ac'
        % Read data
        rawfileValues = regexprep(rawfile(simValuesIni(i)+9:nextSim),',',' ');
        mag = zeros(numVariables, numPoints);
        phase = zeros(numVariables, numPoints);
        tranData = sscanf(rawfileValues,'%f');
        for j=1:numPoints
            for k=1:numVariables
                n1 = tranData((j-1)*(2*numVariables+1)+1+2*k-1);
                n2 = tranData((j-1)*(2*numVariables+1)+1+2*k);
                cNum = n1+1j*n2;
                phase(k,j) = angle(cNum)*180/pi-360;%*(n1<1e-3)*(n2>0);
                mag(k,j) = abs(cNum);
            end
        end
        data(i).f = mag(1,:);
        data(i).mag = mag(2:end,:);
        data(i).phase = phase(2:end,:);
        data(i).varnames = data(i).varnames(2:end);

        % Show data
        numOutVars = length(outVars);
        for j=ind_oV:numOutVars
            index = find(strcmp(data(i).varnames,outVars{j}));
            if isempty(index)
                warning(['Variable ' outVars{j} ' does not exist.']);
            else
                if strcmp(variables(index+1).type,'current')
                    unit = 'A';
                elseif strcmp(variables(index+1).type,'voltage')
                    unit = 'V';
                end

                data(i).outVars(j-ind_oV+1).name = outVars{j};
                data(i).outVars(j-ind_oV+1).mag = data(i).mag(index,:);
```

```matlab
            data(i).outVars(j-ind_oV+1).phase = data(i).phase(index,:);
            if flagShow
                figuremax;
                subplot(2,1,1);semilogx(data(i).f,data(i).mag(index,:));
                title(['Bode ' outVars{j}]);
                ylabel(['Magnitude [' unit '/' unit ']']);
                subplot(2,1,2);semilogx(data(i).f,data(i).phase(index,:));
                ylabel(['Phase [º]'])
                xlabel('Frequency [Hz]');
            end
        end
    end
    otherwise
        error('Simulation type not supported.');
    end
end


% Remove rawfile
delete(rawfilename);   % Delete temp netlist


% Output Data
out = data;

end
```

Obtain amplitude and Frequency without Fast Fourier Transform

```matlab
function out = getFA(y,xq,L)

    flag = 1;
    ind1 = 1;
    f = [];
    A = [];

    while flag==1
        flag1 = 0;
        flag2 = 0;
```

```
        flag3 = 0;
        for i=ind1:L
            if (flag1==0)&&(y(i)>0)&&(flag2==0)
                flag1 = 1;
            end
            if flag1&&(y(i)<0)&&(flag2==0)
                ini = i;
                flag2 = 1;
            end
            if flag2&&(y(i)>0)
                flag3 = 1;
            end
            if (flag3&&(y(i)<0))||(i==L)
                fin = i-1;
                break
            end
        end

        if ((L-(fin+1))<(fin-ini))
            flag = 0;
        else
            ind1 = fin;
        end

        indMax = round(mean(find(max(y(ini:fin))==y(ini:fin))));
        indMin = round(mean(find(min(y(ini:fin))==y(ini:fin))));
        f = mean([f 0.5/abs(xq(indMax+ini)-xq(indMin+ini))]);
        ysec = y(ini:fin);
        A = mean([A max(ysec)]);
    end

    out.A = A;
    out.f = f;
end
```